THE ROLE OF SURFACE ACTIVE AGENTS ON HYDRATE FORMATION

BY

CHI YUEN LO

A DISSERTATION SUBMITTED TO THE GRADUATE FACULTY IN ENGINEERING IN PARTIAL FULFILLMENT OF THE REQUIREMENTS FOR THE DEGREE OF DOCTOR OF PHILOSOPHY, THE CITY UNIVERSITY OF NEW YORK

2011

This manuscript has been read and accepted for the

Graduate Faculty in Engineering in satisfaction of the

dissertation requirement for the degree of Doctor of Philosophy.

Jae W. Lee

_____	_____
Date	Chair of Examining Committee
	Mumtaz Kassir
_____	_____
Date	Executive Officer
Ponisseril Somasundaran	Alexander Couzis
_____	_____
Camille Jones	Lane Gilchrist
_____	_____
	Jeff Morris
	_____
	Supervisory Committee

THE CITY UNIVERSITY OF NEW YORK

Abstract

The Role of Surface Active Agents on Hydrate Formation

by

Chi Yuen Lo

Advisor: Professor Jae W. Lee

The goal of this study is to probe the mechanism for improving gas hydrate formation. Fast hydrate formation for gas storage requires the understanding of hydrate formation mechanism. However the formation kinetics is slow due to the low mass transfer rate of gas to hydrate growth regions. Past hydrate formation studies did not incorporate surface studies to investigate the formation mechanism. Our approach to solving this unknown mechanism is to use surface science techniques to probe the interface of hydrate and water.

From ζ-potential measurements, hydrate surface charge is negative due to bicarbonate ion adsorption. An ion exchange occurs upon adding SDS and DS^- monomers replace the bicarbonate ions and a further negative charge confirms DS^- adsorption. Pyrene fluorescence measures the micropolarity of the hydrate interface. Upon adding 50ppm SDS the hydrate interface's micropolarity decreases and indicates an admicelle formation.

Induction time measurements are correlated to the ζ-potential and Pyrene fluorescence measurements to show that reduced induction periods are due to a formation of an admicelle layer. This is first indication of a mechanism where an admicelle layer led to increased growth of hydrates.

Adsorption Isotherms of SDS and DTAB show similar L-S type adsorption. However, SDS, a hydrate promoter, would form a monolayer at lower surfactant concentrations than DTAB. DTAB, a possible anti agglomerate agent, shows a larger adsorption amount before forming a monolayer. The larger adsorption amount for DTAB indicates that a dense layer of surfactants would prevent hydrate particles from sticking to each other.

Raman spectroscopy reveals a blue shift for CP hydrate interface and a shoulder band. The shoulder implies of the aqueous CP around the hydrate interface. With the addition of SDS, the shoulder is blue shifted. Raman spectroscopy of the 1% CP in water shows the similar red shift for aqueous CP but upon adding 1mM SDS the vibrational band experiences a blue shift, indicating a hydrate-like environment. ATR-IR measurements of the hydrate interface expose that with 100ppm SDS bonded OH shifts from ice-like to water-like. This concentration is the same concentration of where a monolayer forms. A monolayer may loosen the hydrate's hydrogen bonding at the interface.

Acknowledgements

First I would like to thank my advisor, Professor Jae W. Lee, for his attitude towards striving for the best, and pushing to get the best out of each person. It sometimes may seem like a pushy person, but it is to get the best out of you. I am thankful for that push, without that I wouldn't be able to research out on my own.

I also thank all the committee members for their support during this PhD candidacy. Professor Som, I am indebted to your knowledge of solid-liquid interfaces and for your gracious attitude towards me during the times I was in your lab. Professor Couzis, I am not only maize and blue but also thankful for your encouragements and teaching. Professor Jones, I'm glad that you were able to collaborate with us in the hydrates lab because of your presence and attitude toward your students; I aspire to be teaching scholar as you are with your group. Professor Gilchrist, I am thankful for your classes and the motivation you put towards your students. Professor Morris, thank you for looking out for me and suggesting exercising my ankle.

I would like to thank all the people who were there to keep me sane. Everyone, I thank you.

Table of Contents

List of Tables

List of Figures

Chapter 1. Introduction

Gas hydrates are non-stoichiometric crystalline compounds, where the host is a network of hydrogen-bonded water molecules around a guest, usually a low molecular weight molecule[1]. There are three known structures: sI, sII, and sH, with increasing cavity size, respectively. Hydrates of sI tend to be small molecules, typically a van der Waals diameter in the range of 0.4 – 0.55 nm [15], like, CO_2, methane, or ethane. A hydrate of sI type has a hydration number of 5.75 H_2O. [2] Hydrates of sII are of moderate size ranges (van der Waals diameter of 0.6- 0.7 nm[15]) like propane, iso-butane, or cyclopentane; and a hydration number of 17 H_2O. [2] Figure 1.1 and 1.2 show the size and structure relationship.

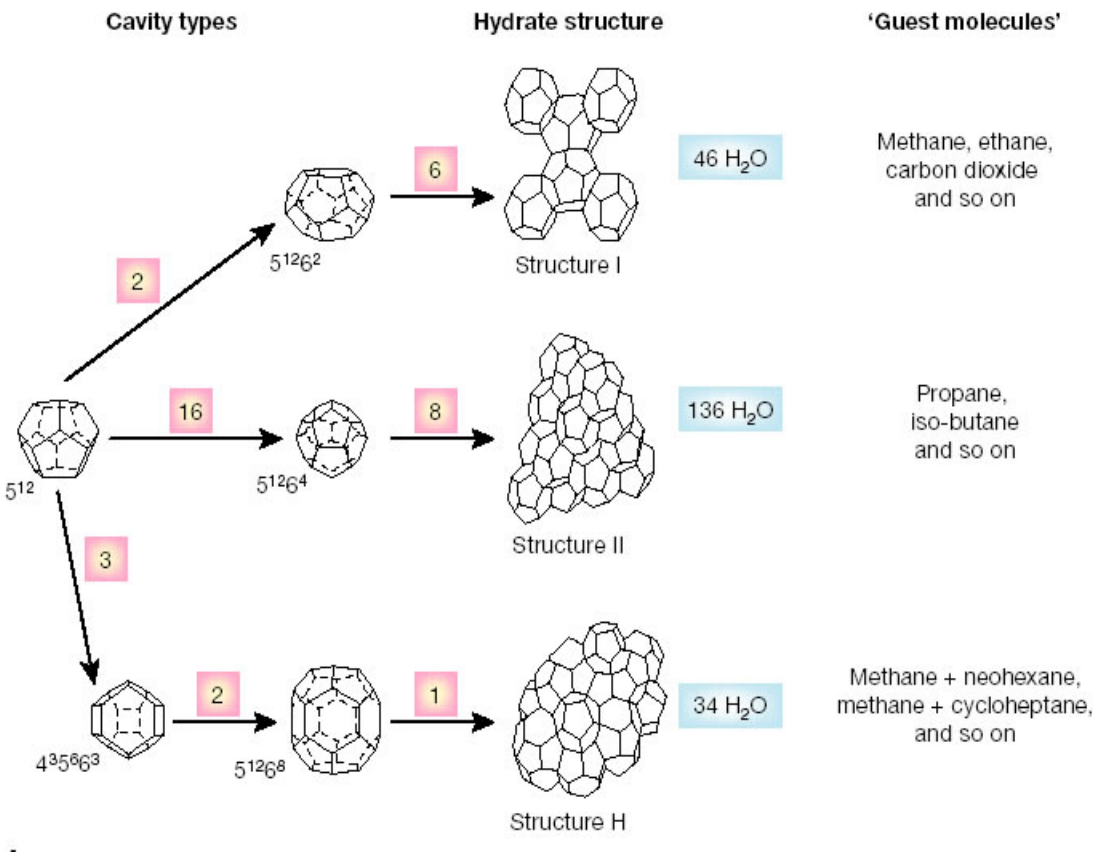

Figure 1.1. Depiction of the hydrate unit cell for sI, sII, and sH hydrates.[1]

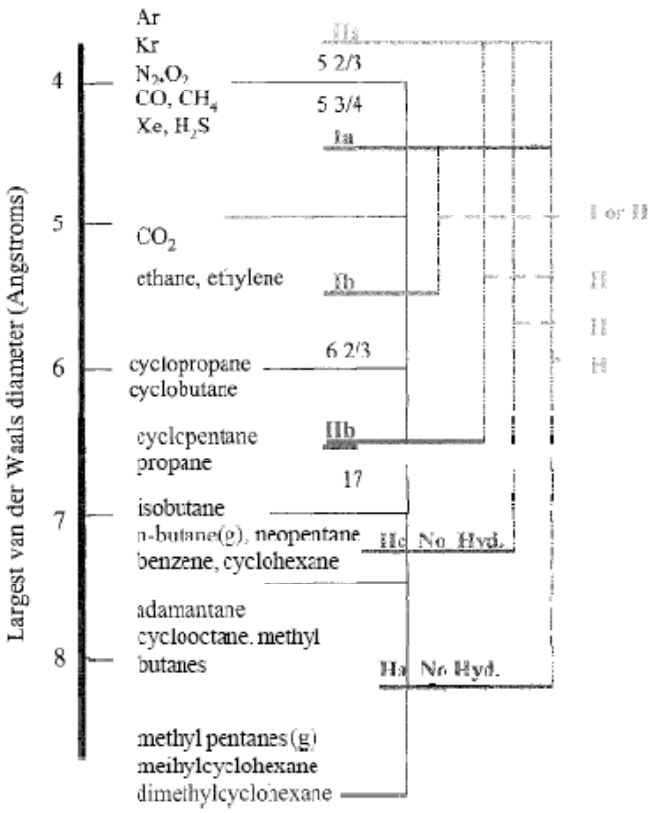

Figure 1.2. Structure-size relationship.[15]

Gas Hydrates were discovered in the early 1800's, by Sir Humphrey Davy. [3] The discovery of the oxymuriatic (chlorine) gas hydrate had spurred more interest into this type of materials. Discoveries of the different gases and phase formations under low temperatures and moderate pressures were of a great interest at that time.

In the 1930's Hammerschmidt discovered gas hydrate formations in oil pipelines, frequently above ice point[4]. This pivotal study led the field into a pragmatic and application-oriented study of gas hydrates. Prevention and risk assessment studies grew rapidly which produced informed protocols for preventing hydrates in the petroleum industry.

Many years later, cursory studies began along the lines of exploration, where an estimated range of 0.2×10^{15}–120×10^{15} m^3 of methane at STP in gas hydrate formations was found around the world[1]. With such an abundance of natural gas, recovery of gas hydrates as a means of energy was a hopeful endeavor. With global warming as a looming threat for relative temperature increases in earth and sea atmospheres, fears of the "clathrate gun" hypothesis spurred a rush for solutions. The "clathrate gun" hypothesis or the late Quaternary climate change 15,000 years ago was thought to be caused by a large methane release due to the dissociation of gas hydrates[5]. So recovery options are being implemented around the world. Along with recovery, hydrate application technologies have been studied as well.

For the oil and gas industry, the mention of gas hydrates is to avoid it and to prevent it. However, new uses of hydrates are to get them to form fast and with a low amount of energy. One volume of gas hydrates is able to store up to 170 volumes of gas at moderate temperatures and high pressures[1]. These storage capacities are comparable to highly compressed gases. Hydrates form at moderately high pressures and low temperatures. However the formation rates are relatively slow and require mechanical agitation to start the stochastic nucleation. More innovative and novel uses of gas hydrates are being implemented as of the last decade. Though most of the research is still in hydrate exploration and recovery[6-10], hydrate technology research is still growing on the outskirts. Most notably, formation studies are being discussed to be implemented in safe gas storage, refrigeration[11], sequestration[12], separation[12] and desalinization[13].

The hurdle for industrial usage of gas hydrates is the slow and stochastic formation rate. One can add mixing and agitation energy to induce formation. However, there is incomplete conversion due to diffusion limitation of guest molecules and the process is energy intensive. This problem is remedied by adding a small amount of surfactant to the process. The effect of adding surfactant is phenomenally fast formation, from weeks to hours[14]; high conversions up to 95-100%. No added energy is used, since this process is a self-assembly process.

We are beginning to understand the dissociation and formation of gas hydrates. Phenomenological studies of fast formation are burgeoning in this field. However, the approach to how the surfactants act on the surface of hydrates is not thoroughly investigated. In the following chapters, fundamental and principal studies will provide an understanding of how surfactants act to promote hydrate formation.

Chapter 2 presents an explanation for fast formation phenomena using ζ- potential measurements and fluorescence spectra measurements. Chapter 3 is a study on the effects of two types of hydrates, one hydrophilic and the other hydrophobic. This study provides a fundamental understanding for similar hydrates and the effects of surfactants upon these interfaces. Chapter 4 is a quantitative analysis of different surfactants using adsorption isotherms as a method of comparison for differing surfactant purposes. Chapter 5 is a quantitative analysis of the two kinetic inhibitors which provides a comparative tool to access the effectiveness of each inhibitor by their surface coverage. By determining coverage and surface amount, it can lead to a better understanding of why these kinetic inhibitors work to inhibit hydrate growth. Chapter 6 uses surface enhanced Raman spectroscopy to probe the hydrate/water interface and the hydrate former/water interface. This study will clarify the

relation of hydrate-like sensitivity upon the hydrate former/water interface and at the hydrate/water interface. Chapter 7 is a study of the hydrate/water interface using infrared absorption, where the interface changes from an ice-like state to a water-like state upon adding surfactants. Chapter 8 is a summary of how surfactants act on hydrate interfaces and how one can deduce the purpose of each individual surfactant. Chapter 9 is the future work chapter which includes the expansion of the work and the ultimate goal of utilizing these fundamental ideas to improve hydrate formation.

References

1. Sloan, E. D.; Koh, C. Clathrate Hydrates of Natural Gas, 3rd ed.; CRC: Boca Raton; 2008.
2. Jeffrey, G. A. Hydrate Inclusion Compounds. In Inclusion Compounds 1; Atwood, J. L., Davies, J. E. D., MacNichol, D. D., Eds.; Academic Press: London, 1983; p 135.
3. Davy. H. On a Combination of Oxymuriatic Gas and Oxygene Gas. Philosophical Transactions of the Royal Society. 1811. 101. 155-162.
4. Hammerschmidt, E. G. Formation of Gas Hydrates in Natural Gas Transmission Lines. Ind. Eng. Chem. 1934. 26. 851–855.
5. Long, D., Lovell, M.A., Rees, J.G., Rochelle, C.A. Sediment-Hosted Gas Hydrates: New Insights on Natural and Synthetic Systems, Geological Society, London, Special Publications. 2009. 319. 1-9.
6. Collett, T.S., Detection and Evaluation of Natural Gas Hydrates from Well Logs, Prudhoe Bay Alaska, M.S. Thesis, University of Alaska. 1983.
7. Collett, T.S., National Assessment of U.S. Oil and Gas Resources on CD-ROM (Gautier, D.L., Goldton, G.L., Takahishi, K.I., eds.), USGS Digital Data Series 30, Washington D.C. (1995).

8. Tréhu, M.A., Bohrmann, G., Rack, R.F., Torres, M.E., Bargs, N.L., et al., in Proc. ODP (Ocean Drilling Program), Initial Repts. 204, Texas A&M University, College Station, TX (2003).
9. Tréhu, A.M., Bohrmann, G., Torres, M.E., Colwell, F.S. (eds.), in Proc. Ocean Drill. Program, Scientific Results 2006, TAMU, College Station, TX, 204.
10. Tréhu, A.M., Ruppel, C., Holland, M., Dickens, G.R., Torres, M.E., Collett, T.S., Goldberg, D.S., Riedel, M., Schultheiss, P., Oceanography. 2006. 19. 124-143.
11. Liang, D., Guo, K., Wang, R., Fan, S. Hydrate equilibrium data of 1,1,1,2-tetrafluoroethane (HFC-134a), 1,1-dichloro-1-fluoroethane (HCFC-141b) and 1,1-difluoroethane (HFC-152a). Fluid Phase Equilibria. 2001. 187–188. 61–70.
12. Kang, S.-P., Lee, H. Recovery of CO2 from Flue Gas Using Gas Hydrate: Thermodynamic Verification through Phase Equilibrium Measurements. Environ. Sci. Technol. 2000. 34. 4397-4400
13. J. Javanmardi, M. Moshfeghian. Energy consumption and economic evaluation of water desalination by hydrate phenomenon. Applied Thermal Engineering. 2003. 23. 845–85
14. Zhong, Y.; Roger, R. E. Surfactant effects on gas hydrate formation. Chem. Eng. Sci. 2000. 55. 4175–4187.
15. Ripmeester, J. A., Ratcliffe, C.I., Udachin, K.A., “Clathrate Hydrates” Encyclopedia of Supramolcular Molecules (2004).

Chapter 2. Adsorption of Sodium Dodecyl Sulfate at THF Hydrate/Liquid Interface.

Published in The Journal of Physical Chemistry C 2008, 112, 12381-12385.

Abstract: Understanding the interaction between sodium dodecyl sulfate (SDS) and gas hydrates provides insight into the role of surfactants in promoting hydrate formation. The aim of this study is to investigate the relationship between tetrahydrofuran (THF) hydrate formation and SDS adsorption at the hydrate/liquid interface. The adsorption behavior of the surfactant is deduced from ζ-potential and pyrene fluorescence measurements. There is a constant negative charge from 0 to 0.17mM SDS from ζ-potential measurements. From 0.17mM to 3.4mM SDS, the ζ-potential becomes more negative indicating adsorption. The micropolarity of the THF hydrate/liquid interface decreases with increasing SDS concentration, starting from 0.17mM SDS. A monolayer of DS^- is completed at 0.17mM SDS. The reduction in induction time in the presence of SDS is indicative of the strong interaction between adsorption and short induction time.

2.1. Adsorption at the THF hydrate/Liquid Interface

This study will endeavor to understand the relationship of SDS adsorption at the THF hydrate/Liquid layer and the gas hydrate induction/nucleation times. We note that below the normal Kraft point (281K - 289K) for SDS there can be no micelles. So it establishes that only the surfactant monomers can acts upon hydrate interfaces. Details of how the interactions between SDS and the hydrate interface are not implicitly understood.

As most gas hydrates like methane, ethane, require high pressures, laboratory studies of these interfaces are difficult. Therefore THF hydrates provide a good alternative for a study at the interface. THF forms sII hydrates and have a maximum melt temperature of 277.9K under atmospheric conditions. In this study, ζ-potential and fluorescence measurements were used to qualitatively study the adsorption density and the surface interactions of SDS and hydrate, which we used to correlate to induction times. The ζ-potential measurements qualitatively measure the charge density on the hydrate interface. Fluorescence measurements obtain information on the micropolarity of the hydrate/liquid interface. Induction time measurements were taken as to correlate the effects of nucleation times to surfactant interaction.

2.2. Experimental Section

2.2.1. Materials

Tetrahydrofuran and sodium dodecyl sulfate with purity of 99+% were purchased from Sigma-Aldrich (ACS reagent grade). The pyrene used for fluorescence had a purity of >99.0% and was supplied by Fluka. All chemicals were used as received without further purification. Deionized water was produced in our laboratory with a resistivity of 17 MΩ cm^{-1}.

2.2.2. ζ- Potential Measurements

Tetrahydrofuran solutions (10wt%) with varying concentrations of SDS were gravimetrically prepared. THF solutions were place in a freezer around 269K and were allowed to freeze for 1 day. The THF hydrate and Ice mixture were melted in an ultrasonic cleaner at room temperature, which removed any excess bubbles from the solution. A one mL aliquot is sampled

from the melted solution and charged into a Folded Capillary Zeta Cell (DTS1060, Malvern Instruments). The cell is placed into a Zetasizer Nano ZS (Malvern Instruments), having set the temperature at 276.4K. THF hydrates were allowed to form to completion in the cell under the temperature setting in the Zetasizer, a process that took 0.5 to 1 hr. ζ-potential measurements then ensued.

2.2.3. Steady-State Fluorescence Measurements

THF solutions (10 wt%) were prepared gravimetrically, where 20g of the solution with different SDS concentrations were placed in a refrigerator at 269K until hydrate formation was observed and then the frozen solutions were maintained at 276.2K overnight. A fluorescent probe, pyrene, was transferred to the slurry with an approximate concentration of 10^{-6} M. Measurements were taken at 276 K. Samples were excited with a UV light source at 335 nm and a fluorescence emission spectra was taken from 350 -500 nm. Fluorescence measurements of the liquid THF solutions were also recorded but at room temperature.

2.2.4. Induction/Nucleation Time

Forty grams of THF solution (20 wt%) was charged to the reactor and was kept at 278.2K for 0.5 hr. Then the temperature is dropped to 268.2K to induce crystallization. We followed the temperature profiles and when the temperature would spike due to THF hydrate formation that would be the induction time, from the flat line of temperature setting to the temperature spike. After every run, to remove memory effect, the reactor is kept at room temperature for several hours, and rinsed with running tap water and a final rinse with DI water, then dried. The

experimental setup to study formation kinetics of THF hydrate with different concentrations of SDS is displayed in Figure 2.1. The vessel is made of stainless steel and holds a volume of 375mL. Reactor temperature is controlled by a recirculation cooler (Isotemp 3006P thermostat, Fisher Scientific) with a stability of ±0.01K. Two T-type thermocouples (Omega Engineering) monitored the inner core and wall temperatures. The variability of the thermocouples is ±0.2K. The temperature was recorded every 20 seconds with a Labview interface.

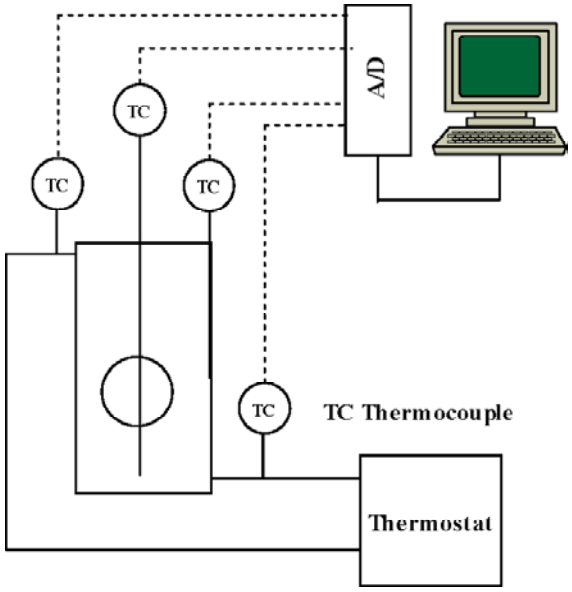

Figure 2.1. Experimental setup for Induction time measurements.

2.2.5. 10 wt% vs. 20 wt% THF hydrates

The reason for the different THF concentrations was that at 20 wt% THF, the phase diagram avoided ice formations in the induction times. 20 wt% THF was not used and 10 wt% THF was

used, is because the mass fraction for 20 wt% is more than 90% of hydrates, which would be above the solids fraction limit of the Zetasizer.

2.3. Results and Discussion

2.3.1. ζ-potential of THF hydrate at 276.4K

10 wt% THF hydrates have a melt temperature of 276.8K under atmospheric conditions[12]. Delahaye, et al.[12] recorded a melt temperature of 276.4K for 9.6 wt% THF. Then the mass solid fraction at 10 wt% THF is estimated at 4%, based on the phase diagram. This small mass fraction is to ensure the size of the hydrate particles is in the range of the detector of the Zetasizer (up to 10μm). The measured hydrate particle sizes fall between 3 to 10 μm.

Figure 2.2 shows a ζ-potential versus SDS concentration for 10wt% THF hydrate particles. The hydrate particle shows a negative charge even in the absence of SDS. This negative charge is due to an anion adsorption at the THF hydrate/Liquid layer. The samples are exposed to the atmosphere and carbon dioxide will come into the aqueous liquid. The anions that can exist in a THF + water system are hydroxide (OH^-), bicarbonate (HCO_3^-), and carbonate (CO_3^{2-}). The pH and partial pressure of CO_2 in the system are 5.8 and 3.5 $x10^{-5}$ MPa. The estimated concentration of bicarbonate is around 3μM according to the Henry's constant at 276.4K[16], which is 2 orders higher than OH^- and 5 orders higher than carbonate.

Drzymala, et al.[17] described that the Ice/water interface has no preferential adsorption of OH^- or H^+ over the other. Thus the surface charge is pH dependent. This analogy can be applied to hydrates because the hydrate surface is similar to ice[18]. Since the pH is 5.8, there should be more H^+ ions and thus hydrate particle should be positive. However, ζ-potential measurements show a negative value. Thus the only ion to subjugate the hydrate to be negative is the

bicarbonate (HCO_3^-). A possible mechanism for the bicarbonate adsorption is a hydrogen bond formation at the hydrate/liquid interface. Compoint, et al.[19] suggested that formic and acetic acids adsorb on ice surfaces via a hydrogen bond formation between the oxygen and hydrogen atoms of the carboxyl group (COOH). Bicarbonate is therefore a possible hydrogen bonding candidate based on the similar functional carboxyl group.

In Figure 2.2, the ζ-potential measurements reveal a flat line from 0 to 0.17mM SDS. In this region, it could be described as an ion exchange between bicarbonate and SDS. With further increases of SDS, ζ-potential decreases with a slope of -336mV mM^{-1} between 0.17 to 0.35mM SDS then -20mV mM^{-1} above 0.35mM SDS. The increase in magnitude qualitatively indicates an adsorption of DS^- monomers ions to the hydrate surface.

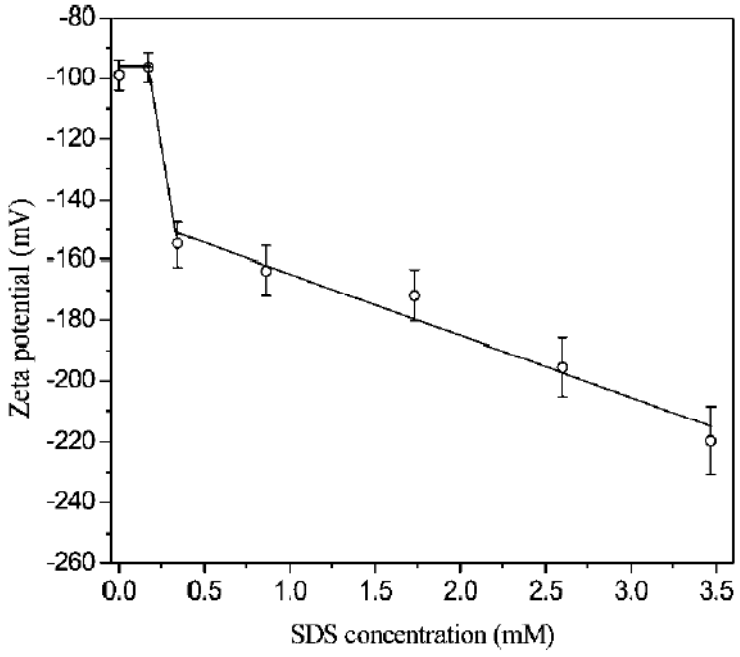

Figure 2.2. ζ-potential versus SDS concentration for 10wt% THF hydrate particles.

2.3.2. Fluorescence Measurements

The fluorescent probe, pyrene, has a low solubility in water and strongly partitions itself into hydrophobic domains. The fluorescent emission spectra of this probe exhibits fine finger like vibronic bands, which indicates the micropolarity of the system it resides in[20]. The use of Pyrene fluorescence to indicate the occurrence of hydrophobic domains in solutions and on solid surfaces is quite prevalent. Steady state fluorescence measurements using an excitation wave length of 335nm on THF hydrate slurries is shown in Figure 2.3. There the fine finger like vibronic bands indicate a hydrophilic microenvironment as determined from the ratio of the third vibronic band (I_3= 384nm) to the first vibronic band (I_1= 374nm) (Kalyanasundaram, et al. 1977). The indication of micropolarity varies from 0.5 to 0.8 for polar solvents and 1.65 to 1.75 for non-polar solvents[20]. The ratio I_3/I_1 (micropolarity parameter) in THF slurries is 0.54 which is equivalently like that of water (I_3/I_1 of water= 0.49). Room temperature 10 wt% THF solution is 0.71, resultantly higher than that of THF hydrates. Since the mass fraction of 10 wt% THF is 4% hydrates, which makes the liquid concentration of THF roughly the same as 10 wt%, what is observed from the fluorescence emission spectra of the pyrene is the hydrate/liquid interface and not the liquid environment.

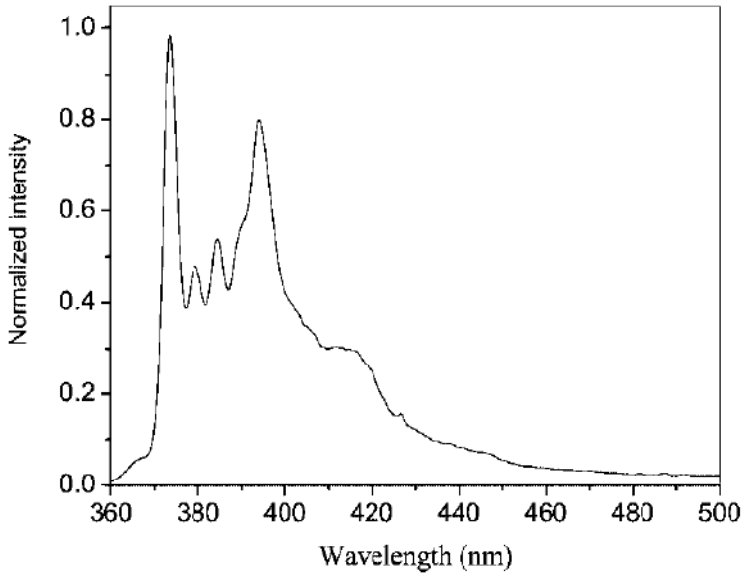

Figure 2.3. Steady state fluorescence measurement of THF hydrate using an excitation wave length of 335nm.

The ratio of I_3/I_1 in THF hydrate slurries with increasing SDS concentration is presented in Figure 2.4. The result is that THF hydrates without SDS has an I_3/I_1 of 0.54 and then with increased SDS beyond 0.17mM SDS the I_3/I_1 is 0.68. This micropolarity parameter value of THF hydrates with SDS (0.68) indicates a hydrophobic domain that forms at the hydrate/liquid interface at these SDS concentrations. Pyrene is able to preferentially partition itself into these hydrophobic domains, to where DS^- monomers are forming these microdomains. With increasing SDS concentration, pyrene is unable to detect any more hydrophobicity. The probe sits in microenvironments with the highest detectable hydrophobicity, however with increasing SDS there is no increase hydrophobicity within the range of 0.17mM to 3.47mM.

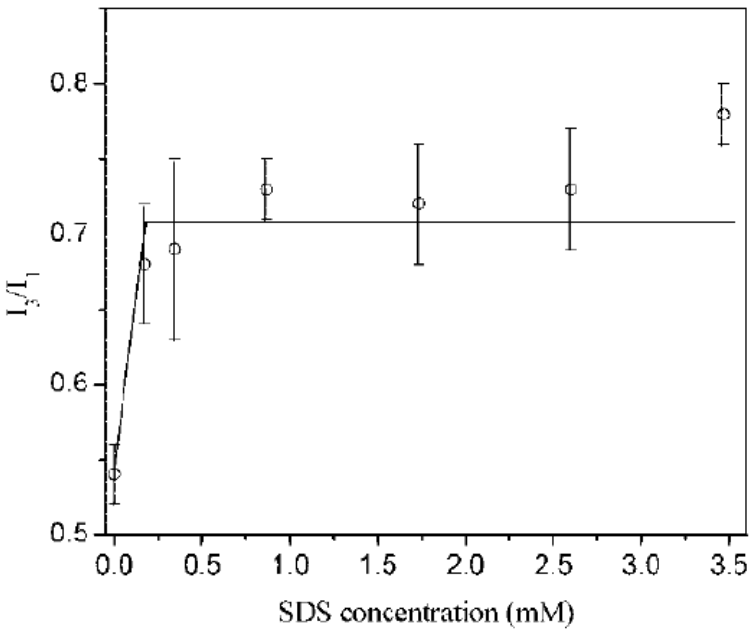

Figure 2.4.The ratio of I_3/I_1 in THF hydrate slurries versus SDS concentration.

2.3.3. Adsorption Mechanism

We have used qualitative methods of studying the adsorption of DS^- monomers onto THF hydrate surfaces. ζ-potential measurements infer a surface charge on the hydrate surface, and fluorescence measurements of pyrene indicate the microenvironment of the hydrate surface. The surface of THF hydrates is similar to that of water or ice, as interpreted by fluorescence measurements. Without any surfactant on hydrates, we inferred that the most prevalent ion, bicarbonate, attaches to the surface of hydrates via hydrogen bonding and is able to compete with DS^- monomers for adsorption sites. While adding surfactant from 0 to 0.17mM SDS the ζ-potential remains flat, but the micropolarity parameter increases. This we can suppose is an ion exchange at the THF hydrate interface, where CO_3^- exchanges with DS^- monomers. So beyond 0.17mM SDS, a consistent hydrophobic domain is formed. With increasing SDS concentration,

additional DS^- monomers would have to associate with the adsorbed DS^- monomers through lateral interactions of the hydrocarbon chains with head groups oriented towards the aqueous phase to offset the charge repulsion. This further increase in DS^- monomer adsorption would make the surface more negative, but the micropolarity remains the same. Figure 2.2 and 2.4 presents this finding of increasing SDS concentration leads to increased negative surface charge, and an unchanged hydrophobic domain.

From Figure 2.2 the region above 0.35mM SDS, the slope of change is less than that from 0.17 to 0.35mM. A possible explanation to the decreased slope is that the adsorption completes at 0.35mM and beyond it is a result of increased charge density in the bulk. This could be a result of increased ionic strength leading to a shrinking of the shear layer. The examination of I_3/I_1 ratio versus SDS concentration reveals that the micropolarity parameter remains unchanged after the formation of hydrophobic domains. This is in agreement to a report of DS^- adsorption on alumina particles where it is observed that the polarity of the microenvironment formed by the DS^- adsorption on the alumina surface is independent of SDS adsorption via hydrophobic interaction[22]. We depict this DS^- monomer adsorption on THF hydrates in Figure 2.5.

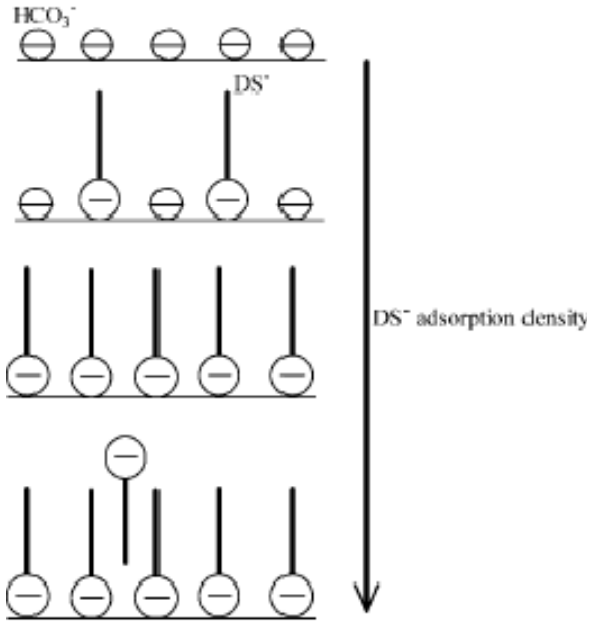

Figure 2.5. Schematic of DS^- monomer adsorption on THF hydrates.

2.3.4. Induction Time

Figure 2.6 present the data of induction time for the formation of THF hydrates versus SDS concentration. In the absence of SDS the induction time on average is 4.75 hr. A decrease in induction time is recorded when SDS concentrations were from 0.17 to 3.47mM SDS. Table 2.1 presents the experimental data for each run and the statistical analysis for each run. The SDS concentrations above 0.17mM were all statistically consistent to each other, revealing that hydrate growth began around the same time for all THF hydrates above 0.17mM SDS.

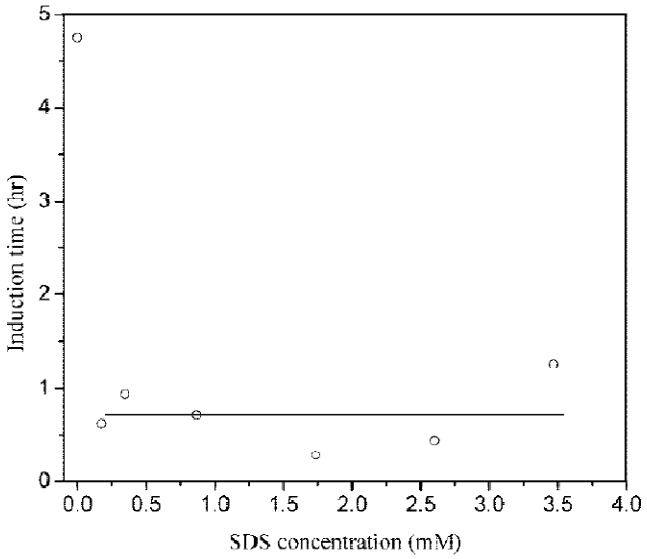

Figure 2.6. Induction time for the formation of THF hydrates versus SDS concentration.

Table 2.1. Experimental data for induction time and statistical analysis.

	induction time (h)							
C_{SDS} (mM)	1st	2nd	3rd	av	sd	se	upper[a]	lower[a]
0.00	8.04	2.28	3.92	4.75	2.42	1.62	7.91	1.58
0.17	0.00	0.00	1.86	0.62	0.88	0.58	1.77	0.00
0.35	1.54	0.51	0.78	0.94	0.44	0.29	1.51	0.37
0.87	0.18	0.00	1.96	0.71	0.88	0.59	1.87	0.00
1.73	0.31	0.18	0.36	0.28	0.08	0.05	0.38	0.18
2.60	0.00	0.00	1.33	0.44	0.63	0.42	1.26	0.00
3.47	1.91	0.30	1.58	1.26	0.69	0.46	2.17	0.36

[a] 95% confidence, av = average, sd = standard deviation, and se = standard error.

We define induction time as the time between the start of consistent temperature to a temperature spike from the exothermic heat of fusion. According to nucleation theory hydrate nuclei are present in the metastable/labile region before the temperature spike[1, 23]. Hydrate nuclei with a radius with less than 100nm is difficult to determine, however the amount should be small. As these nuclei grow and agglomerate, the exothermic heat of formation increases the

temperature and observations of this comes from a temperature spike recorded from the thermocouple. The concentration of SDS in the aqueous phase is nearly constant before the onset of crystallization, as the hydrate nuclei concentration is small. Also the adsorption of DS^- monomers onto the hydrate nuclei reaches equilibrium immediately due to the shear amount of SDS to nuclei, where SDS monomer is in excess to hydrate nuclei. With a concentration of 0.17mM SDS fully grown hydrates can form a monolayer of DS^- at the hydrate/liquid interface. This indicates that the reduced induction time is due to the adsorption of DS^- monomers which forms a monolayer on these nuclei.

A previous study of shortened induction time of methane hydrates in the presence of SDS can be attributed the adsorption of SDS on hydrate nuclei[10], consistent with the results presented in this study. Conjecture of the reasons as to why SDS is able to reduce the induction time is that the interfacial tension of hydrate/liquid decreases after DS^- adsorption. Kashchieva and Firoozabadib[26] reported that the induction time for gas hydrates decreases with decreasing hydrate/liquid interfacial energy. Presently there is no evidence of the effect of SDS on the interfacial tension at the hydrate/liquid interface. Another possible mechanism for the increased growth rate is that hydrate formers like that of methane and THF are likely to be solubilized in the hydrophobic domains formed by adsorbed DS^-. This is a locality mechanism, where solubilized hydrate formers are more accessible at the hydrate/liquid interface. Somasundaran and Moudgil[27] suggested that hydrocarbon gases such as methane would coadsorb with DS^- at the solid/liquid interface.

2.4. Summary

From this study, we were able to qualitatively measure the adsorption of SDS at the THF hydrate/liquid interface from ζ-potential and fluorescence measurements. In the absence of SDS, THF hydrate particles are hydrophilic and negative due to bicarbonate adsorption. From 0 to 0.17mM SDS, there is an ion exchange of DS^- monomers and bicarbonate anions as revealed from both the flat ζ-potential in this region and the increase of the micropolarity parameter. Under these conditions, hydrogen bonding is the main attractive energy that enables DS^- monomers to adsorb on hydrates. The completion of a monolayer of DS^- monomers is at a SDS concentration of 0.17mM SDS. We depict the orientation of the headgroups toward the hydrate interface in Figure 2.4, where the tails are oriented toward the aqueous phase. Increasing the SDS concentration, additional DS^- monomers are able to associate with each other due to the lateral hydrophobic interactions, orienting the headgroup outward to offset the electrical repulsion between DS^-. Micropolarity is unchanged during this further increase of SDS concentration.

In the presence of SDS induction time is decreased to a statistically consistent average time. This decrease in induction time is attributed to the DS^- adsorption on hydrate nuclei to form a monolayer on these surfaces. Two possible mechanisms of fast formation are presented: DS^- adsorption onto hydrate interfaces lowers the interfacial energy to promote growth and coadsorption of hydrate formers, in the presence of a monolayer, at the hydrate interface.

2.5. References

1. Sloan, E. D. Clathrate Hydrates of Natural Gas, 2nd ed.; Dekker: New York, 1998.
2. Sloan, E. D. Fundamental principles and applications of natural gas hydrates. Nature 2003, 426, 353–359.
3. Zhong, Y.; Rogers, R. E. Surfactant effects on gas hydrate formation. Chem. Eng. Sci. 2000, 55, 4175–4187.
4. Gayet, P.; Dicharry, C.; Marion, G.; Graciaa, A.; Lachaise, J.; Nesteroy, A. Experimental determination of methane hydrate dissociation curve up to 55 MPa by using a small amount of surfactants as hydrate promoter. Chem. Eng. Sci. 2005, 60, 5751–5758.
5. Watanabe, K.; Imai, S.; Mori, Y. H. Surfactant effects on hydrate formation in an unstirred gas/liquid system: An experimental study using HFC-32 and sodium dodecyl sulfate. Chem. Eng. Sci. 2005, 60, 4846–4857.
6. Zhang, J. S.; Lee, S. Y.; Lee, J. W. Kinetics of methane hydrate formation from SDS solution. Ind. Eng. Chem. Res. 2007, 46, 6353–6359.
7. Watanabe, K.; Niwa, S.; Mori, Y. H. Surface tensions of aqueous solutions of sodium alkyl sulfates in contact with methane under hydrate forming conditions. J. Chem. Eng. Data 2005, 50, 1672–1676.
8. Di Profio, P.; Arca, S.; Germani, R.; Savelli, G. Surface promoting effects on clathrate hydrate formation: Are micelles really involved. Chem. Eng. Sci. 2005, 60, 4141–4145.
9. Zhang, J. S.; Lee, S. Y.; Lee, J. W. Does SDS micellize under methane hydrate-forming conditions below the normal ambient Krafft point? J. Colloid Interface Sci. 2007, 315, 313–318.
10. Zhang, J. S.; Lee, S. Y.; Lee, J. W. Solubility of sodium dodecyl sulfate near propane and carbon dioxide hydrate-forming conditions. J. Chem. Eng. Data 2007, 52, 2480–2483.

11. Okutani, K.; Kuwabara, Y.; Mori, Y. H. Surfactant effects on hydrate formation in an unstirred gas/liquid system: An experimental study using methane and sodium alkyl sulfates. Chem. Eng. Sci. 2008, 63, 183–194.
12. Delahave, A.; Fournaison, L.; Marinhas, S.; Chatti, I.; Petitet, J. P.; Dalmzaaone, D.; Furst, W. Effect of THF on equilibrium pressure and dissociation enthalpy of CO2 hydrates applied to secondary refrigeration. Ind. Eng. Chem. Res. 2005, 45, 391–397.
13. Anderson, R.; Chapoy, A.; Tohidi, B. Phase relations and binary clathrate hydrate formation in the system H2-THF-H2O. Langmuir 2007, 23, 3440–3444.
14. Devarakonda, S.; Groysman, A.; Myerson, A. S. THF-water hydrate crystallization: an experimental investigation. J. Cryst. Growth 1999, 204, 525–538.
15. Prosser, A. J.; Franses, E. I. Adsorption and surface tension of ionic surfactants at the air-water interface: review and evaluation of equilibrium models. Colloid Surf. A. 2001, 178, 1–40.
16. Carroll, J. J.; Mather, A. E. The system carbon dioxide-water and the Krichevsky-Kasarnovsky equation. J. Solution Chem. 1992, 21, 607–621.
17. Drzymala, J.; Sadowski, Z.; Holysz, L; Chibowski, E. Ice/water interface: Zeta potential, point of zero charge, and hydrophobicity. J. Colloid Interface Sci. 1999, 220, 229–234.
18. Suga, H.; Matsuo, T.; Yamamuro, O. Thermodynamic study of ice and clathrate hydrates. Pure Appl. Chem. 1992, 64, 17–26.
19. Compoint, M.; Toubin, C.; Picaud, S.; Hoang, P. N. M.; Girardet, C. Geometry and dynamics of formic and acetic acids adsorbed on ice. Chem. Phys. Lett. 2002, 365, 1–7.
20. Birks, J. B. Photophysics of Aromatic Molecules; Wiley-Interscience:London, 1970; p 318.

21. Kalyanasundaram, K.; Thomas, J. K. Environmental effects on vibronic band intensities in pyrene monomer fluorescence and their application in studies of micellar systems. J. Am. Chem. Soc. 1977, 97, 2039–2044.
22. Chandar, P.; Somasundaran, P.; Turro, N. J. Fluorescence probe studies on the structure of the adsorbed layers of dodecyl sulfate at the alumina-water interface. J. Colloid Interface Sci. 1987, 117, 31–46.
23. Mullin, J. W., Crystallization, 4th ed., Butterworth-Heinemann: Oxford, U.K., 2001, Chapter 5.
24. Englezos, P.; Kalogerakis, N.; Dholabhai, P. D.; Bishnoi, P. R. Kinetics of formation of methane and ethane gas hydrates. Chem. Eng. Sci. 1987, 42, 2647–2658.
25. Thompson, H.; Soper, A. K.; Buchanan, P.; Aldiwan, N.; Creek, J. L.; Koh, C. A. Methane hydrate formation and decomposition: Structural studies via neutron diffraction and empirical potential structure refinement. J. Chem. Phys. 2006, 124, 164508.
26. Kashchieva, D.; Firoozabadib, A. Induction time in crystallization of gas hydrates. J. Cryst. Growth 2003, 250, 499–515.
27. Somasundaran, P; Moudgil, B. M. The effect of dissolved hydrocarbon gases in surfactant solutions on froth floatation of minerals. J. Colloid Interface Sci. 1974, 47, 290–299.

Chapter 3. Adsorption of Surfactants on Two Different Hydrates.

Published in Langmuir 2008, 24, 12723-12726.

Abstract: The interaction between surfactants and hydrates provides insight into the role of surfactants in promoting hydrate formation. This work aims at understanding the adsorption behavior of sodium dodecyl sulfate (SDS) on cyclopentane (CP) hydrates and its derivative surfactant on tetrabutylammonium bromide (TBAB) hydrates. Cyclopentane (CP) is a hydrophobic former whereas tetrabutylammonium bromide (TBAB) is a salt that forms semiclathrate hydrates. The adsorption on these two hydrates was studied by ζ-potential and pyrene fluorescence measurements. CP hydrates have a negative surface charge in the absence of SDS, and it decreases to a minimum as the SDS concentration increases from 0 to 0.17mM. Then, it increases with further increased SDS concentration. The adsorption density of DS^- on CP hydrates reaches a saturated value at 1.73mM SDS. The micropolarity parameter of the TBAB hydrate/water interface starts to increase rapidly at 0.17mM SDS and levels off at 1.73mM SDS. The presence of Br^- in TBAB hydrate suspensions could compete with TBADS (from association of DS^- and TBA^+) and DS^- for the adsorption on the hydrate surface, but they have a much stronger affinity for the hydrates than does Br^-. From the fluorescence measurements, it was found that the micropolarity of the hydrate/water interface is mainly dependent on the polarity of hydrate formers.

3.1. Adsorption Behavior Around Different Hydrates

It was found that THF hydrate particles become more negative at an SDS concentration above 0.17mM and the change in the micropolarity of the THF hydrate/water interface occurs at SDS

concentrations below 0.17mM. However, whether this adsorption behavior depends on the nature of hydrate formers and/or the presence of other species is still unknown. The main purpose of this work is to investigate the adsorption behavior of SDS and its derivative surfactant on cyclopentane (CP) hydrates and tetrabutyl ammonium bromide (TBAB) semiclathrate hydrates, respectively. CP is immiscible with water, and its polarity is much less than that of THF and water.[8] These two properties are also observed for the components of natural gas (methane, ethane, propane, etc). Therefore, the adsorption of SDS on CP hydrates could provide a better understanding of the interaction between surfactants and natural gas hydrates. CP forms sII hydrates with a melting point of around 280 K at atmospheric pressure,[9-11] making it a suitable system for studying surfactant adsorption under ambient conditions. TBAB forms semiclathrate hydrates in which bromide anions are bound to water through hydrogen bonds and tetrabutyl ammonium cations are encaged in anion-water cavities,[12-14] which are stable at temperatures of up to 285 K at atmospheric pressure. The surface properties of these clathrate hydrates could shed light on the relationship between the micropolarity of the hydrate surface and nature of hydrate formers. We will study the adsorption of surfactants on the CP and TBAB hydrates by using ζ- potential and pyrene fluorescence measurements to understand how the different hydrate formers can affect the adsorption behavior. ζ- potential measurements provide qualitative information on the adsorption density, whereas fluorescence spectroscopy is used to obtain the micropolarity of the hydrate surface. A plausible adsorption mechanism for DS^- on the CP hydrate will be discussed in detail on the basis of ζ- potential measurements.

3.2. Experimental Section

3.2.1. Materials

Cyclopentane, tetrabutylammonium bromide, and sodium dodecyl sulfate were purchased from Sigma-Aldrich with a purity of + 99%. Pyrene used in fluorescence measurements was supplied by Fluka with a purity of>99.0%. All chemicals were used as received without further purification. Deionized water with a resistivity of 17M Ω cm^{-1} was produced in our laboratory.

3.2.2. Sample Preparation

CP was added to water in a molar ratio of 1:17, and the sample was placed in a freezer overnight at a temperature of around 269 K. The sample was then transferred to a chiller and kept at 277 K for 1 week. A 20 g aliquot of SDS solutions in a 25-mL glass vial was kept in the chiller at 277 K overnight, and then 1 g of CP hydrates was added to the solutions. The slurries were kept at 277 K for at least 2 days before conducting ζ-potential and pyrene fluorescence measurements. TBAB was added to SDS solutions in a 25mL glass vial at a TBAB weight fraction of 15%. The samples were placed in a freezer at a temperature of around 269 K, and then they were transferred to a chiller once a small amount of hydrates was observed. The slurries were kept at 277 K for more than 2 days.

3.2.2. ζ-Potential and Particle Size

A 1mL sample of the hydrate slurries was quickly transferred to a folded capillary zeta cell (DTS1060, Malvern Instruments). The cell was then inserted into a Zetasizer Nano ZS (Malvern

Instruments) where the temperature was set to 277 K. The ζ- potential and particle sizes of hydrates were measured after the cell was maintained at 277 K for 10 min.

3.2.3. Pyrene Fluorescence

An appropriate amount of pyrene was added to 20 g of hydrate slurries, and then the samples were kept in a chiller at 277 K overnight. The pyrene concentration in the aqueous phase was approximately 1 μM. The samples were excited at 335 nm, and emissions were recorded between 360 and 500 nm at 277 K. Emissions were also collected between 360 and 500 nm at room temperature for 15 wt% TBAB solution with an SDS concentration between 0 and 3.47mM.

3.3. Results and Discussion

3.3.1. ζ- Potential at 277 K

The mass fraction of CP hydrates in slurries is about 5% if all added CP is converted to hydrates at 277 K. This low hydrate mass fraction was employed to ensure that hydrate slurries have a solid concentration below the upper limit of the measurement in the Zetasizer Nano ZS. The average diameter of CP hydrates is about 0.5 μm whereas that of TBAB hydrates is about 2.1 μm under the measurement conditions. These particle sizes are in the recommended range for measuring the zeta potential. Figure 3.1 shows that a negative charge exists at the shear plane of the CP hydrate/water interface. This negative charge comes from the adsorption of $HCO3^-$ in open systems as suggested by Zhang et al.[7] The change in the ζ-potential versus SDS concentration can be divided into four regions. In region I (0 to 0.17mM), the zeta potential

becomes less negative with increasing SDS concentrations whereas the zeta potential of THF hydrates was found to remain unchanged in the same SDS concentration range.[7] This indicates that the DS^- adsorption behavior is dependent on the nature of hydrate formers. In region II (0.17 to 0.34mM), the ζ- potential decreases rapidly with a slope of -377.7 mV mM^{-1}. In region III (0.34 to 1.73mM), the ζ- potential decreases much more slowly, and the slope is about -28.4 mV mM^{-1}. In region IV (1.73 to 3.47mM), the ζ- potential is a constant, indicating that no further adsorption of DS^- at the CP hydrate/water interface occurs. The ζ- potential of TBAB hydrates using a Zetasizer Nano ZS is inconclusive because of the relatively high concentration of Br^- in the aqueous phase. Lipkowski[13] reported that the equilibrium concentration of aqueous TBAB solution is 5 wt % in TBAB hydrate slurries at 277.15 K; therefore, the concentration of Br^- is about 0.16 M in the aqueous phase. Copper bromide forms and covers the electrode when applying an electrical field to the TBAB hydrate slurries, which interferes with the ζ- potential measurements.

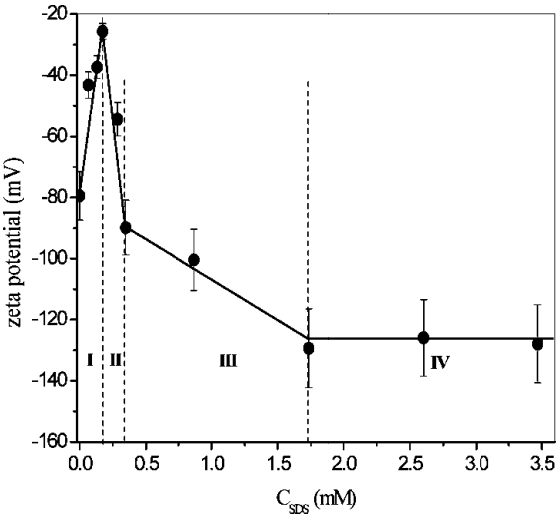

Figure 3.1. ζ-Potential of CP hydrates as a function of increasing SDS concentration.

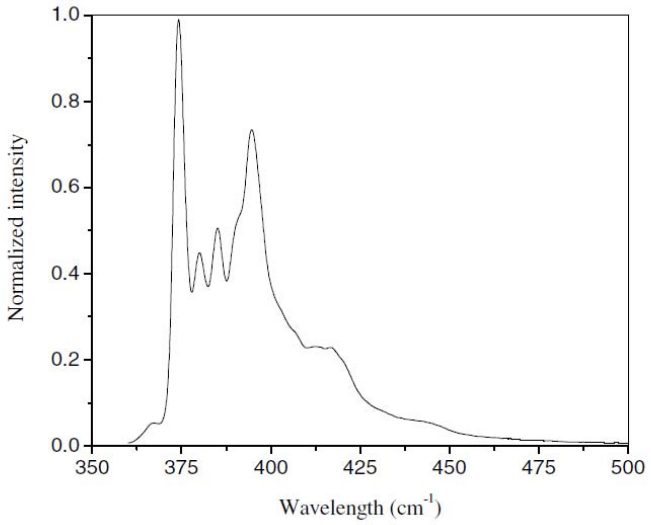

Figure 3.2. Steady-state fluorescence spectra of TBAB hydrate slurries using an excitation wavelength of λ_{ex}= 335 nm.

Fluorescence Spectra of Hydrates at 277 K. Steady-state fluorescence spectra of pyrene using an excitation wavelength of λ_{ex}= 335 nm in TBAB hydrate slurries are obtained (Figure 3.2). The intensity ratio of the third vibronic band (I_3, λ= 384 nm) to the first one (I_1, λ =374 nm) is a qualitative measure of the polarity of the microenvironment around the pyrene probe, which varies from 0.50 to 0.80 for simple polar solvents and from 1.65 to 1.75 for hydrocarbon solvents.8 The value of I_3/I_1 (also known as the micropolarity parameter) in TBAB hydrate slurries without SDS is 0.49, which is the same as water (0.49) under ambient conditions and close to that in THF hydrate slurries (0.54) in the absence of SDS.[7] The effect of SDS on the value of I_3/I_1 in TBAB hydrate slurries and TBAB solutions is given in Figure 3.3a. The micropolarity parameter of TBAB hydrate slurries remains unchanged at SDS concentrations below 0.17mM, and it increases to a steady value of 0.69 as the SDS concentration increases to 1.73mM. A similar trend is also observed for the micropolarity parameter of TBAB solutions; however, the

values of I_3/I_1 level off to 0.55 at an SDS concentration of 0.86mM. When SDS is added to TBAB solutions or TBAB hydrate slurries, DS^- reacts with TBA^+ to form TBADS, which is a colorless liquid surfactant with very high solubility in water.[15,16] The dissociation constant of TBADS is reported to be 6.25×10^{-4},[17] suggesting that almost all added DS^- is converted to TBADS. The concentration of TBADS in water is 3 orders of magnitude higher than that of the remaining DS^- but 3 orders of magnitude lower than that of Br^-. No increase in the value of I_3/I_1 in TBAB hydrate slurries at SDS concentrations of less than 0.17mM is possible because Br^- prevents TBADS and/or DS^- adsorption, and the increases in the micropolarity parameter originates from the TBADS and/ or DS^- adsorption on the hydrate surface. The increase in the value of I_3/I_1 in TBAB solutions with SDS comes from the formation of TBADS micelles (cmc = 1.0mM in pure water[15]), and a similar pattern has been reported for others surfactant systems.[8] The effect of SDS on the value of I_3/I_1 in CP hydrate slurries is presented in Figure 3.3b. The value of I_3/I_1 in the absence of SDS is about 0.75, which is higher than that in TBAB hydrate slurries without SDS (0.49 in Figure 3.3a). The change in the value of I_3/I_1 is within the experimental error in the SDS concentration range of 0 to 3.47mM, indicating that the probe (pyrene) has hydrophobic interaction with CP in water cavities even in the absence of SDS and the micropolarity of the CP hydrate/water interface is independent of DS^- adsorption, although the ζ- potential results suggest that adsorption density of DS^- on the CP hydrate surface increases as the SDS concentration increases from 0 to 1.73mM.

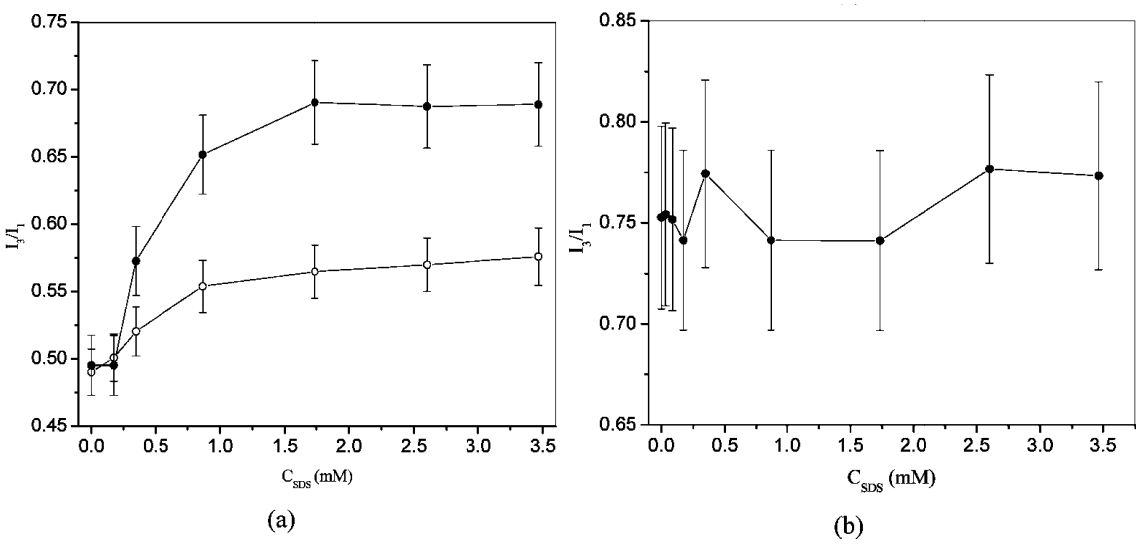

Figure 3.3. Variations of I3/I1 in two different hydrate slurries: (a) TBAB hydrate slurries (b) at 277 K and 15 wt % TBAB solutions and (O) at room temperature as a function of SDS concentration. (b) CP hydrate slurries at 277 K.

3.3.2. Adsorption Mechanism

The results of ζ- potential and fluorescence measurements provide insight into the mechanism of DS^- adsorption at the hydrate/water interface. The density of negative charge at the CP hydrate/water interface decreases as the SDS concentration increases up to 0.17mM (Figure 3.1). Our previous study suggested that the negative charge of THF hydrate particles in the absence of SDS arises from the adsorption of $HCO3^-$ and its competition with DS^- for the adsorption sites.[7] The surface structure of clathrate hydrates is given in a previous review article.[18] The decrease in the negative charge is due to the fact that one DS^- occupies more adsorption sites than does one $HCO3^-$. This adsorption mechanism is different from that on THF hydrates because the negative charge on the THF hydrate surface is constant in the SDS concentration range of 0-0.17mM, indicating that the number of DS^- adsorption sites is the same

as that of $HCO3^-$ adsorption sites.[7] A plausible explanation for this difference is that the tail of DS^- lies down on CP hydrates as shown in Figure 3.4 but stands up on THF hydrates. The CP hydrate/water interface is more hydrophobic than water; therefore, the tail of DS^- lies down on CP hydrates to favor the hydrophobic interaction. However, the tail of DS^- stands up on THF hydrates because the bulk THF solution is more hydrophobic than the THF hydrate/water interface.[7] The density of $HCO3^-$ on CP hydrates is negligible at an SDS concentration of 0.17mM because the negative charge reaches a minimum under this condition (Figure 3.1). The ζ-potential of CP hydrate particles decreases at an SDS concentration above 0.17mM, and the particle charge at an SDS concentration of 0.34mM is close to that without SDS (Figure 3.1). The shift to more negative charge originates from an increase in the adsorption density of DS^- on CP hydrates. The main force for DS^- adsorption on hydrates is hydrogen bonding, although the van der Waals force cannot be ignored.[7,18] The hydrogen bonding between the headgroups of DS^- and the hydrate surface is stronger than the hydrophobic force between the tails of DS and the hydrate surface. As more DS^- adsorbs on the hydrate surface, the configuration of adsorbed DS^- changes from lying down to standing up, with headgroups attaching to the surface and tails orienting toward water as shown in Figure 3.4. A further decrease in the zeta potential as the SDS concentration increases from 0.34 to 1.7mM is possibly due to the fact that DS^- associates with adsorbed DS^- via hydrophobic interaction with headgroups orienting toward water to offset the electrical repulsion between adsorbed DS^- ions.

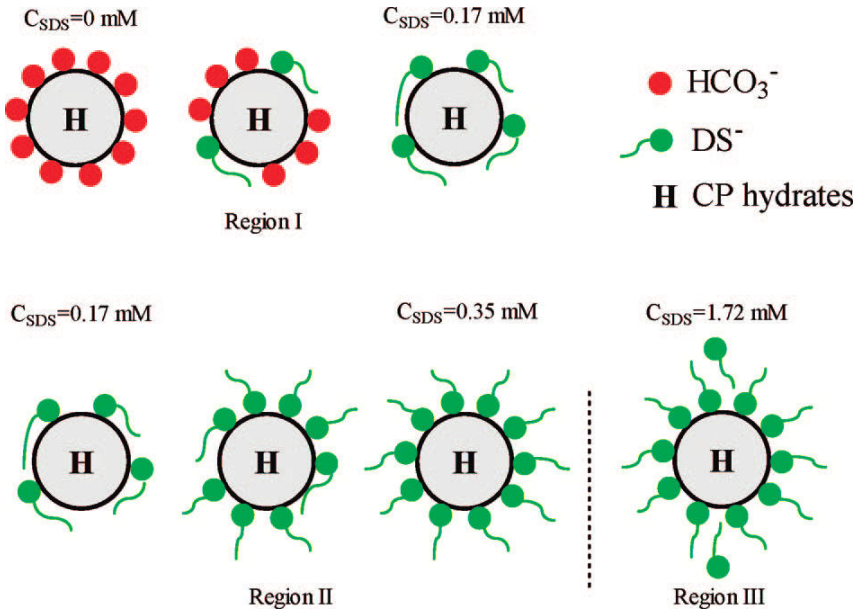

Figure 3.4. Schematic representation of SDS adsorption at the CP hydrate/water interface.

3.4. Adsorption Behavior and the Dependency of the Nature of the Hydrate

The adsorption behavior of SDS and its derivative on clathrate hydrates is dependent on the nature of hydrate formers and the presence of other anions. The headgroup of DS^- binds to the surface of clathrate hydrates in which the polarity of the hydrate surface is close to that of water. However, both the headgroup and tail of DS^- attach to clathrate hydrates at low adsorption densities if the polarity of the hydrate former is much lower than that of water. The headgroups predominantly interact with the hydrate surface via hydrogen bonding whereas the tails interact via a hydrophobic force. The hydrophobic interaction is negligible at high adsorption densities. The micropolarity of the hydrate surface is mainly determined by the nature of hydrate formers. The higher the polarity of hydrate formers, the higher the micropolarity of the hydrate surface. However, the adsorption of surfactants on hydrates increases the value of the micropolarity parameter of the hydrate surface.

3.5. References

1. Sloan, E. D.; Koh, C. Clathrate Hydrates of Natural Gas, 3rd ed.; CRC: Boca Raton, FL, 2008.
2. Gayet, P.; Dicharry, C.; Marion, G.; Graciaa, A.; Lachaise, J.; Nesterov, A. Experimental determination of methane hydrate dissociation curve up to 55 MPa by using a small amount of surfactant as hydrate promoter. Chem. Eng. Sci. 2005, 60, 5751–5758.
3. Watanabe, K.; Imai, S.; Mori, Y. H. Surfactant effects on hydrate formation in an unstirred gas/liquid system: An experimental study using HFC-32 and sodium dodecyl sulfate. Chem. Eng. Sci. 2005, 60, 4846–4857.
4. Zhang, J. S.; Lee, S. Y.; Lee, J. W. Kinetics of Methane Hydrate Formation from SDS Solution. Ind. Eng. Chem. Res. 2007, 46, 6353– 6359.
5. Zhong, Y.; Roger, R. E. Surfactant effects on gas hydrate formation. Chem. Eng. Sci. 2000, 55, 4175–4187.
6. Zhang, J. S.; Lee, S. Y.; Lee, J. W. Does SDS micellize under methane hydrate-forming conditions below the normal Krafft point? J. Colloid Interface Sci. 2007, 315, 313–318.
7. Zhang, J. S.; Lo, C.; Somasundaran, P.; Lu, S.; Couzis, A.; Lee, J. W. Adsorption of Cationic and Anionic Surfactants on Cyclopentane Hydrates. J. Phys. Chem. C 2008, 112, 12381–12385.
8. Kalyanasundaram, K.; Thomas, J. K. Environmental effects on vibronic band intensities in pyrene monomer fluorescence and their application in studies of micellar systems. J. Am. Chem. Soc. 1977, 97, 2039– 2044.
9. Werezak, G. N. Aqueous solution concentration by a clathrate type of gas hydrate formation. Chem. Eng. Prog. Symp. Ser. 1969, 65, 6–18.

10. Zhang, Y.; Debenedetti, P. G.; Prud'homme, R. K.; Pethica, B. A. Differential Scanning Calorimetry Studies of Clathrate Hydrate Formation. J. Phys. Chem. B 2004, 108, 16717–16722.
11. Zhang, J. S.; Lee, J. W. Equilibrium of Hydrogen + Cyclopentane and Carbon Dioxide + Cyclopentane Binary Hydrates. J. Chem. Eng. Data 2009, 54, 659-661.
12. Jeffrey, G. A.; McMullan, R. W. The Clathrate Hydrates. Progress in Inorganic Chemistry; John Wiley: New York, 1967; 8, 43-108.
13. Lipkowski, J. The Structure of Tetrabutylammonium Bromide Hydrate $(C_4H_9)_4NBr \cdot 2^1/_3H_2O$. J. Supramol. Chem. 2002, 2, 435–439.
14. Chapoy, A.; Anderson, R.; Tohidi, B. Low Pressure Molecular Hydrogen Storage in Semi-Clathrate Hydrates of Quaternary Ammonium Compounds. J. Am. Chem. Soc. 2007, 129, 746–747.
15. Bales, B. L.; Zana, R. Cloud Point of Aqueous Solutions of Tetrabutylammonium Dodecyl Sulfate Is a Function of the Concentration of Counterions in the Aqueous Phase. Langmuir 2004, 20, 1579–1581.
16. Zana, R.; Benrraou, M.; Bales, B. L. Effect of the Nature of the Counterion on the Properties of Anionic Surfactants. 3. Self-Association Behavior of Tetrabutylammonium Dodecyl Sulfate and Tetradecyl Sulfate: Clouding and Micellar Growth. J. Phys. Chem. 2004, 108, 18195– 18203.
17. Pradines, V.; Lavabre, D.; Micheau, J.C.; Pimienta, V. Determining the Association Constant and Adsorption Properties of Ion Pairs in Water by Fitting Surface Tension Data. Langmuir 2005, 21, 11167–11172.
18. Koh, C. A. Towards a fundamental understanding of natural gas hydrates. Chem. Soc. Rev. 2002, 31, 157–167.

Chapter 4. Adsorption of Cationic and Anionic Surfactants on Cyclopentane Hydrates.

Published in Journal of Physical Chemistry C. 2010, 114, 13385-13389.

Abstract: This work presents the adsorption of an anionic surfactant, sodium dodecyl sulfate (SDS), and a cationic one, dodecyl-trimethylammonium bromide (DTAB), on cyclopentane (CP) hydrates. Adsorption isotherms were obtained by liquid−liquid titrations. Also, the adsorption was qualitatively studied by zeta potential measurements. The isotherm of both SDS and DTAB exhibits a two-plateau (L-S) type. The saturated adsorption amount in the first step (Langmuir type) is 0.01 and 0.03mmol g^{-1} for SDS and DTAB, respectively. The Langmuir equilibrium constant is 1.17mM^{-1} for SDS and 0.32mM^{-1} for DTAB. The maximum adsorption amount of SDS in the second step (S type) is 2.5 times higher than that in the Langmuir step. The similar trend is observed for DTAB. SDS adsorption shifts the zeta potential from −60 to −90 mV in the first step, followed by a further 30 mV decrease as the adsorption approaches the second plateau. For DTAB, the zeta potential increases from −60 to 50 mV in the Langmuir step and then it approaches 90 mV in the second step. On the basis of these results, the role of surfactants in enclathration is discussed and the adsorption mechanism of surfactant on clathrate hydrates is also presented.

4.1. Quantifying Adsorption of Surfactants on Cyclopentane Hydrates

Clathrate hydrates, a nonstoichiometric crystalline compound, have attracted a lot of attention because they are not only a potential cause of pipeline blockage in oil and gas industries but also a promising storage medium for natural gas[1]. To meet challenges in the application of hydrate

storage, surfactants are desired to accelerate the hydrate formation over other methods including mechanical stirring, dry water, and semiclathrates due to their low cost and the low-dosage[2-5]. Over the past decade, much effort has been paid to understanding the promoting mechanism of surfactants in enclathration; however, the mechanism remains poorly understood. The first explanation is that surfactants form micelles and then they initiate the nucleation of clathrate hydrates[2]. However, several recent studies suggest no micelles are present in the aqueous phase that contacts with hydrate formers at a high pressure and low temperature if the temperature is below the Kraft point for surfactants[6-8]. Moreover, a recent study found that sodium dodecyl sulfate (SDS), one of the most effective promoters for the enclathration of natural gas, has no significant effect on the heterogeneous nucleation of clathrate hydrates[9]. Therefore, it is most likely that SDS accelerates the hydrate growth by DS^- adsorption on clathrate hydrates.

Lo et al.[10] qualitatively investigated the adsorption of DS^- on cyclopentane (CP) hydrates, and it was proposed that the configuration of adsorbed DS^- on CP hydrates changes from "lie-down" to "stand-up" mode as the SDS concentration increases. In the configuration of stand-up, the headgroups attach to the open cavities via hydrogen bonding, whereas the tails orient toward the liquid phase. Thus, hydrophobic microdomains[10-12] occur on the hydrate surface at higher SDS concentrations. Hydrate formers such as methane could solubilize into these domains, increasing their concentration at the hydrate−water interface and then enhancing the growth rate.

Quantifying the adsorption of surfactants on hydrates will provide a better understanding of influences of different surfactants on the enclathration. At this point, the quantitative information of surfactant adsorption on the hydrate surfaces is still not available. This work is

the first attempt to determine adsorption isotherms of two surfactants, SDS, an anionic surfactant, and dodecyl trimethylammonium bromide (DTAB), a cationic surfactant, on cyclopentane (CP) hydrates. The main reason to choose CP hydrates is that they are stable at temperatures below 280 K under ambient pressure[13], compared with natural gas hydrates that exist at high pressures and low temperatures, making them unsuitable for investigating surfactant adsorption with currently available analytic techniques. Additionally, the crystal structure of CP hydrate is the same as that of natural gas hydrates.

This work presents the determination of the isotherm of both SDS and DTAB on CP hydrates using single and double liquid titrations. Also, it will show that the affinity of surfactants to hydrates is proportional to the number of hydrogen bonding formed between headgroups and the hydrate surface. An adsorption mechanism will be proposed based on these results. The effectiveness of the surfactants enhancing the enclathration will also be discussed in terms of the adsorption isotherms and zeta potential measurements.

4.2. Materials and Methods

4.2.1. Materials

Cyclopentane (CP), dodecyl trimethylammonium bromide (DTAB), and sodium dodecyl sulfate (SDS) were purchased from Sigma-Aldrich with a purity of 99%. Methylene Blue and Methyl Orange were obtained from Sigma-Aldrich with indicator purity. Sulfuric acid 96% and sodium sulfate 99% were supplied by Sigma-Aldrich. All chemicals were used as received without further purification. Deionized (D.I.) water was produced in our lab with a resistivity of 18 MΩ cm^{-1}.

4.2.2. Preparations of CP Hydrate Slurries

A 10 wt % CP−water mixture was charged to a 1 L glass bottle and hermetically sealed, and then it was placed in a freezer at a temperature of 263 K. After ice formation, the bottle was vigorously shaken at ambient conditions. When ice melts, CP is enclathrated at the same time. The formation of CP hydrates was confirmed by the appearance of white particles. The bottle was put in a chiller at 277 K for one week and shaken from time to time to accelerate the enclathration. The concentration of CP hydrates in slurries was found to be 51 wt % by calorimetric measurements. The reason why we started with CP hydrate slurries instead of solid CP hydrates in adsorption measurements is to avoid the variation of total hydrate surface area when adding pure hydrates in surfactant solutions. Preparing CP hydrates from surfactant solutions first could result in different particle sizes due to the effect of surfactants on the enclathration.

4.2.3. Adsorption Isotherms

Ten grams of surfactant solutions were charged to a 25mL vial followed by putting the vial in a chiller at 277 K overnight. Ten grams of CP hydrate slurries were quickly added to the solutions (both the slurries and solutions were put in an ice bath). Then, the vial was sealed and kept in a chiller at 277 K for more than one week to allow the adsorption to reach equilibrium. From time to time the vial was shaken to accelerate surfactant adsorption on hydrates. Because of the density difference between hydrates and solutions, all of CP hydrates were located at the upper portion of vials. Finally, several milliliters of solution were withdrawn from the lower portion of the vial by using a 6mL plastic syringe. The sampling usually lasted less than one minute. The concentration of SDS in solutions was analyzed by Methylene Blue titration as described by

Epton[14]. The DTAB concentration was determined by Methyl Orange and Methylene Blue liquid−liquid titration. The details of this titration are described below. The adsorption amount is the depletion of surfactants in the aqueous phase.

4.2.4. ζ- Potential

The procedure of sample preparation for zeta potential measurements is the same as described in our previous work[10]. One milliliter of hydrate slurry was quickly transferred to a Folded Capillary zeta cell (DTS1060, Malvern Instruments). The cell was then inserted into a Zetasizer Nano ZS (Malvern Instruments) where the temperature was set to 277 K. The ζ- potential was measured after the cell was maintained at 277 K for 10 min. The average diameter of CP particles is around 0.5 μm.

4.2.5. Liquid–Liquid Titration

One milliliter of an unknown DTAB concentration was pipetted into a 20mL test tube, and then 1.25mL of solutions containing 0.003 wt % Methylene Blue, 1.20 wt % sulfuric acid, and 5.00 wt % sodium sulfate was added, followed by charging another 1.9 mL of solutions containing 0.003 wt % Methyl Orange, 1.20 wt % sulfuric acid, and 5.00 wt % sodium sulfate. Finally, 1.70mL of chloroform was added to the test tube. The tube was vigorously shaken for several seconds to achieve a well mixed system. At the start of the titration, the top layer was dark blue and the lower organic layer was yellow as shown in Figure 4.1. A relatively diluted SDS solution was used to titrate the DTAB solution to ensure a more precise titration. The end-point is identified when the top layer becomes pink and the lower layer turns to blue. Figure 4.1 shows three images

from the starting point to end point during the titration. Both Methylene Blue and Methyl Orange are firstly employed to determine DTAB concentrations, although previous works have studied titration methods of using other indicators to determine surfactant concentrations as well[15-17]. The accuracy of concentration measurements using this method is estimated to be within 2%.

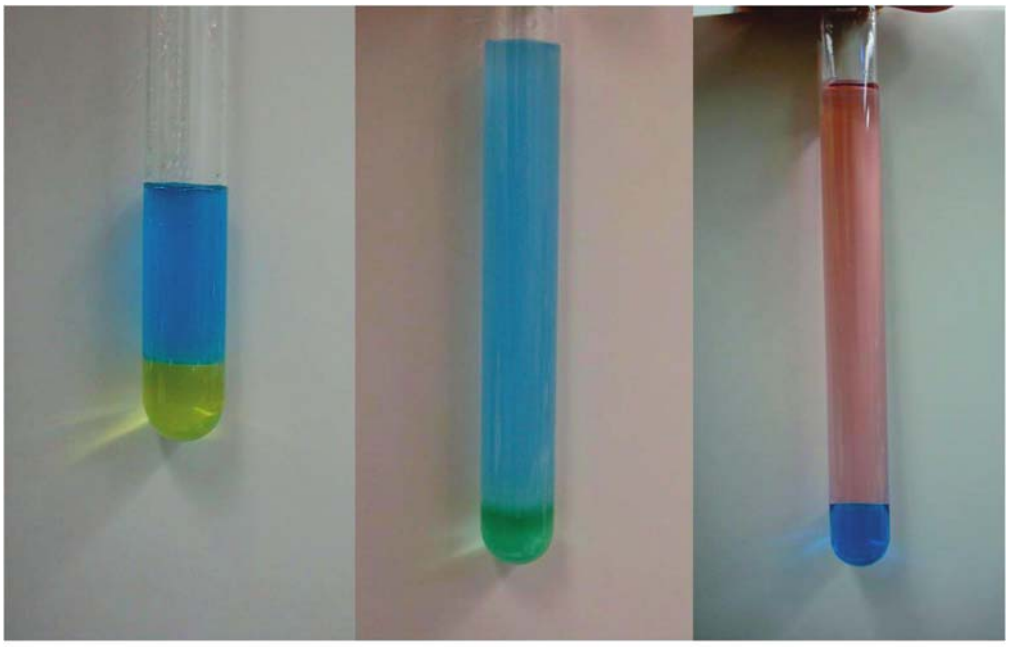

Figure 4.1. Liquid−liquid titration for determining DTAB concentrations.

4.3. Results and Discussion

4.3.1. SDS Adsorption

The adsorption isotherm of SDS on CP hydrates is shown in Figure 4.2, which belongs to a two-plateau type (L-S) as described by Zhu and Gu.[18] In the first step (0.15 to 1.6mM), the data is well fitted to the Langmuir isotherm (insert in Figure 4.1). The Langmuir equilibrium constant is

estimated to be 1.17mM^{-1}. In the second step (1.6 to 3.9mM), the maximum adsorption amount is 0.025mmol g^{-1} that is 2.5 times as high as that in the Langmuir step. It should be noted here that the adsorption amount at SDS concentrations less than 0.15mM cannot be determined, because it is impossible to identify the end-point in our titration. SDS adsorption under the above condition can be inferred from the zeta potential measurements.

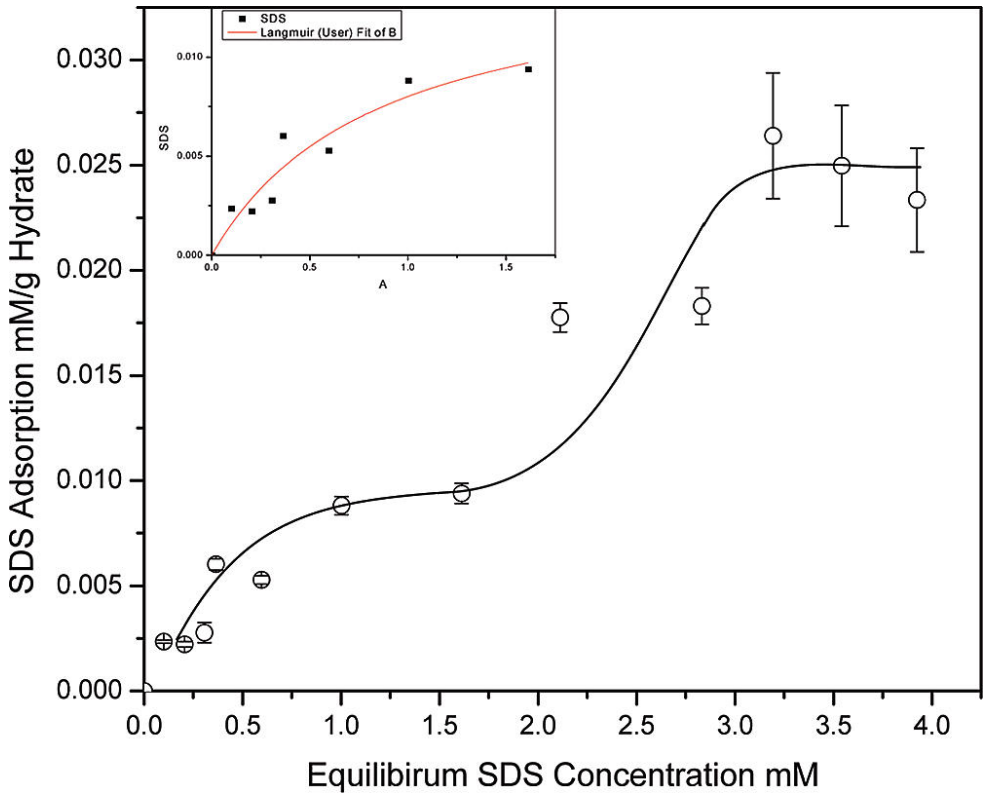

Figure 4.2. Adsorption isotherm of SDS on CP hydrates at 277 K.

Figure 4.3 presents the variation of particle charge on CP hydrates with increasing SDS concentrations. The zeta potential decreases from −35 to −90 mV as the SDS concentration increases from 0.33 to 1.7mM; followed by a steady level at −90 mV at SDS concentrations up to 2.4mM. With a further increase in the SDS concentration, the zeta potential reduces again and

reaches another plateau (−125 mV) at 3.4mM SDS. As Figure 4.3 shows, the concentration-dependent particle charge is consistent with the L-S type adsorption isotherm. Another notable observation is that the zeta potential reaches a maximum at a SDS concentration of 0.34mM, which is interpreted as adsorbed DS^- on the hydrate surface changing from lay-down to stand-up mode. Both headgroups and tails attach to the hydrate surface at SDS concentrations below 0.34mM, and tails start to orient toward the aqueous phase when the SDS concentration exceeds the above value[10].

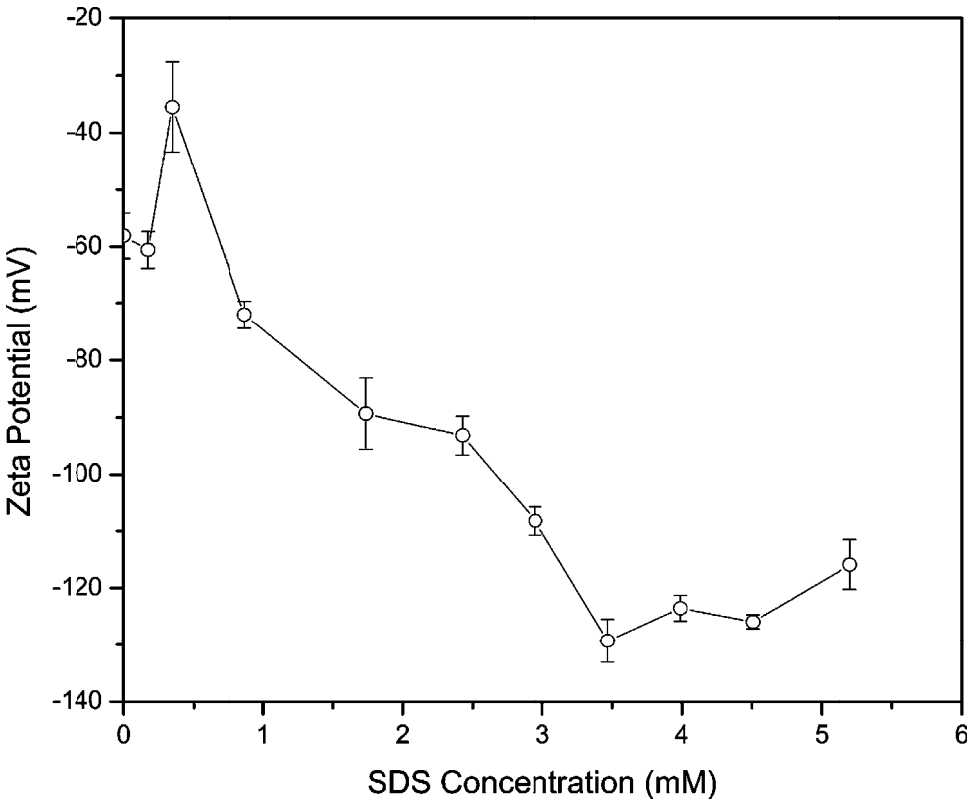

Figure 4.3. Zeta potential of CP hydrates with SDS.

4.3.2. DTAB Adsorption

Figure 4.4 shows the adsorption isotherm of DTAB, which also exhibits an L-S type adsorption. The Langmuir equilibrium constant is estimated to be 0.32mM^{-1}, which is lower than that of SDS. The saturated adsorption amount in the Langmuir step is 0.03mmol g^{-1}, which is three times higher than that for SDS. Also, it is observed that maximum adsorption amount in the second step (4 to 8mM) is 0.065mmol g^{-1}. Thus, the adsorption amount doubles in this step.

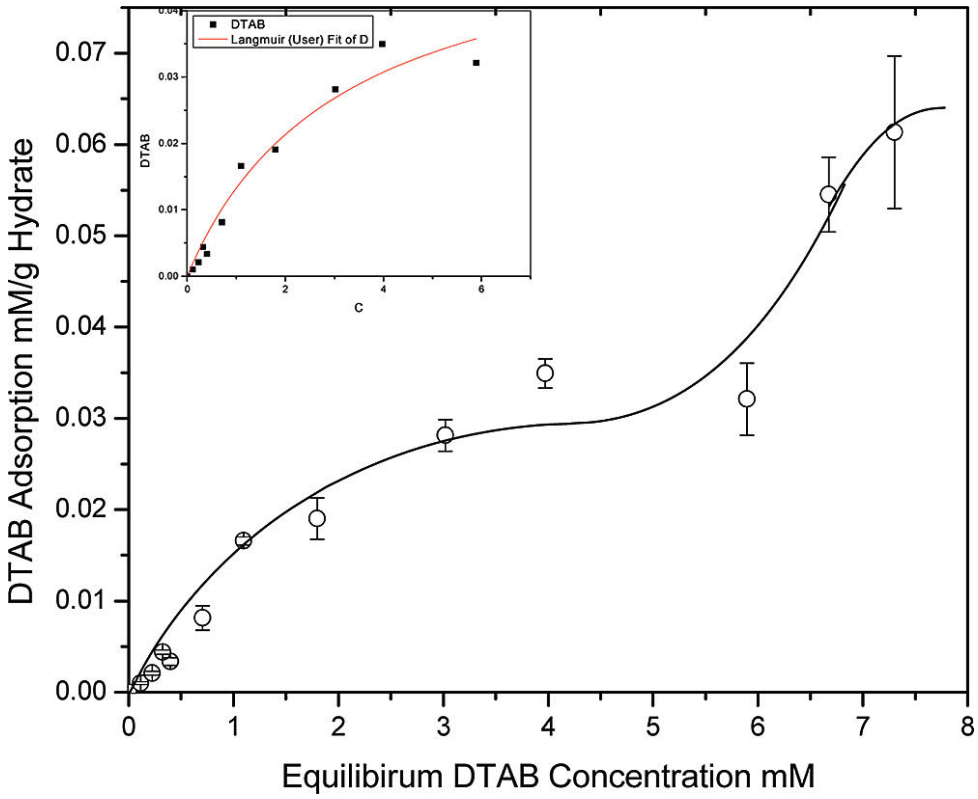

Figure 4.4. Adsorption isotherm of DTAB on CP hydrates at 277 K.

ζ- potential measurements provide supporting information on the adsorption of DTAB on CP hydrates. Hydrate particle charges are negative without any surfactants because of the presence of other anions like bicarbonate that comes from the dissolution of carbon dioxide in water[10].

Figure 4.5 shows increasing DTAB adsorption, shifting the particle charge from negative to positive. The ζ- potential first changes from −60 to 15 mV as the DTAB concentration increases from 0 to 0.17mM, followed by another 50 mV increase at DTAB concentrations up to 1mM, beyond which the ζ- potential keeps at 55 mV until the DTAB concentration increases to 3.8 mM. Finally, the ζ- potential reaches the second plateau (90 mV) at 4.8mM DTAB in the second step.

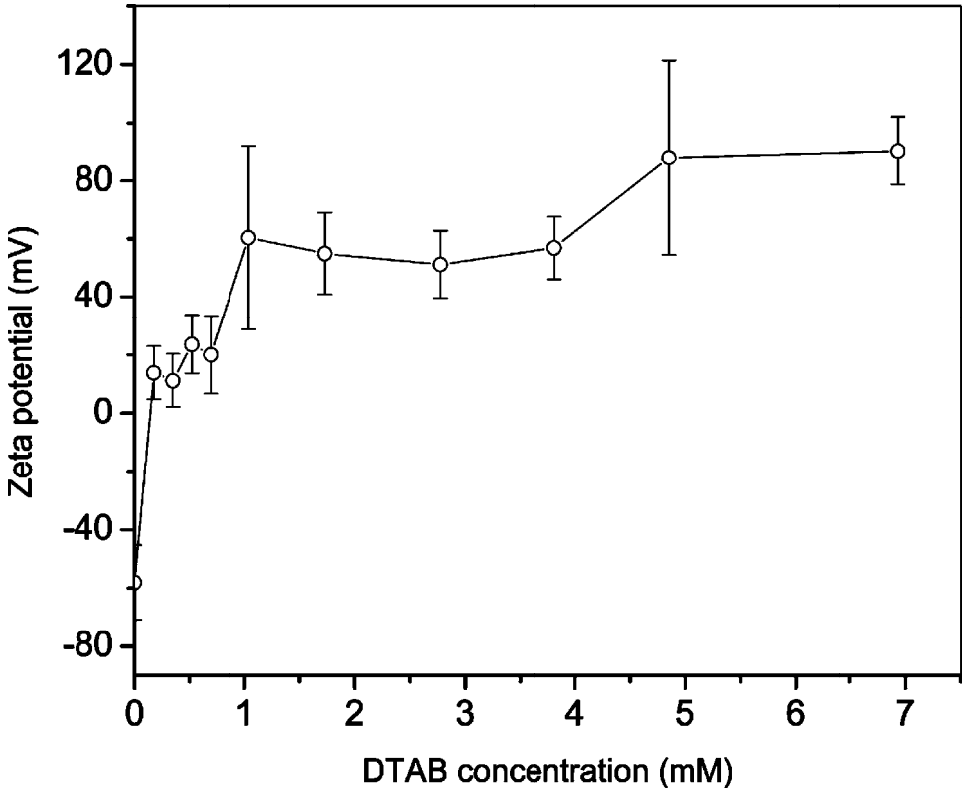

Figure 4.5. ζ- potential of CP hydrates with DTAB.

It is also noted that the dramatic increase in zeta potential at DTAB concentrations of 0 to 0.17mM is not related to a significant change in the adsorption amount as shown in Figure 4.4, suggesting that the small amount of DTA^+ would be enough to replace the adsorption sites that

are occupied by bicarbonates. As mentioned in the previous section, the configuration of adsorbed DS^- changes as the more DS^- adsorbs on the hydrate surface at low SDS concentrations. We believe that the same is also true for adsorbed DTA^+ on hydrates as the DTAB concentration increases from 0 to 1mM, because tails of these two surfactants are almost identical.

4.3.3.Adsorption Mechanism

The results presented above can be used to elucidate the adsorption mechanism of surfactants on hydrates. At relatively low concentrations, surfactant chains lay down on the surface, with both headgroups and tails attaching to the surface. This configuration results in a decrease in the net surface charge for anionic surfactant adsorption, because one anionic surfactant chain occupies more adsorption sites than other anions that contribute to the negative surface charge of hydrates in the absence of any surfactants[10, 11]. As the surfactant concentration in the aqueous increases, tails of surfactant chains start to align parallel to each others. The main driving force for this configuration transformation is the hydrophobic force.

The change in the configuration of adsorbed surfactant chains, as shown in Figure 4.6, comes from the hydrophobic interaction between surfactant chains. In the lie-down configuration, both the head groups and alkyl chain tails favor the hydrate surface because the hydrate surface allows for hydrogen bonding and is also slightly hydrophobic[10]. As the surfactant concentration in the bulk aqueous solutions increases, more surfactant chains adsorb on the surface, whose head-groups prefer to interact with the surface. This factor, combined with the hydrophobic force between surfactant chains, causes the configuration change as the surfactant concentration increases.

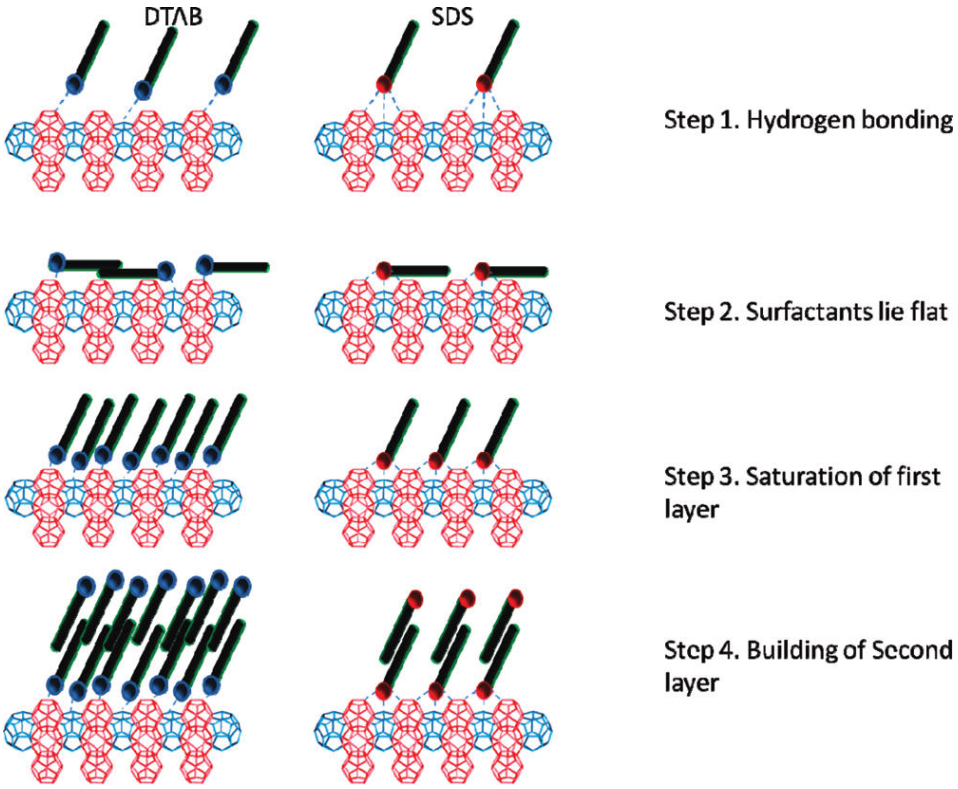

Figure 4.6. Schematic of surfactant adsorption on clathrate hydrates.

With a further increase in the surfactant concentration, a monolayer in which headgroups attach to the surface with tail orienting toward the aqueous phase forms. This explains the existence of the first plateau on adsorption isotherms of SDS and DTAB. Surfactant chains in this layer act as the adsorption sites for further surfactant adsorption, which proceeds via forming another layer in which tails interact with those in the first layer with headgroups orienting toward the aqueous phase. Finally, a surfactant bilayer occurs once the space between surfactant chains of the first layer cannot accommodate more tails, resulting in a second plateau on the adsorption isotherm. A schematic description of this mechanism is presented in Figure 4.6.

It should be emphasized here that the affinity of surfactant chains to the hydrate surface is mainly dependent on the number of hydrogen bonds formed between the headgroup and pendant hydrogens of open cavities of hydrates. The pendant hydrogens on the hydrate surface are believed to be adsorption sites. The headgroup of DS^- can form at least 3 hydrogen bonds; whereas the headgroup on DTA^+ can only form 1[19]. This explanation is consistent with the observation that the Langmuir equilibrium constant in the first step is higher for SDS ($1.17mM^{-1}$) than for DTAB ($0.32mM^{-1}$). Also, the low saturated adsorption amount for SDS ($0.01mmol\ g^{-1}$) in the Langmuir step compared with DTAB ($0.03mmol\ g^{-1}$) supports the above argument. The second step resembles a lipid-bilayer composition. DTA^+ has a one-to-one composition to the first and the second layers as in a bilayer[20]. However DS^- monomers must assemble itself to a denser composition (1.5 times) to the first layer, because the void spaces left by the first layer must be fulfilled in the second layer by an increase in surfactant amount. The first layer is anchored by hydrogen bonding forces; the second layer must fulfill the void spaces by hydrophobic force which is a denser second layer depicted in Figure 4.6.

4.3.4. Role of Surfactants

The above results of isotherms and zeta potentials can offer clear understanding of the role of surfactants in promoting the enclathration. Zhong and Rogers[2] found that the effectiveness of SDS promoting ethane enclathration is observed at a SDS concentration around 1.0mM (Figure 4.2), which corresponds to the single layer configuration (step 3 in Figure 4.6) where tails of surfactants orient toward the aqueous phase while headgroups attach to the hydrate surface. As tails orient parallel to each other, hydrophobic microdomains form at the hydrate−water interface, into which hydrate formers like methane molecules could solubilize. On the other

hand, adsorption of DS^- makes the hydrate surface more negative at higher SDS concentrations, which could change the water structure at the interface. The water structure at the solid−water interface is strongly dependent on the surface charge[21]. Becraft and Richmond[22] found that the water hydrogen-bonding structure at the CaF_2^-water interface becomes relatively weak as the surface charge approaches zero, but it becomes strong if the net surface charge increases, which is favorable for the enclathration. We believe that the water structure at the hydrate−water interface follows the same behavior. The increased concentration of hydrate former, favorable water structure, or both give rise to a fast growth rate.

We cannot also exclude that the surfactant adsorption could reduce the adhesion force between hydrate particles[23], via increasing the net surface charge (repulsion between hydrate particles), or forming an adsorbed layer around hydrate particles, or both, lowering the possibility of agglomeration. As a consequence, more small hydrate particles form[24] and the total hydrate−water interfacial area, at which the hydrate growth prefers to proceed, is higher than that in a system without surfactants, causing more guest molecules to be enclathrated for a given period. Besides, a low possibility of agglomeration also gives rise to a longer period of contact between water and guest molecules for a given hydrate−water interfacial area. These may lead to favorable enclathration kinetics[2, 24].

4.4. Conclusions

The adsorption isotherms of both SDS and DTAB on CP hydrates show a two-plateau (L-S) type. The Langmuir equilibrium constant in the first step is higher for SDS than for DTAB. The saturated adsorption amount of SDS in both steps is lower than that of DTAB. The affinity of these two surfactant chains to hydrates is proportional to the number of hydrogen bonds

formed between headgroups and pendant hydrogens on the hydrate surface. Hydrophobic microdomains, into which hydrocarbon molecules could solubilize, occur on the hydrate surface at high surfactant concentrations. Also, adsorption of ionic surfactant chains enhances the water hydrogen-bonding structure at the hydrate−water interface and reduces the adhesion force between hydrate particles. These three factors may contribute to a fast enclathration rate.

4.5. References

1. Sloan, E. D.; Koh, C. Clathrate Hydrates of Natural Gas, 3rd ed.; CRC: Boca Raton; 2008.
2. Zhong, Y.; Roger, R. E. Surfactant effects on gas hydrate formation. Chem. Eng. Sci. 2000, 55, 4175-4187.
3. Englezos, P.; Kalogerakis, N.; Dholabhai, P. D.; Bishnoi, P. R. Kinetics of gas hydrate formation from mixtures of methane and ethane. Chem. Eng. Sci. 1987, 42, 2659-2666.
4. Wang, W. X.; Bray, C. L.; Adams, D. J.; Cooper, A. I. Methane Storage in Dry Water Gas Hydrates. J. Am. Chem. Soc. 2008, 230, 11608-11609.
5. Wang, W. X.; Carter, B. O.; Bray, C. L.; Steiner, A.; Bacsa, J.; Jones, J. T.; Croper, C.; Khimyak, Y. Z.; Adams, D. J.; Cooper, A. I. Reversible Methane Storage in a Polymer-Supported Semi-Clathrate Hydrate at Ambient Temperature and Pressure. Chem. Mater. 2009, 21, 3810-3815.
6. Watanabe, K.; Imai, S.; Mori, Y. H. Surfactant effects on hydrate formation in an unstirred gas/liquid system: An experimental study using HFC-32 and sodium dodecyl sulfate. Chem. Eng. Sci. 2005, 60, 4846-4857.
7. Gayet, P.; Dicharry, C.; Marion, G.; Graciaa, A.; Lachaise, J.; Nesterov, A. Experimental determination of methane hydrate dissociation curve up to 55 MPa by using a small amount of surfactant as hydrate promoter. Chem. Eng. Sci. 2005, 60, 5751-5758.
8. Zhang, J. S.; Lee, S. Y.; Lee, J. W. Does SDS micellize under methane hydrate-forming conditions below the normal Krafft point? J. Colloid Interface Sci. 2007, 315, 313-318.
9. Zhang, J. S.; Lee, J. W. Effect of Sodium Dodecyl Sulfate on the Supercooling Point of Ice and Clathrate Hydrates. Energy Fuel 2009, 23, 3045-3047.
10. Lo, C.; Zhang, J. S.; Somasundaran, P.; Couzis, A.; Lee, J. W. Adsorption of Surfactants on Two Different Hydrates. Langmuir 2008, 24, 12723-12726

11. Zhang, J. S.; Lo, C.; Somasundaran, P.; Lu, S.; Couzis, A.; Lee, J. W. Adsorption of Sodium Dodecyl Sulfate at THF Hydrate/Liquid Interface. J. Phys. Chem. C 2008, 112, 12381-12385.
12. Chandar, P.; Somasundaran, P.; Turro, N. J. Fluorescence probe studies on the structure of the adsorbed layer of dodecyl sulfate at the alumina—water interface. J. Colloid Interface Sci. 1987, 117, 31-46.
13. Zhang, J. S.; Lee, J. W. Equilibrium of Hydrogen + Cyclopentane and Carbon Dioxide + Cyclopentane Binary Hydrates. J. Chem. Eng. Data 2009, 54, 659-661.
14. Epton, S. R. A new method for the rapid titrimetric analysis of sodium alkyl sulphates and related compounds. Trans. Faraday Soc. 1948, 44, 226-230
15. Corso, J. V. Mixed Indicator Composition. U.S. Patent 2663692, 1953.
16. Wang, L. K.; Panzardi, P. Determination of anionic surfactants with Azure A and quaternary ammonium salt. J. Anal. Chem. 1975, 47, 1472-1475.
17. Steveninck, J. V.; Riemersma, J. C. Determination of Long-Chain Alkyl Sulfates as Chloroform-Soluble Azure A Salts. Anal. Chem. 1966, 38, 1250-1251
18. Zhu, B. Y.; Gu, T. R. General isotherm equation for adsorption of surfactants at solid/liquid interfaces. Part 1. Theoretical. J. Chem. Soc., Faraday Trans. 1989, 85, 3813-3817.
19. Pimentel, G. C.; McClellan, A. L. The Hydrogen Bond; WH Freeman: New York, 1960.
20. Patrykiejew, A.; Sokolowski, S.; Zientarski, T.; Binder, K. Monte Carlo Study of Dense Monolayer and Bilayer Films on the (100) Plane of Face-Centered Cubic Crystals. Langmuir 1999, 15, 3642-3652.
21. Richmond, G. L. Molecular Bonding and Interactions at Aqueous Surfaces as Probed by Vibrational Sum Frequency Spectroscopy. Chem. Rev. 2002, 102, 2693-2724.

22. Becraft, K.; Richmond, G. L. In Situ Vibrational Spectroscopic Studies of the CaF_2/H_2O Interface. Langmuir 2001, 17, 7721-7724.

23. Anklam, M. R.; York, J. D.; Helmerich, L.; Firoozabadi, A. Effects of antiagglomerants on the interactions between hydrate particles. AIChE J. 2008, 54, 565-574.

24. Zhang, J. S.; Lee, S.; Lee, J. W. Kinetics of Methane Hydrate Formation from SDS Solution. Ind. Eng. Chem. Res. 2007, 46, 6353-6359.

Chapter 5. Adsorption of Kinetic Inhibitors on Clathrate Hydrates.

Published in The Journal of Physical Chemistry C. 2009,113, 17418-17420.

Abstract: Adsorption studies of kinetic inhibitors on clathrate hydrates are essential for understanding the inhibition mechanism at the hydrate−water interface. This work presents the adsorption behaviors of two kinetic inhibitors, polyvinyl pyrrolidone (PVP) and polyvinylcaprolactam (PVCap), on cyclopentane (CP) hydrates. The particle charge of CP hydrates is negative in the absence of any inhibitors, and it becomes neutral as the inhibitor concentration increases. The isotherm of PVP is well fitted to the Langmuir-type whereas the adsorption isotherm of PVCap is of the BET-type. Although PVCap monomers preferably adsorb on hydrates compared with PVP monomers, the isotherms of PVP and PVCap overlap with each other at concentrations up to 50 μM that corresponds to a water-based weight fraction of 0.6% for PVP or 0.5% for PVCap. Above this concentration, a multilayer adsorption occurs for PVCap. This multilayer adsorption gives rise to a thicker adsorption layer than that for the PVP case, which makes PVCap more effective in reducing the diffusion of hydrate formers from the bulk phase to the hydrate surface where the hydrate growth prefers to proceed. The determination of polymer inhibitor adsorption isotherms can provide the implication of adsorption behaviors and can be utilized to screen a new effective kinetic hydrate inhibitor.

5.1. Evaluating Kinetic Inhibitors on Cyclopentane Hydrates

Clathrate hydrates are nonstoichiometric crystalline compounds in which guest molecules such as methane, carbon dioxide, and cyclopentane (CP) stabilize the hydrogen-bonded water cavities[1]. These solids are identified as a potential cause of pipeline blockage in oil and gas

industries. To counter this problem, low-dosage hydrate inhibitors (LDHIs) have been developed and studied extensively over the past three decades[2]. However, the inhibiting mechanism of LDHIs in hydrate formation is still poorly understood.

A number of theoretical studies have suggested that an inhibitor molecule binds to the surface of hydrate nuclei[3-6]. Two microscopic studies investigated inhibitor adsorption on tetrahydrofuran (THF) hydrates[7, 8]; however, it should be noted that the surface property of THF hydrates is different from that of natural gas hydrates because THF is miscible with water and less hydrophobic than most light hydrocarbons[9]. Another hydrate guest that can readily enclathrate is CP. CP is as hydrophobic as hydrocarbons, and thus the interfacial nature of CP hydrate−water is close to that of natural gas hydrate−water. Furthermore, CP hydrates are stable at temperatures up to 280 K at atmospheric pressure[10]; therefore, they are a better model system than THF hydrates in adsorption studies.

In this work, we present the adsorption study of two kinetic inhibitors, polyvinyl pyrrolidone (PVP) and polyvinylcaprolactam (PVCap), on CP hydrates. To our best knowledge, this study is the first attempt to determine the adsorption isotherms of the kinetic inhibitors and to relate them to an inhibition mechanism. The particle charge measurements provide additional information about the accumulation of these two inhibitors at the hydrate−water interface.

5.2. Experimental Procedures

5.2.1. Materials

CP was purchased from Sigma-Aldrich with a purity of 99%+. PVCap (Mr = 100,000) solution (40 wt % in ethanol) was generously supplied by BASF. PVP (Mr = 40,000) was purchased from Spectrum Chemical. Figure 5.1 shows the molecular structure of these two inhibitors. All chemicals were used as received without further purification. Deionized water with a resistivity of 18 MΩ cm−1 was produced in the lab.

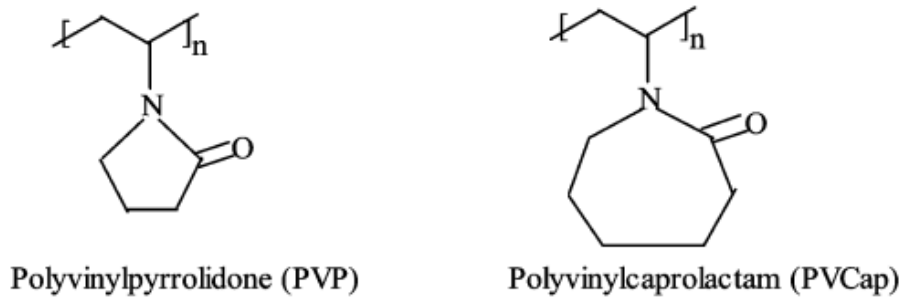

Polyvinylpyrrolidone (PVP) Polyvinylcaprolactam (PVCap)

Figure 5.1. Structure of polyvinylpyrrolidone and polyvinylcaprolactam.

5.2.2. CP Hydrate Slurries

Thirty grams of CP and 270 g of water were added to a 1 L glass bottle and then placed in a freezer at a temperature of around 263 K after sealing the bottle. After the water was frozen, the bottle was vigorously shaken at ambient conditions and CP was enclathrated. The bottle was then put in a chiller at 277 K for 7−10 days and was frequently shaken to promote the enclathration. These hydrate slurries were mixed with the polymer solutions, and another week was spent for the equilibration of polymer adsorption on the hydrates as described below in the

determination of isotherms. The concentration of CP hydrates in slurries was estimated to be 53.6 wt % assuming complete enclathration of CP in hydrates.

5.2.3. ζ-Potential

Our previous work describes the procedure of sample preparation for zeta potential measurements[11]. A 1mL sample of the hydrate slurries was quickly transferred to a Folded Capillary zeta cell (DTS1060, Malvern Instruments). The cell was then inserted into a Zetasizer Nano ZS (Malvern Instruments) where the temperature was set to 277 K. The ζ-potential was measured after the cell was maintained at 277 K for 10 min.

5.2.4. Adsorption Isotherms

Ten grams of polymer solutions were prepared in a 25mL vial, and the vial was placed in a chiller at 277 K overnight. Ten grams of CP hydrate slurries were quickly added to the polymer solutions (both the slurries and solutions were placed in an ice bath). Then, the vial was sealed and kept in a chiller at 277 K for 1 week to achieve the adsorption equilibrium. The vial was shaken from time to time to accelerate the adsorption during this period. Due to its low density compared with water, all of the CP hydrates were located in the upper portion of the vial. About 5mL of solution was withdrawn from the lower portion of the vial by using a 10mL syringe in less than 1 min. The concentration of polymers in solutions was analyzed by using a Total Organic Carbon Analyzer (Shimadzu TOC 5000A). The adsorption amount is calculated from the depletion of the polymers from the aqueous phase.

5.2.5. Error Analysis

The uncertainty in determining adsorption isotherms is mainly due to the variation of solid concentrations in hydrate slurries. When the slurries are exposed to atmospheric conditions, some CP hydrates will dissociate even though at a temperature below the equilibrium temperature. To minimize the dissociation, transferring hydrate slurries to the vial was carried out as quickly as possible (within less than 1 min). The mean percent deviation of triplicate measurements of the adsorption density is 8%.

5.3. Results and Discussion

The electrokinetic measurement of CP hydrates provides valuable information on inhibitor adsorption. Figure 5.2 shows the ζ-potential of CP hydrates at different PVP or PVCap concentrations at 277 K. The surface charge of CP hydrate particles is negative without any inhibitors. Lo et al.[11] have proposed that the negative charge results from the adsorption of bicarbonate because the hydrate slurries are open to air during preparation and measurements. Other anions, if they are present in water, could compete with bicarbonates for adsorption sites. The surface charge of CP hydrates becomes less negative as the nonionic inhibitor concentration increases, indicating that the inhibitors compete with anions for the adsorption sites.

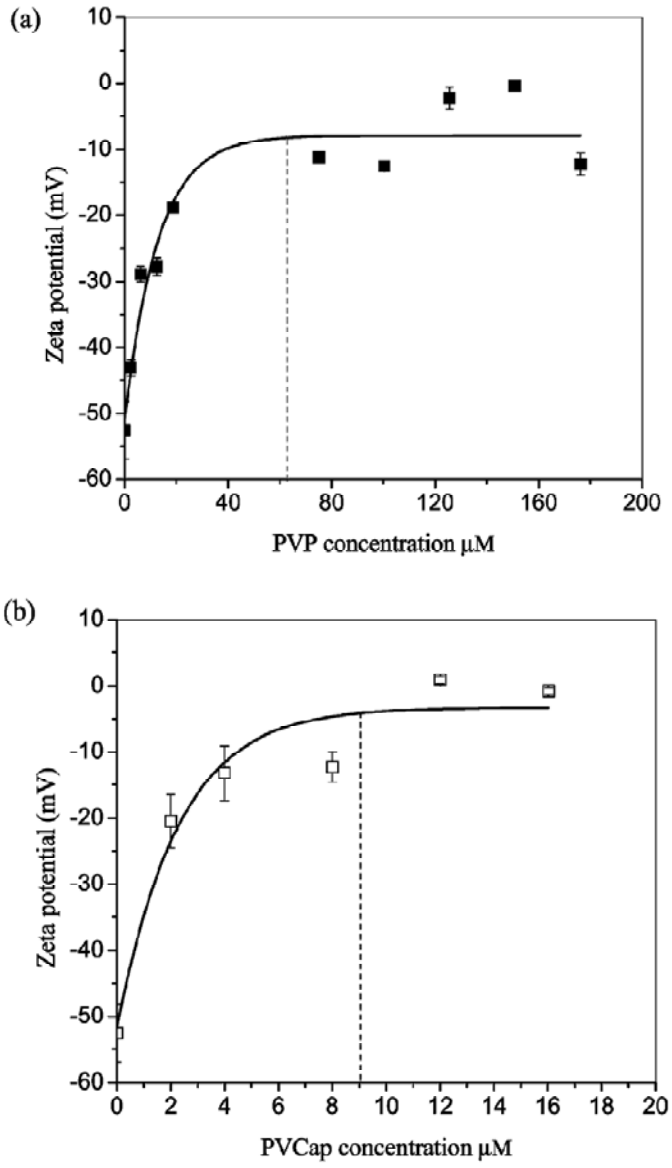

Figure 5.2. Zeta potential of CP hydrates as a function of PVP (a) and PVCap (b) concentrations.

The inhibitors bind to the hydrate surface via hydrogen bonding and hydrophobic interactions. Hydrogen bonds can form between oxygen of the cyclic amide group and pendant hydrogens on the hydrate surface. Hydrophobic interaction between the inhibitor molecules and the hydrate surface cannot be ignored since the hydrate surface is more hydrophobic than water[11]. The ζ-

potential fluctuates around −8 mV at PVP (or PVCap) concentrations above 63μM (or 9μM). This can be regarded as the zero charge because the error of the ζ-potential measurements is within ±6 mV. Thus, the surface of CP hydrates is neutral at sufficiently high inhibitor concentrations. However, whether more nonionic PVP or PVCap adsorbs on hydrate particles at higher concentrations is unclear from ζ-potential measurements because more adsorption has no effect on the particle charge after it becomes neutral. Adsorption isotherms can identify the variation of adsorbed amounts in the wide range of the inhibitor concentrations.

The adsorption isotherms of PVP and PVCap on CP hydrates at 277 K are presented in Figure 5.3. The adsorption data of PVP can be fitted to the Langmuir isotherm, whereas the isotherm of PVCap belongs to the BET-type. The isotherm of PVP overlaps with that of PVCap at inhibitor concentration below 50 μM, suggesting that the affinity of PVP to CP hydrates is the same as that of PVCap in this low concentration range. This observation is not consistent with the free energy of binding (ΔG) for PVP and PVCap monomers that was obtained from molecular dynamic simulations[3]. It was reported that ΔG is 0.5 ± 3.8 and −9.4 ± 3.7 kcal mol−1 for PVP and PVCap monomers, respectively[3]. Thus, the PVCap monomers preferably adsorb on hydrates compared to the PVP monomers.

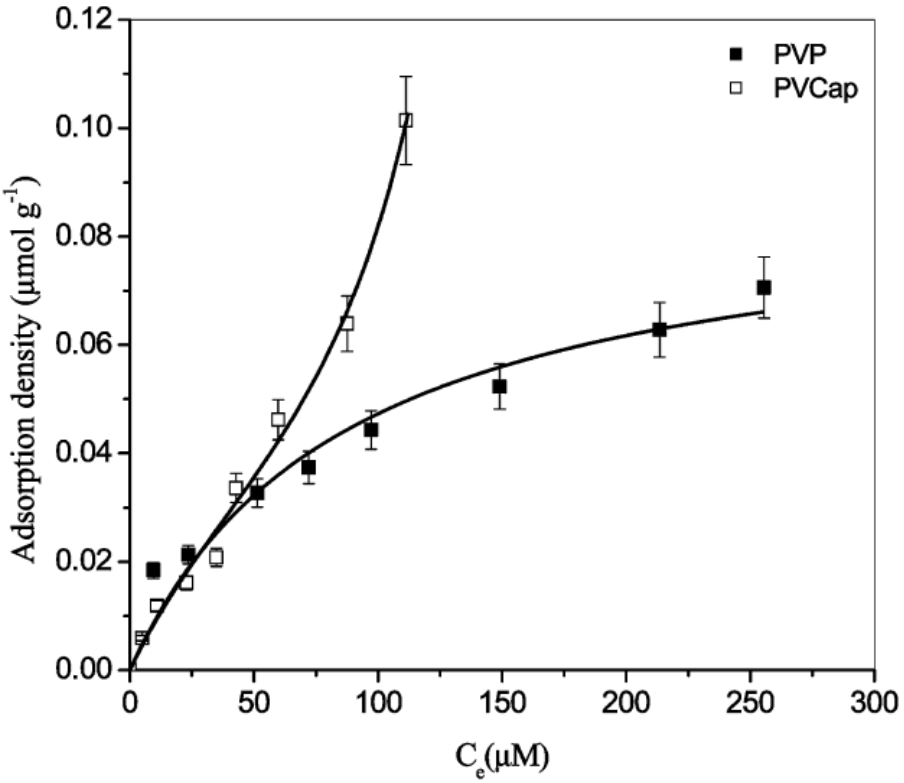

Figure 5.3. Adsorption isotherms of two inhibitors on CP hydrates.

However, when the polymers adsorb on clathrate hydrates, more than one monomer can bind to the surface; therefore, ΔG for the polymers is not proportional to ΔG for the monomers because the number of monomer units of PVP and PVCap bound to open cavities on the hydrate surface is not identical. Furthermore, ΔG for the polymers is also dependent on the configuration of adsorbed polymers because the entropy change of polymer adsorption is related to the configuration. Thus, the binding energies of monomer would not be directly used to predict the affinity of polymers without knowing both the number of monomer units bound to the surface and the configuration of adsorbed molecules.

The adsorption density at which the hydrate surface becomes neutral in Figure 5.2 corresponds to 0.035 μmol g^{-1} for PVP and 0.011 μmol g^{-1} for PVCap, indicating that a single PVP chain occupies less surface area than one PVCap chain does. This difference is attributed to the molecule sizes of these two polymers. The size of polymers in solutions is characterized by the radius of gyration (R_g). King et al.[8] reported that R_g is 8 nm for PVP and 15.5 nm for PVCap. The monolayer density of PVP and PVCap is also inversely proportional to the molecule size. The calculated monolayer density is 0.09 μmol g^{-1} for PVP and 0.04 μmol g^{-1} for PVCap.

Kinetic inhibitors are usually effective at high concentrations around 1 wt %. Although the fraction of open cavities involved in inhibitor adsorption increases with higher inhibitor concentrations, the impact of the thickness of adsorption layer on the effectiveness of inhibitors is also important. Figure 5.3 shows that the multiple-layer adsorption of PVCap can occur at concentrations above 56 μM that correspond to a water-based weight fraction of 0.6%. The larger molecule size and its multiple-layer adsorption of PVCap give rise to a larger thickness of adsorption layer compared to the adsorption case of PVP. One important step in hydrate growth is the transport of individual molecules or clusters formed by water and guest molecules from the bulk phase to the hydrate−water interface[1]. The rate of hydrate growth decreases as the path of this transport increases. This decelerating effect becomes stronger with the increased thickness of the adsorbed layer because the agglomeration between hydrate particles in water becomes weak as the thickness of the polymer adsorption layer increases[12]. Furthermore, the existence of the polymer layer increases the resistance of diffusion of the individual molecules and clusters. Therefore, PVCap more effectively decelerates the diffusion from the bulk phase to the hydrate−water interface than PVP does.

5.4. Adsorption Behavior and Its Effect on Inhibition

Adsorption of PVP or PVCap reduces the charge density of hydrate particles. The adsorption of PVP follows the Langmuir isotherm whereas the PVCap adsorption isotherm is the BET-type. However, the adsorption density of PVP overlaps with that of PVCap at inhibitor concentrations below 50 μM. The results suggest that the affinity of polymers to the hydrate surface is not simply proportional to the free energy of binding of corresponding monomers, but it is affected by both the number of monomers bound to the surface and the configuration of adsorbed polymers. The multilayer adsorption of PVCap with a large molecule size makes PVCap more effective than PVP in terms of reducing the tendency of particle agglomeration or decelerating the diffusion of guest molecules, water molecules, or both from the bulk phase to the hydrate−water interface.

5.5. References

1. Sloan, E. D.; Koh, C. Clathrate Hydrates of Natural Gas, 3rd ed.; CRC: Boca Raton, FL, 2008.
2. Kelland, M. A. History of the Development of Low Dosage Hydrate Inhibitors. Energy Fuels 2006, 20, 825–847.
3. Anderson, B. J.; Tester, J. W.; Borghi, G. P.; Trout, B. L. Properties of Inhibitors of Methane Hydrate Formation via Molecular Dynamics Simulations. J. Am. Chem. Soc. 2005, 127, 17852–17862.
4. Carver, T. J.; Drew, M. G. B.; Rodger, P. M. Characterisation of the {111} growth planes of a type II gas hydrate and study of the mechanism of kinetic inhibition by poly(vinylpyrrolidone). J. Chem. Soc., Faraday Trans. 1996, 92, 5209–5033.
5. Kvamme, B.; Kuznetsova, T.; Aasoldsen, K. Molecular dynamics simulations for selection of kinetic hydrate inhibitors. J. Mol. Graphics Modell. 2005, 23, 524–536.
6. Storr, M. T.; Taylor, P. C.; Monfort, J. P.; Rodger, P. M. Kinetic Inhibitor of Hydrate Crystallization. J. Am. Chem. Soc. 2004, 126, 1569–1576.
7. Hutter, J. L.; King, H. E.; Lin, M. Y. Polymeric Hydrate-Inhibitor Adsorption Measured by Neutron Scattering. Macromolecules 2000, 33, 2670–2679.
8. King, H. E.; Hutter, J. L.; Lin, M. Y.; Sun, T. Polymer conformations of gas-hydrate kinetic inhibitors: A small-angle neutron scattering study. J. Chem. Phys. 2000, 112, 2523–2532.
9. Kalyanasundaram, K.; Thomas, J. K. Environmental effects on vibronic band intensities in pyrene monomer fluorescence and their application in studies of micellar systems. J. Am. Chem. Soc. 1977, 97, 2039–2044.
10. Zhang, J. S.; Lee, J. W. Equilibrium of Hydrogen + Cyclopentane and Carbon Dioxide + Cyclopentane Binary Hydrates. J. Chem. Eng. Data 2009, 54 (1), 659–661.

11. Lo, C.; Zhang, J. S.; Somasundaran, P.; Couzis, A.; Lee, J. W. Adsorption of Surfactants on Two Different Hydrates. Langmuir 2008, 24, 12723.
12. Gregory, J. Particles in water: properties and processes; CRC: Boca Raton, FL, 2006; pp 90-92.

Chapter 6. Raman Spectroscopic Studies of Surfactant Effect on the Water Structure around Hydrate Guest Molecules.

Published in Journal of Physical Chemistry Letters 2010, 1, 2676-2679.

Abstract: The addition of a small amount of surfactants enhances hydrocarbon enclathration rates without any mechanical agitation, but the role of surfactants has yet to be clarified. This work presents the effect of sodium dodecyl sulfate (SDS) on the water structure around cyclopentane (CP), a sII hydrate former, at the hydrate−water interface. The arrangement of local water molecules was obtained using surface-enhanced Raman spectroscopy (SERS). The Raman spectra reveal that the water structure around CP at the water−hydrate interface is identical to the hexakaidecahedron ($5^{12}6^4$) cavity of sII hydrates at a SDS concentration higher than 0.087mM. However, at the CP−water interface, with and without SDS, the water arrangement is clathrate-like. Additionally, we found that the microenvironment of CP in bulk aqueous solutions is close to that in hydrates at a SDS concentration higher than 0.35mM.

6.1. Local Hydrate-Like Environments Around Hydrate Formers

Gas hydrates, also known as clathrate hydrates, are nonstoichiometric crystalline compounds in which guest molecules such as hydrogen, methane, and cyclopentane (CP) stabilize cavities formed by hydrogen-bonded water molecules[1]. They pose nuisances as detrimental oil and gas pipeline blockages. On the other hand, they have been considered as a safe and economical storage medium for natural gas and a possible option for carbon capture and storage[1-5].

Controllability for inhibiting or accelerating clathrate hydrate formation is based on a solid understanding of the enclathration kinetic including both hydrate nucleation and crystal growth. The enclathration is usually carried out with a small amount of surfactants, for example, sodium dodecyl sulfate (SDS), to enhance enclathration kinetics in the absence of mechanical agitation[6-8]. The promoting role of surfactants is still poorly understood, although a lot of effort has been made to clarify the mechanism. The first explanation was that SDS molecules form micelles, and then they initiate the crystallization of gas hydrates[7]. However, recent studies suggest that micelles cannot form in the aqueous phase below the Kraft point, even with a high pressure of hydrate formers[9, 10]. To date, the fast enclathration kinetics is believed to originate from the interaction between surfactant monomers and hydrates[11, 12].

One step in the process for rapid formation is the adsorption of anionic surfactants on hydrates. The surfactant adsorption brings negative charges to the surface, and thus hydrate crystals become more negatively charged as more surfactant chains accumulate at the water−hydrate interface[11,12], causing an increase in the repulsion force between hydrate particles, which reduces the possibility of particle agglomeration and then results in high enclathration rates. Also, the adsorption of surfactant chains can change the water structure of the interfacial region because simulation results found that the aqueous environment around surfactant chains seems to be compatible with the structure of hydrate surface[13]. Despite the importance of the changed aqueous environment for the enclathration, no experimental investigation has been done on the local structure of water around hydrate formers.

6.2. Experimental Section

6.2.1. Materials

Cyclopentane, 1-butanol, 1-dodecanol, and SDS were purchased from Sigma-Aldrich with a purity of 99+%. An aqueous colloid of silver (the silver concentration is 20ppm) was provided from Purest Colloids, Inc. with a size of 0.65 nm. All chemicals were used as received without further purification. Deionized (DI) water was produced in our lab with a resistivity of 18 mΩ cm^{-1}.

6.2.2. Synthesis of CP Hydrate Slurries

CP and water mixture (300 g; the mass ratio of CP to water was 1:9) were charged to a 1 L glass bottle and then hermetically sealed. The bottle was placed in a freezer at 263 K until all water converted to ice, and then the bottle was shaken vigorously at room temperatures. As the ice melted, CP was enclathrated at the same time. The occurrence of CP hydrates was confirmed by the appearance of fine white particles. After visually observing that large portions of ice had melted, the bottle was placed in a chiller at 277 K for 1 week, and it was shaken daily to enhance the enclathration. The concentration of CP hydrates in slurries was 51 wt % by calorimetric measurements.

6.2.3. Preparation of CP Microemulsions, CP Aqueous Solutions, and Dodecanol Solutions

CP microemulsions were prepared according to the method proposed by Rosano and Nixon[17]. In a typical experiment, 4.1 g of SDS, 4.2 g of CP, and 41.5mL of colloidal silver were mixed

vigorously together to form an emulsion; then, this emulsion was titrated to clarity with 3.0 g of butanol. We prepared CP bulk aqueous solutions by mixing SDS, CP, and colloidal silver (the mass ratio of CP to colloidal silver was 1:99). We prepared the dodecanol solution (62mM) by dissolving dodecanol in CP.

6.2.4. Micro-Raman Analysis

SDS was dissolved in an aqueous colloid of silver; then, the SDS solution was preserved in a chiller at 277 K. CP hydrate slurries (10 g) were added to 10 g of the SDS solution in a 20mL chilled vial. The mixture was then placed in the chiller at 277 K for 1 week, which allowed the system to reach equilibrium. Finally, the sample was put in an aluminum crucible chilled at 275 K, and the Raman spectra of CP hydrate−water interface were obtained around 275 K by using an HR800 Horiba Jobin Yvon Raman Microprobe. The samples were excited with 632.8 nm HeNe laser radiation; a 10× object lens was used. The spectrum was recorded from 100 to 3500 cm^{-1}. The Raman spectra of CP−water (oil−water) interface, bulk CP aqueous solutions, CP microemulsions, and dodecanol solutions were also collected at room temperature from 100 to 3500 cm^{-1}.

6.3. Results and Discussion

This work is the first experimental attempt to understand the effect of SDS on the water structure around CP both at the hydrate−water interface and in bulk aqueous solutions using surface-enhanced Raman spectroscopy (SERS). With an SDS concentration higher than 0.087mM, the structure of water molecules at the water−CP hydrate interface is the same as

that in the large cavity of sII hydrates. It is observed that the microenvironment of CP in bulk aqueous solutions is clathrate-like at SDS concentrations above 0.35mM.

The Raman spectrum of liquid CP exhibits five prominent bands at 888, 1030, 1445, 2869, and 2942 cm^{-1} (Figure 6.1). The bands at 888 and 2869 cm^{-1} have been assigned to ring breathing and C−H stretching modes of A_1' (symmetric vibration) species, the Raman bands at 1030 and 2942 cm^{-1} are assigned to ring and C−H stretching modes of E_2' (degenerate vibration) species, and the 1445 cm^{-1} frequency represents the CH_2 deformation mode of E_2' species[14-16]. As Figure 6.1 shows, five bands appear in the Raman spectrum of the water−CP hydrate interface, and all bands are blue-shifted from those of liquid CP. Again, the strongest band at 894 cm^{-1} is assigned to the A_1' ring breathing mode, and the weaker band at 2874 cm^{-1} is assigned to the A_1' C−H stretching mode. This high-frequency shift of the ring breathing and C−H stretching bands is due to encaging CP molecules in large cavities ($5^{12}6^4$) of sII hydrates. Also, a shoulder (left dotted line) is observed at the low-frequency side of the 894 cm^{-1} band, which is attributed to the dissolved CP at the interface. A close examination of Figure 6.1 reveals that the A_1' ring breathing mode at the liquid CP−water interface appears at 890 cm^{-1}, indicating that the water structure surrounding CP in this region becomes clathrate-like. Additionally, A_1' ring breathing mode of dissolved CP both in bulk aqueous solutions and at the water-hydrate interface (Figure 6.1a) experiences a red shift compared with that of liquid CP.

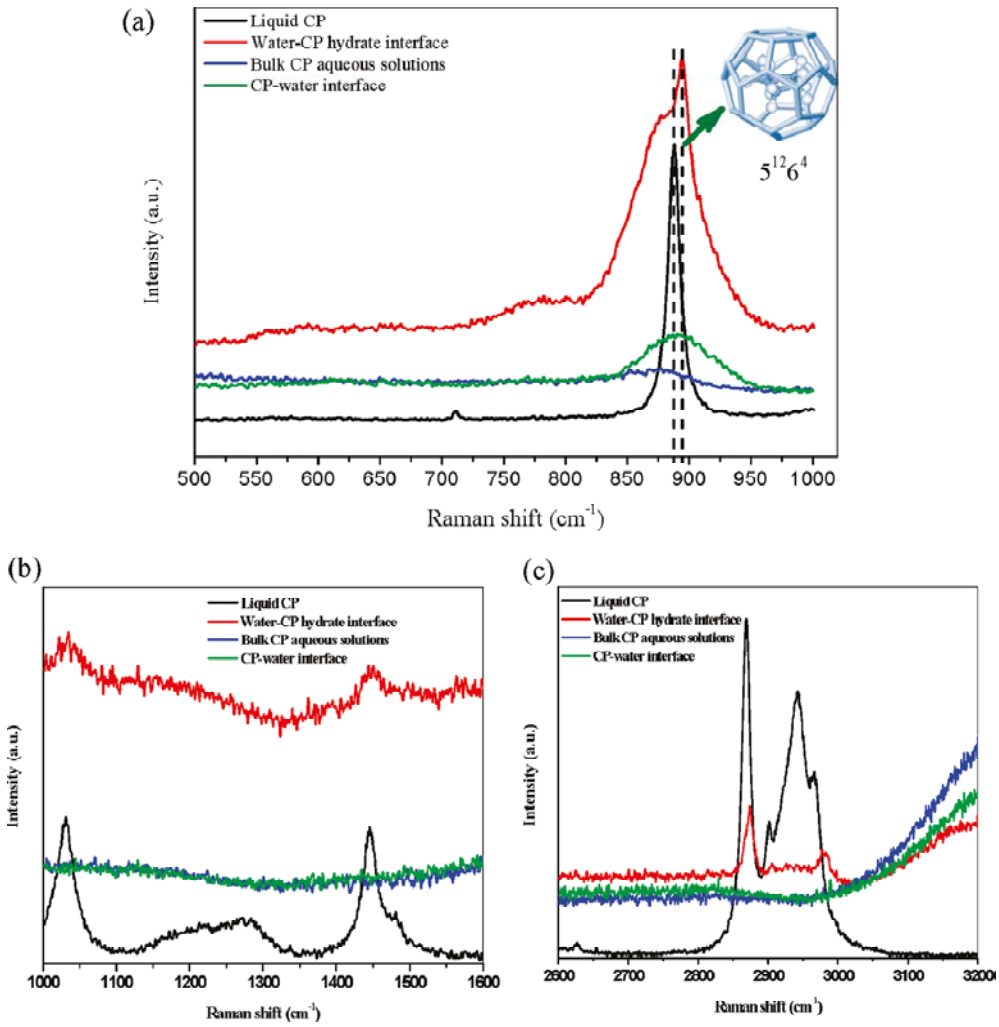

Figure 6.1. Raman spectra of liquid CP, and Raman spectra of water−CP hydrate interface, bulk aqueous solution, and CP−water interface without any SDS in an aqueous colloid of silver: (a) in the region of 500−1000 cm^{-1} frequency, (b) in the region of 1000−1600 cm^{-1} frequency and (c) in the region of 2600−3200 cm^{-1} frequency.

With 0.087 to 1.0mM SDS, the shoulder of 894 cm^{-1} band in CP at the water−hydrate interface vanishes, as shown in Figure 6.2. This observation can be interpreted in terms of the effect of surfactant chains on the local water structure. A previous simulation work suggests that the

aqueous environment around the nonpolar tails of surfactants is similar to the structure of hydrate surface[13]. Therefore, adsorption of DS^- on hydrates causes the local microenvironment of dissolved CP at the water−hydrate interface to be identical to the water structure of the large cavity of sII hydrates, even with 0.087mM SDS.

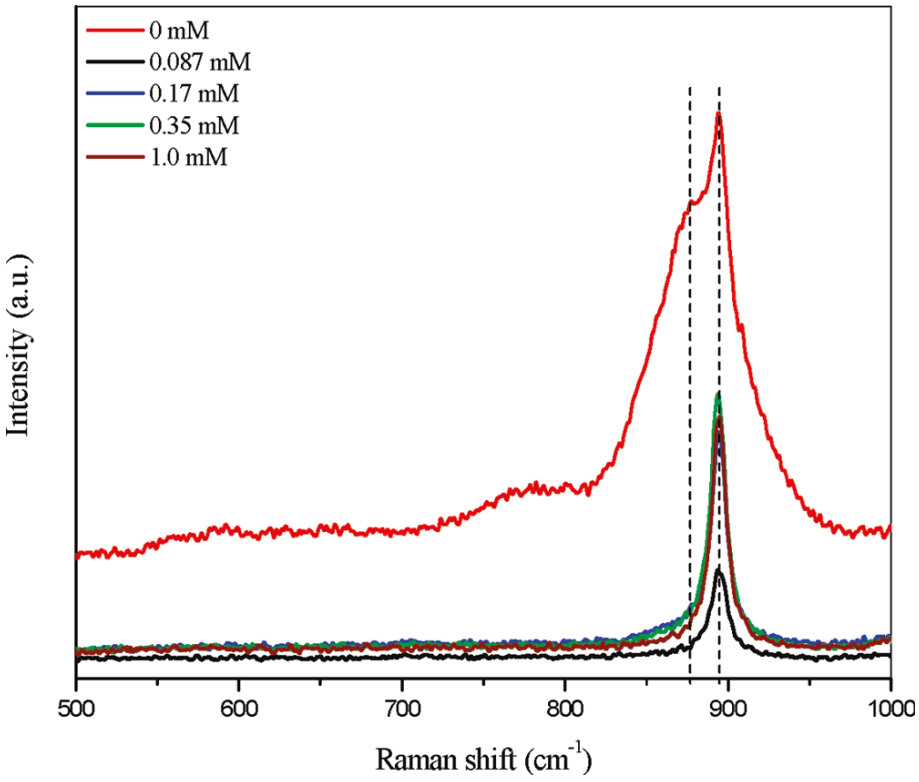

Figure 6.2. Raman spectra of water−CP hydrate interface with different SDS concentrations in an aqueous colloid of silver.

To confirm further the influence of surfactants on the local water structure, we measured the Raman spectra of dissolved CP in bulk CP aqueous solutions. As shown in Figure 6.3, we observe that the Raman band at 877 cm^{-1} shifts to a higher wavenumber as the SDS concentration increases from 0.17 to 0.35mM, despite the signal being relatively weak because of the low

solubility of CP in water. With 0.35 and 1.0mM SDS, the A_1' ring breathing appears near 890 cm^{-1}, which corresponds to the A_1' ring breathing of CP in clathrate-like clusters. This blue shift is due to the change in the microenvironment around dissolved CP but not to the interaction between tails and CP because SDS has no significant effect on the Raman spectrum of the CP–water interface (Figure 6.4). The Raman spectrum of liquid CP is also not affected by the existence of the hydrocarbon chain in dodecanol solutions and the tail of SDS in CP microemulsions (Figure 6.5).

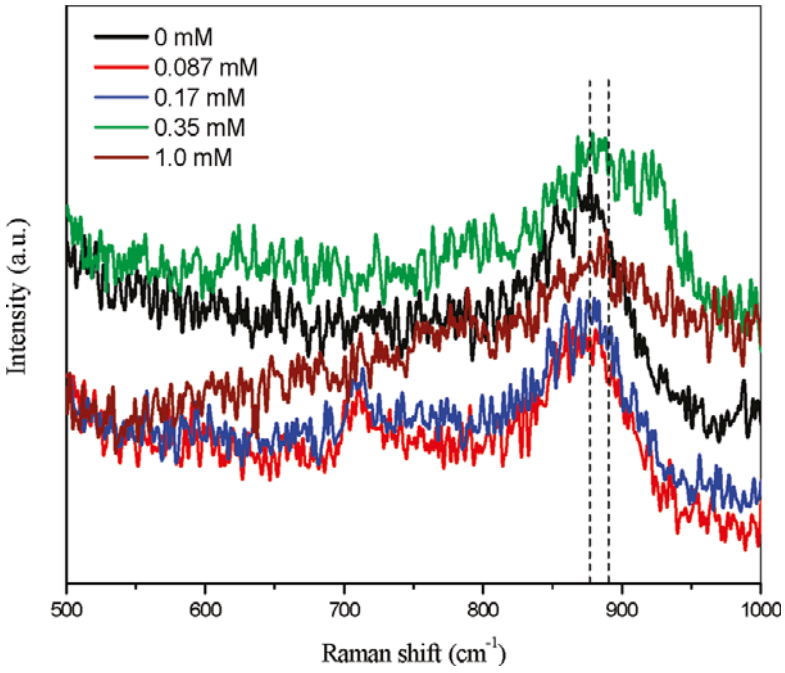

Figure 6.3. Raman spectra of dissolved CP in the bulk aqueous solutions with different SDS concentrations in an aqueous colloid of silver.

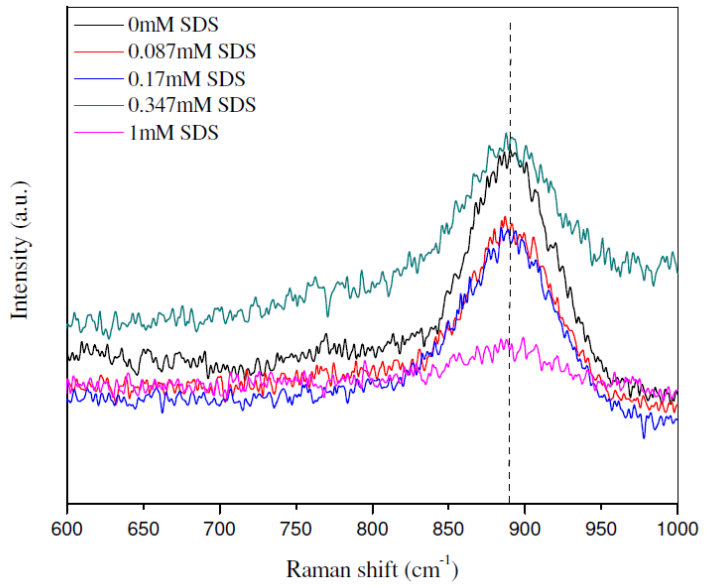

Figure 6.4. Raman spectra for the CP-Water interface with varying SDS concentrations.

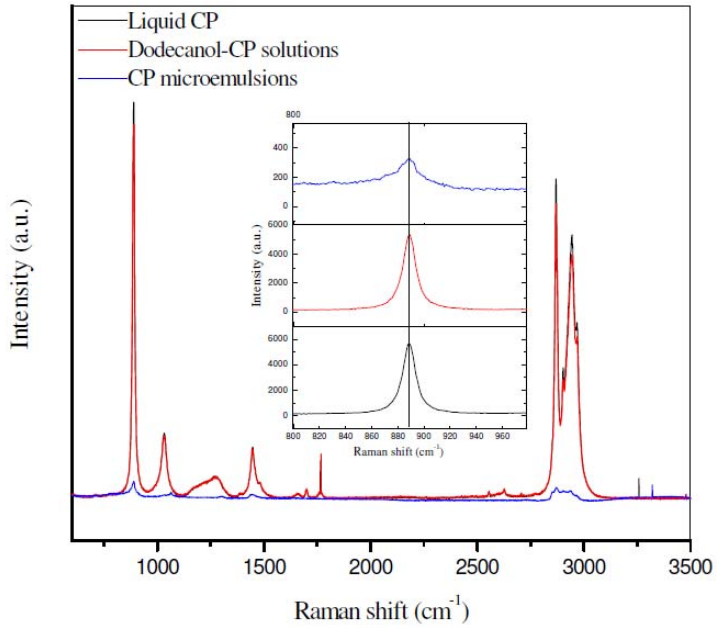

Figure 6.5. Raman spectra for pure liquid CP, and liquid CP in dodecanol and microemulsions.

Inset: No shift in symmetric A1' ring breathing.

6.4. Spectroscopic Evidence for Hydrate-Like Environments

In summary, we have inferred the structure of water molecules around CP, a sII hydrate former, both at the water−hydrate interface and in bulk aqueous solutions with a surfactant, SDS, from surface-enhanced Raman measurements. At an SDS concentration above 0.087mM (or 25ppm), the arrangement of water molecules around the hydrate former at the water−hydrate interface is the same as the hexakaidecahedron ($5^{12}6^4$) cavity of sII hydrates. Also, the microenvironment of CP in bulk aqueous solutions is close to that in hydrates when a SDS concentration is higher than 0.35mM (or 100ppm). Additionally, the water structure around CP at the CP−water interface, regardless of the presence of surfactants, is clathrate-like. Adsorption of surfactants at the water−hydrate interface causes hydrogen-bonded water molecules to arrange in the same way as in clathrate hydrates, which enhances the intrinsic enclathration rate. Moreover, the presence of surfactants in bulk aqueous solutions increases the concentration of clathrate-like water aggregates, shortening the induction period.

6.5. References

1. Sloan, E. D. Fundamental Principles and Applications of Natural Gas Hydrates Nature 2003, 426, 353– 359.

2. Hammerschmidt, E. G. Formation of Gas Hydrates in Natural Gas Transmission Lines Ind. Eng. Chem. 1934, 26, 851– 855.

3. Gudmundsson, J. S.; Borrehaug, A. A Frozen Hydrate for Transport of Natural Gas. In The Second International Conference on Natural Gas Hydrate, Toulouse, France, 1996; pp 415− 422.

4. Mao, W. L.; Mao, H. K.; Goncharov, A. F.; Struzhkin, V. V.; Guo, Q. Z.; Hu, J. Z.; Shu, J. F.; Hemley, R. J.; Somayazulu, M.; Zhao, Y. S. Hydrogen Clusters in Clathrate Hydrate Science 2002, 297, 2247– 2249.

5. North, W. J.; Blackwell, V. R.; Morgan, J. J. Studies of CO2 Hydrate Formation and Dissolution Environ. Sci. Technol. 1998, 32, 676– 681.

6. Kutergin, O. B.; Mel'nikov, V. P.; Nesterov, A. N. Influence of Surfactants on the Mechanism and Kinetics of the Formation of Gas Hydrates Dokl. Akad. Nauk SSSR 1992, 323, 549– 553.

7. Zhong, Y.; Rogers, R. E. Surfactants Effects on Gas Hydrate Formation Chem. Eng. Sci. 2000, 55, 4175– 4787.

8. Gayet, P.; Dicharry, C.; Marion, G.; Graciaa, A.; Lachaise, J.; Nesterov, A. Experimental Determination of Methane Hydrate Dissociation Curve up to 55 MPa by Using a Small Amount of Surfactant as Hydrate Promoter Chem. Eng. Sci. 2005, 60, 5751– 5758.

9. Zhang, J. S.; Lee, S. Y.; Lee, J. W. Does SDS Micellize under Methane Hydrate-Forming Conditions below the Normal Ambient Krafft Point? J. Colloid Interface Sci. 2007, 315, 313– 318.

10. Okutani, K.; Kuwabara, Y.; Mori, Y. H. Surfactant Effects on Hydrate Formation in an Unstirred Gas/Liquid system: An Experimental Study Using Methane and Sodium Alkyl Sulfates Chem. Eng. Sci. 2008, 63, 183– 194.

11. Lo, C.; Zhang, J. S.; Somasundaran, P.; Couzis, A.; Lee, J. W. Adsorption of Surfactants on Two Different Hydrates Langmuir 2008, 24, 12723– 12726.

12. Zhang, J. S.; Lo, C.; Somasundaran, P.; Couzis, A.; Lee, J. W. Adsorption of Sodium Dodecyl Sulfate at THF Hydrate/Liquid Interface J. Phys. Chem. C 2008, 112, 12381– 12385.

13. Storr, M. T.; Taylor, P. C.; Monfort, J.; Roger, P. M. Kinetic Inhibitor of Hydrate Crystallization J. Am. Chem. Soc. 2004, 126, 1569– 1576.

14. Rosenbaum, E. J.; Jacobson, H. F. Raman Spectra of Cyclopentane and Some of Its Monoalkyl Derivatives J. Am. Chem. Soc. 1941, 63, 2841– 2842.

15. Miller, F. A.; Inskeep, R. G. The Infra-Red and Raman Spectra of Cyclopentane, Cyclopentane-d1, and Cyclopentane-d10 J. Chem. Phys. 1950, 18, 1519– 1531.

16. Schettino, V.; Marzocchi, M. P.; Califano, S. Infrared Spectra of Crystalline Cyclopentane and Cyclopentane-d10 J. Chem. Phys. 1969, 51, 5264– 5276.

17. Rosano, H. L.; Nixon, A. L.; Cavallo, J. L. Interfacial Stoichiometry of a Microemulsion System J. Phys. Chem. 1989, 93, 4536– 4539.

Chapter 7. Attenuated Total Reflectance-Infrared Spectroscopic Study on the Effect of Surfactants on Cyclopentane Hydrates

To be submitted to Journal of Physical Chemistry Letters

Abstract: Infrared spectroscopy of hydrates is limited due to the overwhelming signal saturation of the OH bonding. Thus, the aim of this study is to use this increased signal of the OH bonding to identify the water structure sensitivities, and then identify the changes in water structure when there is added surfactant upon hydrate interfaces. The data suggests a change from hydrate-like to water-like upon adding surfactants and identifies the reasons for the increased growth phase during hydrate formation.

7.1. Spectroscopy on the Hydrate Interface by the use of Surface Enhancement

In the study of gas hydrates, usually a guest molecule of typically low molecular weight i.e. methane, ethane, cyclopentane, etcetera, is surrounded by a hydrogen bonded network of water molecules. These hydrates have three known structures: sI, sII, and sH, and the hydration number varies due to the structure type. [1] Typically, gas hydrates require low temperatures and high pressures to form.

Hydrate formation requires the stabilization of the host network i.e. the water cage. This host network stabilization is detectable by near-infrared spectroscopy. The OH stretching indicates an ordered or unordered hydrogen bonding. However, there are only a few gas hydrate studies using mid-IR[2-4] since OH broadening is quite extensive and covers a lot of the spectra. Therefore, chemical vibrations are covered by the absorption of OH. The technical problem of IR

absorptivity of water is actually an advantage for this study of hydrogen bonding at hydrate interfaces. The other technical problem for using IR for hydrate studies is cool temperature. IR is quite sensitive to temperature. The absorption intensity can be lowered due to the lower temperature.

Surface studies of hydrates are limited due to the difficulties of detecting scattered particles and uneven hydrate formations. Many have used intricate methods of growth on ATR surfaces like vapor deposition and epitaxial growth.[2-4] These methods try to increase the surface area contact to increase signal strength.

We incorporated silver nano-particles to enhance the signal strength at the hydrate interface. Since the silver particles situate at the surface of hydrates, the returning IR signal is primarily of hydrate surfaces. This increased signal does not follow Beer-Lambert's Law because this method employs the incident flux to induce resonance and produce a stimulated emission. This is a vital distinction for the use of surface enhanced ATR-IR. Silver nano-particles act as signal increasing probes, via the surface plasmon resonance phenomena.[5] In the absence of silver nano-particles, signal from the free OH bands (3500-3800cm^{-1}) are not visible (Figure 7.1).

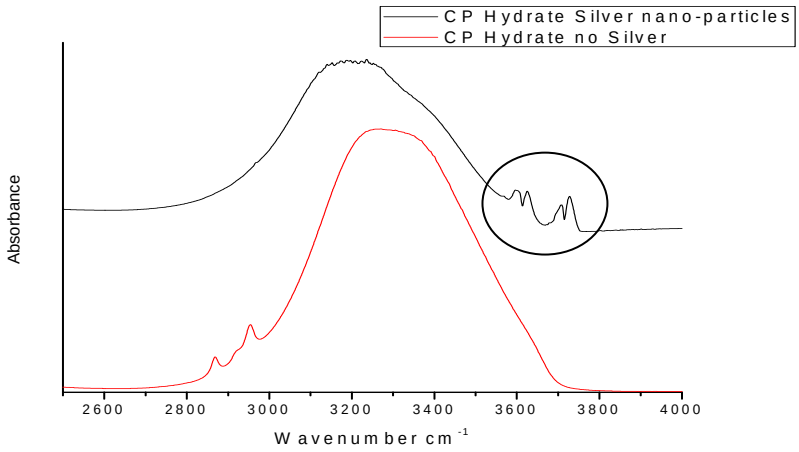

Figure 7.1. CP hydrates with and without silver nano-particles.

Clathrate hydrate vibrational spectroscopic studies have been mainly in the field of Raman. Raman has revealed spectroscopic evidence for hydrate-like sensitivity related to nucleation.[6] However this does not explain the extended growth phase. This hydrate-like sensitivity was detectable because of surface enhancement, which is the method we employed in this study. In this paper, we will expose why SDS not only as a nucleator but also as a growth promoter. This study will tie together the full role of SDS on hydrates and the reasons for fast hydrate formation.

7.2. Materials and Methods.

7.2.1. Materials

Cyclopentane and SDS were purchased from Sigma-Aldrich with a purity of 99+%. An aqueous colloid of silver (the silver concentration is 20ppm) was provided from Purest Colloids, Inc. with a diameter of 0.65 nm. All chemicals were used as received without further purification. Deionized (DI) water was produced in our lab with a resistivity of 18 mΩ cm^{-1}.

7.2.2. Synthesis of CP Hydrate Slurries

In a hermetically sealed 500mL polypropylene bottle, a CP-water mixture (300 g; the mass ratio of CP to water was 1:9) is charged. The bottle is placed in a freezer at 263 K until all water converted to ice the bottle is then taken out and shaken vigorously at room temperatures. As the ice melts, CP was enclathrated at the same time. CP hydrate formation was confirmed by the appearance of fine white particles. After visually observing that large portions of ice had melted, the bottle is placed in a chiller at 277 K for 1 week, and it was shaken daily to enhance

the enclathration. The concentration of CP hydrates in slurries was 51 wt % by calorimetric measurements. The addition of surfactants follows the method described in Lo et al.[7] with exception that the water contains 20ppm silver nano-particles. The surfactant solutions are allowed to equilibriate for ten days.

7.2.3. Attenuated Total Reflectance Infrared Spectroscopy

A Perkin Elmer Spectrum 100 is used to take measurements using a cooled MCT sensor. The ZnSe Horizontal Attenuated Total Reflectance (HATR) trough is cooled to 1-5°C during the experiment. Hydrate slurry mixture is ladled onto the crystal surface. The cooled HATR surface is taken as the background. 100 measurements were taken for each sample.

7.3. Results and Discussion

The OH stretching and free OH stretching is the focus of the study. The OH stretching indicates an ordered “ice-like” or unordered “water-like” environment.[8] Free OH stretching is able to determine the penetration depth of a water molecule into an oil phase. The free OH stretching can also determine structure, like the magic number clathrate.[9]

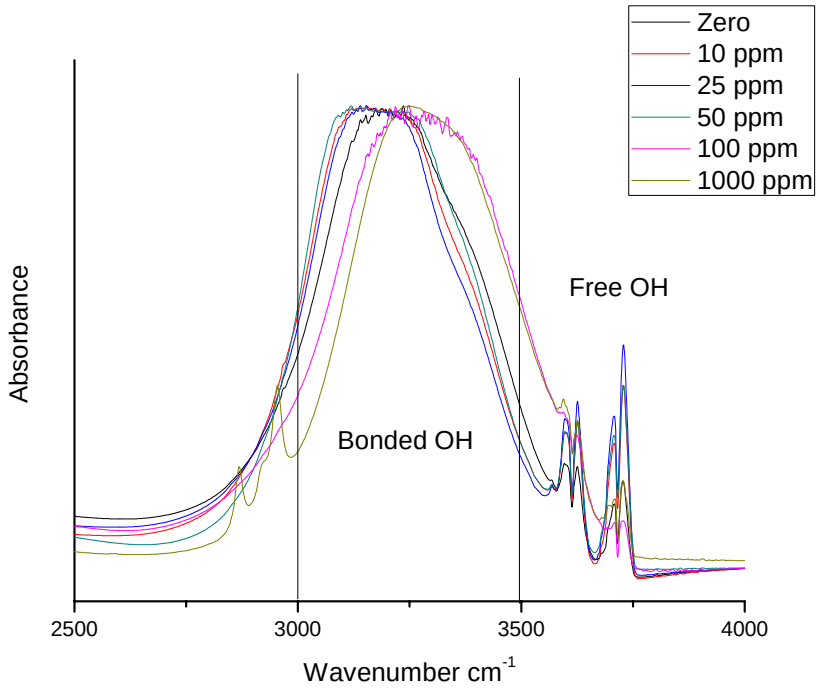

Figure 7.2. ATR-IR measurements of CP Hydrate with varying SDS concentrations.

The ATR-IR measurements for the CP hydrate interface with varying SDS concentrations are depicted in Figure 7.2. The definitions of "ice-like" and "water-like" are in regards to the 3100 cm^{-1} and 3400 cm^{-1} bands in the bonded OH region[8] From 0 to 75ppm SDS there is an inclination towards the left. A red shift for the OH stretch is indicative of ice-like tendencies, to an ordered and static state. However, at 100ppm SDS the OH stretch shifts to right, the additional SDS acts upon the surface to induce water-like environments. This is similar to adding salt to bulk water where the OH band blue shifts. So above 100ppm SDS the hydrate interface is similar to hydrogen bonded water, which is less ordered and able to vibrate more. SDS is added to 1000ppm to emphasize this shifting.

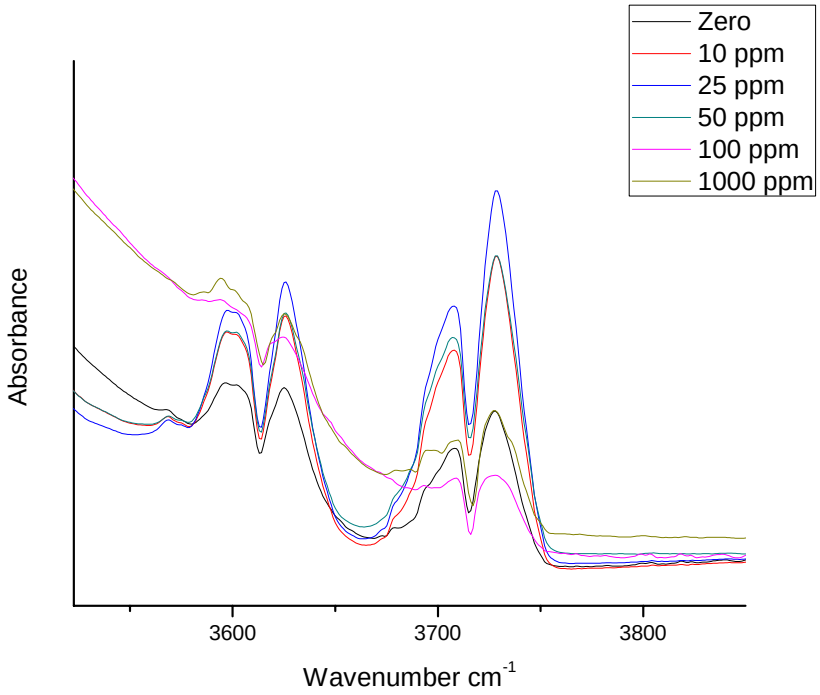

Figure 7.3. The free OH bands 3690 to 3760 cm^{-1} is the asymmetric OH stretch, 3580 to 3650 cm^{-1} is the symmetric OH stretch with varying SDS concentrations.

The free OH bands are depicted in Figure 7.3 from 3500 to 3800 cm^{-1}. These free OH bands come from non-colligative interactions of the individual molecules. The high frequency band is due to the asymmetric OH stretch, the low frequency band is due to the symmetric OH stretch[10]. These two bands are indicative of the oil environment and the penetration of free OH into the oil. The wings on the bands indicate the hydration number[9]. This is due to the rotational moments of free OH. Shin et al.[9] showed that n = 6 - 27 water clusters have a different vibrational predissociation for each hydration cluster. In our data we can identify this be an n = 11 water cluster, meaning this is a half clathrate or the surface of the clathrate. We take the

ratio of the area of Free OH to the area of hydrogen bonded OH and compared them to each other in Figure 7.4.

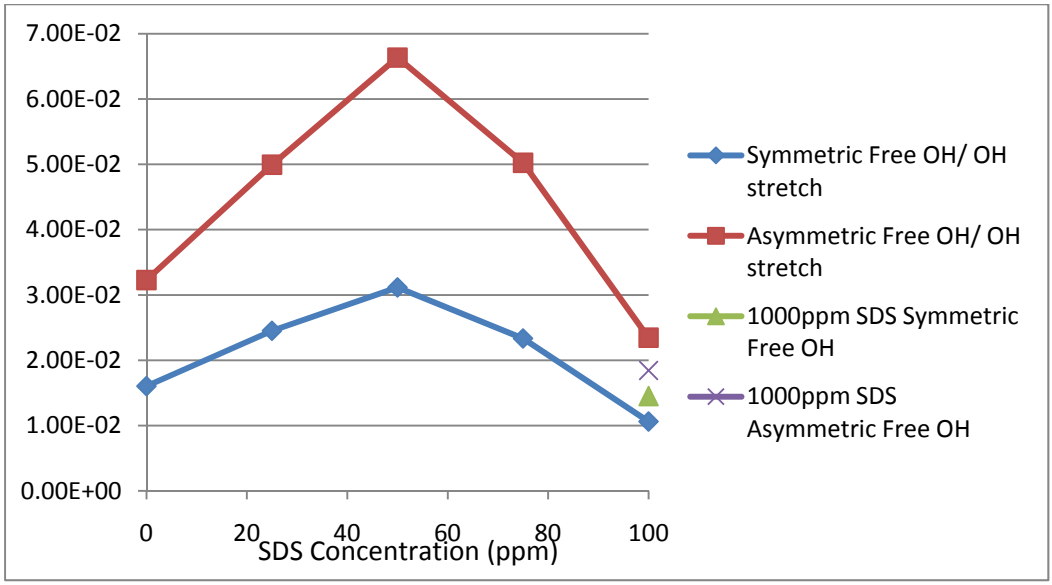

Figure 7.4. Band ratio of Free OH to Hydrogen bonded OH.

The band ratio maximum is at 50ppm SDS, where we note from Lo et al.[7] that this is when the surfactant is lying flat on the hydrate surface. The penetration into the oil phase is greater since the oily chain is contacting the surface of the clathrate and may bring along with it oil/hydrate former. Beyond 50ppm SDS the half clathrate is unable to diffuse into the oil layer. So we are unable to detect an increased localization of more hydrate former in the adsorbed surfactant layer. Possibly a diffusion of more hydrate former to the interface is not acting upon the hydrate interface but on the monolayer formation which is subsequently the length of the alkyl chain.

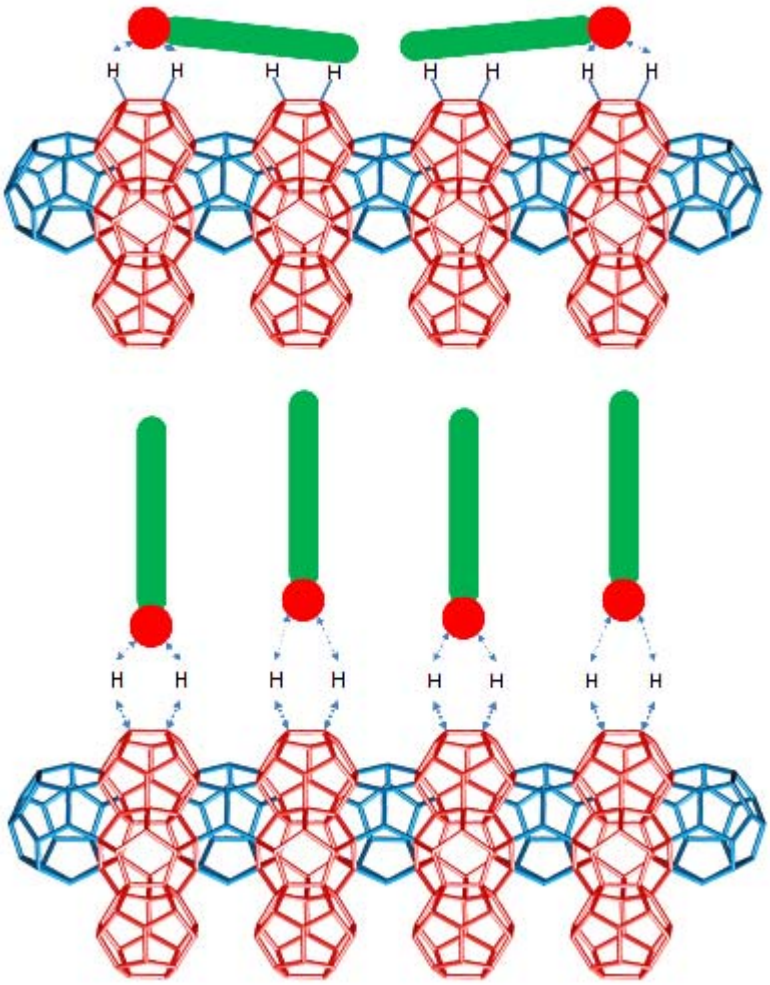

Figure 7.5. A depiction of the hydrate interface.

7.3.1. Mechanism for Growth

SDS acts to induce nucleation as noted from Raman studies by Lo et al.[6], where hydrate-like water structure was detected. Then, as hydrate nuclei form, SDS is able to adsorb upon the hydrate surface via hydrogen bonding. As more SDS accumulates onto the surface, a monolayer

can form and induce an increased diffusion of hydrate formers to the bulk and onto these interfaces[11].

From the ATR data, similar patterns of surface adsorption can be described as from our previous papers. At 50ppm SDS, the free OH band ratio is at the highest penetration into the oil phase. From this, we infer that the half clathrate structure is closer to oil layer or alkyl chain. As we increase the SDS concentration the monolayer forms, the bonded OH starts to become mobile as inferred from the ATR-IR of the OH bonding. The loose hydrogen bonding at the surface is kinetically mobile and seeking hydrate formers to fulfill the host-guest structure. This continual growth process is due to this factor of looser hydrogen bonding at the hydrate interface, enabling hydrate surfaces to seek for guests/hydrate formers to fulfill the matrix. Figure 7.5 is an animated schematic of the adsorption process.

7.4. Summary

We have deduced that there is a loosening of hydrogen bonding at the hydrate interface above 100ppm SDS. This measurement infers that the growth process starts once there can be fluctuating hydrogen bonding at these hydrate interfaces. ATR-IR also confirms the lying down on surfactants at 50ppm SDS, where the free OH band ratio is higher than at other concentrations. At 50ppm SDS, the interface is in contact with an increased amount of hydrate former, however since the interface is still “ice-like” it would be difficult to incorporate the hydrate former into the matrix. The spectroscopic data presents a direct measurement of the hydrate interface and supplies a way of indentifying interfacial properties upon hydrate interfaces.

7.5. References

1. Sloan, E. D.; Koh, C. Clathrate Hydrates of Natural Gas, 3rd ed.; CRC: Boca Raton; 2008.
2. Dobbs, G. T.; Luzinova, Y.; Mizaikoff, B. Infrared Spectroscopy for Monitoring Gas Hydrates in Aqueous Solution. Proceedings of the 6th International Conference on Gas Hydrates (ICGH 2008)
3. Fleyfel, F.; Devlin, J. P. FT-IR Spectra of 90 K Films of Simple, Mixed, and Double Clathrate Hydrates of Trimethylene Oxide, Methyl Chloride, Carbon Dioxide, Tetrahydrofuran, and Ethylene Oxide Containing Decoupled D_2O. Journal of Physical Chemistry 92, 1988, 3, 631-635.
4. Fleyfel, F.; Devlin, J. P. Carbon Dioxide Clathrate Hydrate Epitaxial Growth: Spectroscopic Evidence for Formation of the Simple Type-II CO_2 Hydrate. Journal of Physical Chemistry 95, 1991, 9, 3811-3815.
5. Osawa, M. Surface-Enhanced Infrared Absorption. NEAR-FIELD OPTICS AND SURFACE PLASMON POLARITONS Topics in Applied Physics, 2001, 81, 163-187.
6. Lo, C.; Zhang, J. S.; Somasundaran, P.; Lee, J. W. Raman Spectroscopic Studies of Surfactant Effect on the Water Structure around Hydrate Guest Molecules. *J. Phys. Chem. Lett.* , 2010, 1, 2676–2679.
7. Lo, C.; Zhang, J. S.; Somasundaran, P.; Couzis, A.; Lee, J. W. Adsorption of Cationic and Anionic Surfactants on Cyclopentane Hydrates. *J. Phys. Chem. C* 2010, 114, 13385–13389.
8. Tian, C.S.; Shen, Y.R. Isotopic Dilution Study of the Water/Vapor Interface by Phase-Sensitive Sum-Frequency Vibrational Spectroscopy. J.AM. CHEM. SOC. 2009, 131, 2790–2791.

9. Shin, J.-W.; Hammer, N.I.; Diken, E.G.; Johnson, M.A.; Walters, R.S.; Jaeger, T.D.; Duncan, M.A.; Christie, R.A.; Jordan, K.D. Infrared Signature of Structures Associated with the $H^+(H_2O)_n$ (n=60 to 27) Clusters. Science , 2004, 304, 1137-1140.
10. Conrad, M.; Strauss, H. L. The Vibrational Spectrum of Water in Liquid Alkanes. Biophysical Journal, 48, 1985, 117-124.
11. Somasundaran, P; Moudgil, B. M. The effect of dissolved hydrocarbon gases in surfactant solutions on froth floatation of minerals. J. Colloid Interface Sci. 1974, 47, 290–299.

Chapter 8. Conclusion

The previous chapters provided fundamental insight into hydrate formation. Firstly surfactants like SDS can induce hydrate-like structure, which is visibly detectable by Surface Enhanced Raman Spectroscopy[1]. This hydrate-like sensitivity can be used as a screening method for other hydrate promoters. However, some surfactants like DTAB are not detectable by this method, due to the similar vibrational bands of anime or bromine to the CP ring breathing band. Therefore screening should also include ATR-IR spectroscopy methods, especially for the OH region to sense ice-like activity. The hydrate-like/ice-like sensitivity seems to have corollary properties to induction times. This hydrate-like environment can induce hydrate formation. In Zhang et al. 2008[2], we recognized that with the addition of 50ppm SDS there is a reduction of induction time for THF hydrates. From Lo et al. 2010[1], Raman results revealed upon adding 0.35mM or 100ppm SDS to a CP aqueous solution the appearance of hydrate-like environments are visible.

However we can note that at 50ppm SDS on THF Hydrate[2] and at 100ppm SDS on CP hydrate[3] is when these hydrate particles are saturated with a monolayer. The detection of a monolayer for THF hydrate is confirmed through ζ-potential and fluorescence measurements. The detection of a monolayer for CP hydrates is confirmed by ζ-potential measurements and an adsorption Isotherm.

CP hydrate being a more suitable model hydrate, because of its hydrophobicity, high melt temperature and exhibits no other phase changes, we continue the use of this type of hydrate.

Adsorption Isotherms of SDS and DTAB on CP hydrates revealed differences in adsorption behavior[3]. Regardless of charge, both surfactants are able to adsorb onto the hydrate interface. The result is a difference in adsorption amounts and readiness to form a monolayer on the hydrate interface. DTAB is unable to form a monolayer at the same concentrations as that of SDS, but is able to adsorb more upon the surface. DTAB is a known surfactant that is used as an anti-agglomerate agent and SDS is a known promoter. SDS being a promoter is able to adsorb and form a monolayer at lower concentrations, which may help in the growth process of hydrate formation. DTAB forms a monolayer but at higher concentrations, the density of the adsorbed layer is 3 times larger than that of SDS[3]. This higher density prevents the agglomeration of the hydrate particles to each other.

We can also see similarities with the adsorption of kinetic inhibitors on CP hydrates, where the adsorption density plays a large part on the effectiveness of preventing hydrate formation and agglomeration. From Zhang et al.[4], we are able to distinguish the effectiveness of the kinetic inhibitor by the surface coverage and surface excess on hydrates. PVP and PVCAP are popular kinetic inhibitors, however their effectiveness was previously based on their monomer structures [5]. From the adsorption isotherms we are able to compare the adsorption behavior of both inhibitors. PVP is able to adsorb onto the hydrate interface following a Langmuir type isotherm adsorbing up to one layer, but PVCAP is able to adsorb with a BET type isotherm with multiple layers. These comparison studies allow the evaluation of the effectiveness of the surfactant upon hydrate interfaces.

From many hydrate formation studies, the most effective surfactant is SDS and the most effective SDS concentration is between 100 to 500ppm. This concentration range is where we distinguish a monolayer concentration[3]. So how does this monolayer formation increase formation? We hypothesized that as these surfactant monolayer formations appear, hydrophobic hydrate formers would co-adsorb on to these hydrophobic domains. We have tried trials to identify these co-adsorbed elements from ATR-IR spectroscopy. However what resulted was a hydrate surface that changed from ice-like to water-like with the addition of 100ppm SDS[6]. The significance confirms that in the presence of a monolayer, the hydrate surface becomes "water-like". With loose hydrogen bonding, the cage structure is able to "seek" guest molecules rather than frozen/slow growth at the interface, similar to stopped growth at gas hydrate films.

With these fundamental ideas of how surfactants act upon hydrate interface in promoting hydrate formation and in stopping hydrate formation, we can assess a multitude of surfactants to see similar behavior. Thus we have deduced the methods to identify the surfactants' role on hydrates. Raman, ATR, ζ-potential, Pyrene fluorescence measurements, and adsorption isotherms provide the methods to deduce the role of surfactants on hydrate interfaces.

8.1. References

1. Lo, C., Zhang, J.S., Somasundaran, P., Lee, J.W. Raman Spectroscopic Studies of Surfactant Effect on the Water Structure around Hydrate Guest Molecules. *J. Phys. Chem. Lett.* 2010. 1. 2676–2679.
2. Zhang, J. S.; Lo, C.; Somasundaran, P.; Lu, S.; Couzis, A.; Lee, J. W. Adsorption of Sodium Dodecyl Sulfate at THF Hydrate/Liquid Interface. J. Phys. Chem. C 2008, 112, 12381-12385.
3. Lo, C., Zhang, J.S., Couzis, A., Somasundaran, P., Lee, J.W. Adsorption of Cationic and Anionic Surfactants on Cyclopentane Hydrates. J. Phys. Chem. C. 2010. 114. 13385-13389.
4. Zhang, J.S., Lo, C., Couzis, A., Somasundaran, P., Wu, J., Lee, J.W. Adsorption of Kinetic Inhibitors on Clathrate Hydrates. *J. Phys. Chem. C*, 2009, 113 (40), 17418–17420.
5. Anderson, B. J.; Tester, J. W.; Borghi, G. P.; Trout, B. L. Properties of Inhibitors of Methane Hydrate Formation via Molecular Dynamics Simulations. J. Am. Chem. Soc. 2005, 127, 17852–17862.
6. Lo, C., Zhang, J.S., Somasundaran, P., Lee, J.W. Attenuated Total Reflectance-Infrared Spectroscopic Study on the Effect of Surfactants on Cyclopentane Hydrates. to be submitted to JCIS.

9. Future Work

9.1. Improving Hydrate Formation Using Doubly Charged Surfactants

To be submitted after the addition of formation experiments and adsorption data.

Abstract: Hydrate formation is a stochastic and slow process. However, with the use of surfactants, it has become phenomenally faster. This work addresses the isotherms of two novel Dow surfactants for promoting hydrate growth. These Dowfax surfactants have doubly charged head groups which may promote hydrate formation more effectively than that of SDS. Though structurally similar these surfactants behave differently in solution. The scissors movement of the C-O-C bonds between the head groups is contracted open for Dowfax C6L. However, Dowfax 2A1 is able to move freely and have gauche transitions. Thus, two different titration paths are used to determine their aqueous concentrations. The adsorption behavior between these two surfactants will determine the active roles of these Dowfax surfactants and the potential purpose they serve. The extension of this work will also contain more adsorption data to identify the types of isotherms and hydrate formation data for a comparison of hydrate formation performance under SDS and the two Dowfax surfactants.

9.1.1. Evaluating Doubly Charged Surfactants

Gas hydrates or clathrates are non-stoichiometric crystalline compounds, where the host structure is composed of hydrogen bonded water molecules and the guest is usually a low molecular weight molecule i.e. methane, ethane, carbon dioxide, or cyclopentane[1]. These structures are formed under high pressure and low temperature conditions. They have thermodynamic or physical properties which can be exploited for industrial applications. They

are potential storage media, refrigeration coolant[2], separation[3], and desalinization material[4]. However utilizing this type of media requires an efficient and effective means to form hydrates.

The promoting hydrate formation has been done via employing a small amount of surfactants without mechanical agitation[5]. However, the exact usage of different types of surfactants was unclear as to how they would improve formation. The reasons for usage have been inferred on the surfactant's interfacial property or chemical structure.

From Lo et al.,[6] there is a spectroscopic evidence for inducing fast formation. Such evidence is provided by RAMAN spectroscopy. Hydrate like environments result in a blue shift in the ring breathing of cyclopentane, typically around 890cm^{-1}. Evidence for using doubly charged surfactants comes from the idea of how the head group, sulfate, acts to provide a semi-stable hydrate-like environment for the hydrate former. From our Raman data collected (Figure 9.1) there is a blue peak shift for Dowfax 2A1. However, C6L did not exhibit such a blue shift.

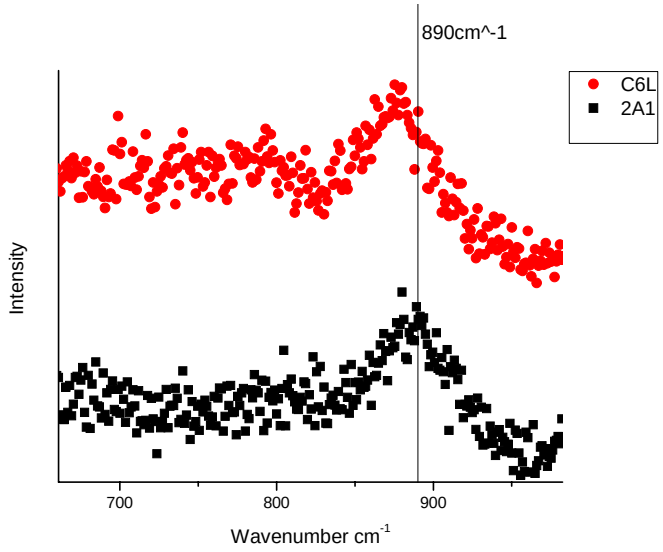

Figure 9.1. Raman Spectra of the CP ring breathing for 1wt% CP in two 1 wt% Dowfax Surfactants.

Dowfax surfactants are doubly charged with 2 anionic sulfate heads. Along with the idea of more negative charges being the contributing factor for promotion[8], having 2 heads may lead to increased hydrate promotion.

Preliminary works have been done to titrate these doubly charged surfactants and present adsorption isotherms for these surfactants. Titration of these similar Dowfax surfactants requires a vibrational analysis. Though structurally similar, ATR measurements reveal the difference in C-O-C bending movements. Figure 9.2 shows the vibrational spectra of bending movements of the C-O-C bond for the two Dowfax surfactants. Dowfax 2A1 has a steady parabolic curve over the 1170-1190 cm^{-1} range for C-O-C vibrational bending, but C6L a bi-modal curve indicating hindered bending movements. This hindered movement allows a bulky indicator like methylene blue to attach to the two head groups on the surfactant. However, the free moving bond for Dowfax 2A1 does not allow methylene blue to attach to both head groups due the steric hindrances. A back titration method is used to titrate the doubly charged surfactant. This method utilizes Methyl Orange, which is an anionic indicator. The charged headgroup for this molecule is at an end, rather than in the middle like Methylene Blue. Methyl Orange is able to attract only positively charged molecules like DTAB, which we use to titrate. Figure 9.3 shows the structure of the different surfactants and indicator molecules.

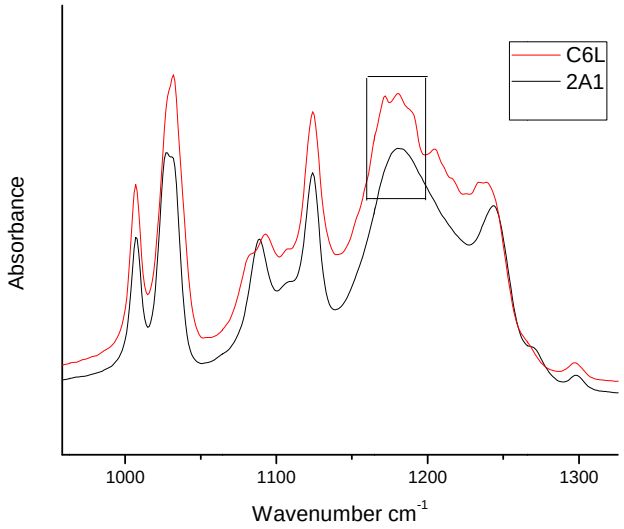

Figure 9.2. ATR-IR spectra for Dowfax 2A1 and C6L. Circled in the region for C-O-C stretch.

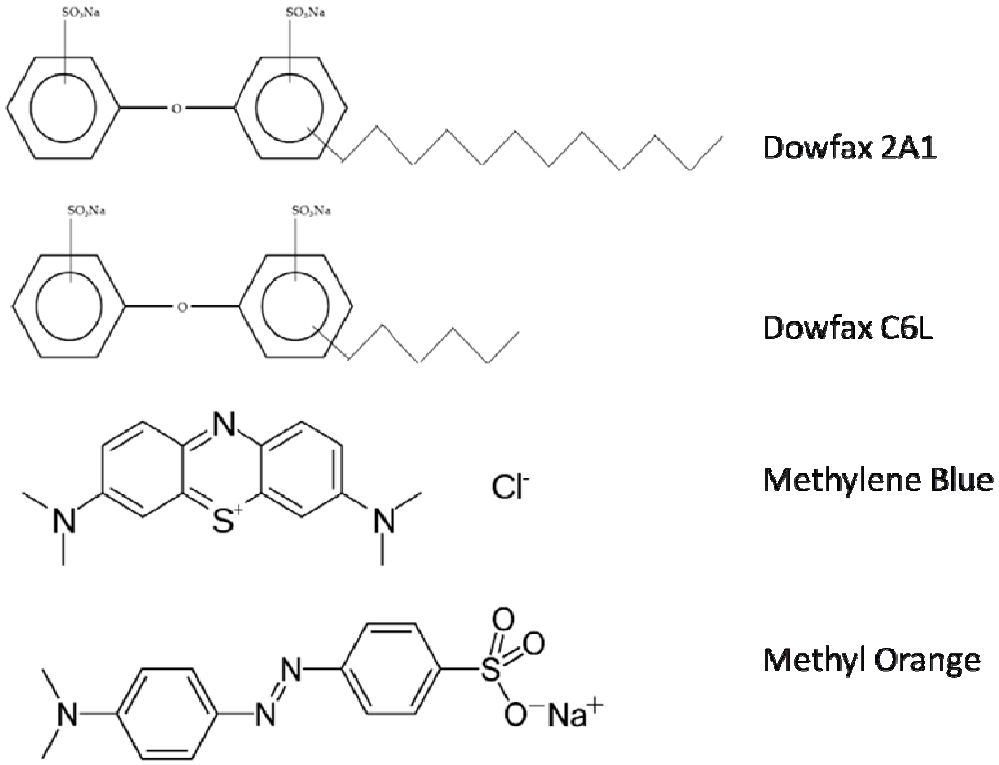

Figure 9.3. Structures of Dowfax C6L, Dowfax 2A1, Methylene Blue, and Methyl Orange.

The adsorption isotherms can reveal the mechanisms of the surfactant adsorption on hydrates. Hydrate formation activity seems to increase as the surfactant layer forms a hemi-micelle layer. Zhang et al. 2008[7] suggests that the hemi-micelle layer would allow for co-solubilization of hydrophobic hydrate formers, which can easily be incorporated into the growing front of hydrate and water interface.

9.1.2. Materials and Methods

9.1.2.1. Materials

Cyclopentane (CP) and dodecyl trimethylammonium bromide (DTAB) were purchased from Sigma-Aldrich with a purity of + 99%. Methylene Blue and Methyl Orange were obtained from Sigma-Aldrich with indicator purity. Sulfuric acid 96% and sodium sulfate 99% were supplied by Sigma-Aldrich. Dowfax 2A1 and C6L samples were generously supplied by Dow Chemical. All chemicals were used as received without further purification. Deionized (D.I.) water was produced in our lab with a resistivity of 18 MΩ cm^{-1}.

9.1.2.2. Preparations of CP Hydrate Slurries

A 1:9 CP-water mixture by weight was charged to a 500 mL polypropylene bottle and hermetically sealed. It was then placed in a freezer at a temperature of 263 K. After ice formation, the bottle was vigorously shaken at ambient conditions. When ice melts, CP is enclathrated at the same time. The formation of CP hydrates was confirmed by the appearance of white particles. The bottle was put in a chiller at 277 K for one week and shaken daily to

accelerate the enclathration. The concentration of CP hydrates in slurries was found to be 51 wt % by calorimetric measurements. The reason we started with CP hydrate slurries instead of solid CP hydrates in adsorption measurements is to avoid the variation of vapor condensation on hydrate particles and to avoid variation of total hydrate surface area when adding hydrate former in surfactant solutions. Preparing CP hydrates from surfactant solutions first could result in different particle sizes due to the effect of surfactants on the enclathration.

9.1.2.3. Adsorption Isotherms

The determination of adsorption isotherms follows the procedure proposed by Lo et al.[8]. Ten grams of surfactant solutions were charged to a 25 mL vial followed by putting the vial in a chiller at 277 K overnight. Ten grams of CP hydrate slurries were quickly added to the solutions (both the slurries and solutions were put in an ice bath). Then, the vial was sealed and kept in a chiller at 277 K for more than one week to allow the adsorption to reach equilibrium. The vial was shaken daily to accelerate surfactant adsorption on hydrates. Because of the density difference between hydrates and solutions, all of CP hydrates were located at the upper portion of vials. Finally, several milliliters of solution were withdrawn from the lower portion of the vial by using a 10 mL plastic syringe. The sampling usually lasted less than one minute. The concentration of Dowfax C6L in solutions was analyzed by Methylene Blue titration, similarly described by Epton[9]. Dowfax 2A1 concentration was determined by Methyl Orange liquid-liquid back titration method due to the steric hindrance as described above. A detailed titration procedure is given in the subsequent section. The adsorption amount is the depletion of surfactants in the aqueous phase.

9.1.2.4. Attenuated Total Reflectance-Infrared

Samples of Dowfax surfactants were placed directly onto a perkin elmer HATR trough plate. Using the MCT detector, the measurements were taken at atmospheric conditions. 100 sample measurements were accumulated.

9.1.2.5. Titration

A measured aliquot of the unknown surfactant solution is place into a 20 mL test tube. For Dowfax C6L, 2.5 mL of blue indicator solution containing 0.003 wt % Methylene Blue, 1.20 wt % sulfuric acid, and 5.00 wt % sodium sulfate was added, and then 2.5 mL of Chloroform was charged to the test tube. For Dowfax 2A1, 2.5 mL of orange indicator solution containing 0.003 wt % Methyl Orange, 1.20 wt % sulfuric acid, and 5.00 wt % sodium sulfate was added, and then 2.5 mL of Chloroform was charged to the test tube. These were then shaken to promote mass transfer. Then titrate with a known DTAB solution. The end points for both Dowfax 2A1 and C6L are shown in Figure 9.4.

Epton[9] described titration methods for sulfonate surfactants. Methylene Blue is able to complex with the anionic surfactant and move towards the hydrophobic chloroform layer. DTAB, a cationic surfactant, is able to displace Methylene Blue from the Methylene Blue-anionic surfactant complex and form the cationic-anionic surfactant complex. Thus the color moves from the lower hydrophobic layer to the upper hydrophilic layer.

The liquid-liquid back titration method is used for Dowfax 2A1. Methyl Orange is able to attract only positively charged molecules like DTAB, which we use to titrate. Once DTAB-Dowfax 2A1 complexes are fulfilled DTAB-Methyl Orange can form complexes with each other. The result is a yellow color in the chloroform layer.

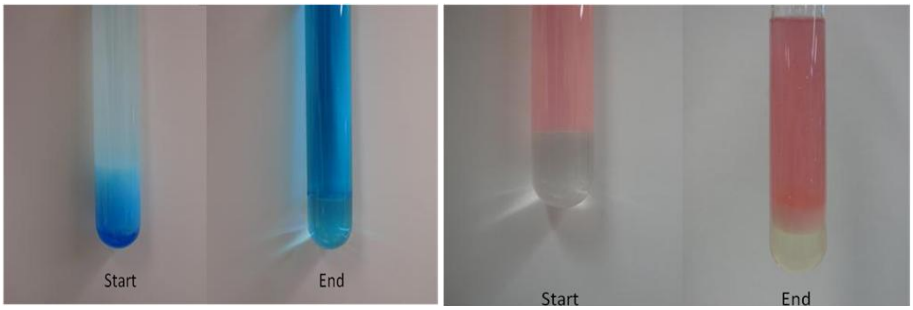

Figure 9.4. Start and End point for Dowfax C6L (left: White/Blue and Blue/Blue) and Dowfax 2A1(Right: Pink/Clear and Pink/Yellow).

9.1.3. Results and Discussion

The adsorption of Dowfax 2A1 and C6L are shown in Figures 9.5 and 9.6. They both exhibit favorable affinity to the hydrate interface. However, the adsorption behaviors are distinctly different. Dowfax C6L adsorption appears to be a Langmuir type isotherm, with a maximum adsorption amount of approximately 0.11mM/g hydrate. This adsorption amount of Dowfax C6L is large in comparison to DTAB or SDS adsorption amounts[8]. Indications of the Dowfax C6L isotherm seem to point that it should act as an anti-agglomerating agent. It shows a high adsorption amount and does not shift the raman vibrational CP ring breathing (Figure 9.1) to indicate a hydrate-like state, making this molecule a favorable candidate for an anti-agglomerating agent for hydrates. The dense and highly charged layer would act to reduce the adhesion of hydrates to each other and provide a barrier for hydrate growth.

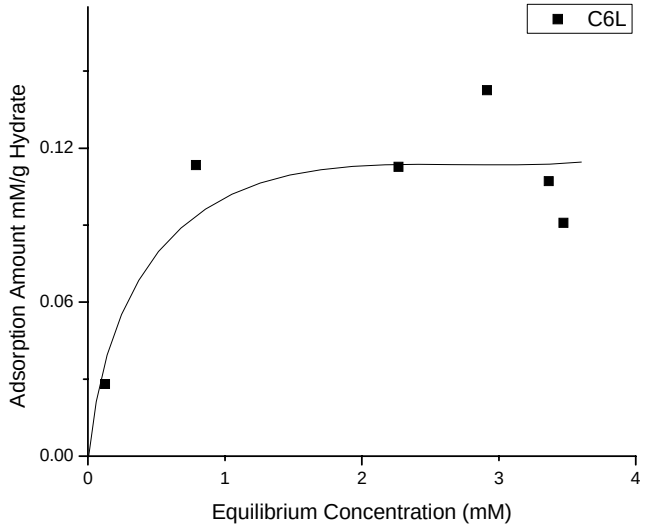

Figure 9.5. An adsorption isotherm of Dowfax C6L on CP hydrates.

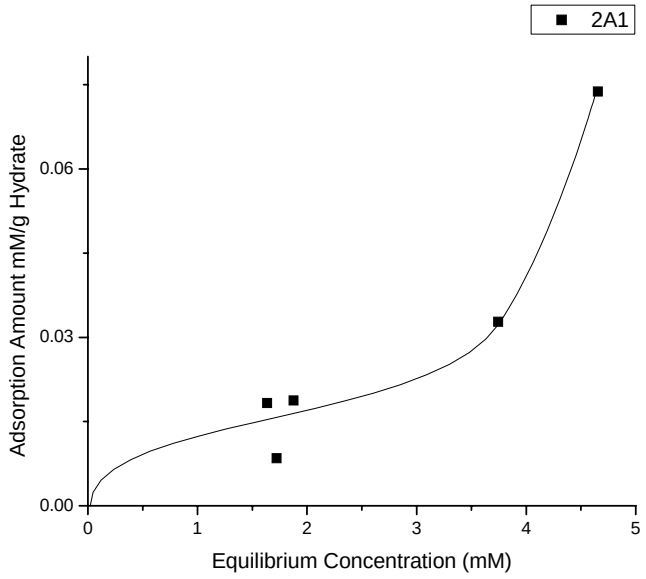

Figure 9.6. An adsorption isotherm of Dowfax 2A1 on CP hydrates.

The adsorption isotherm of Dowfax 2A1 is supposed to have an L-S type isotherm as described by Zhu and Gu[10]. The first step (1.0 to 3.5mM) has a leveling off about 0.025mM/g hydrate. The second step is above the equilibrium concentration of 4.5mM. This adsorption isotherm is similar to SDS in respect to its low adsorption amount and its Raman blue shift of the CP ring breathing to 890cm^{-1} as shown in Figure 9.1. This similarity to the SDS adsorption behavior and the induced hydrate sensitivity, leads to the inclination that this molecule is a favorable hydrate promoter. However from Figure 9.6, the start of the formation of the monolayer begins at a higher concentration. The effective concentration of Dowfax 2A1 to promote formation of hydrate may require more than 1 mM of the surfactant[6]. These similar behaviors behooves us to think that Dowfax 2A1 is a hydrate promoter molecule.

9.1.4. Preliminary Conclusions

We have deduced the roles of these two similar surfactants and how they can be used on hydrate formation processes. Though the structure and surfactant head groups are similar, each surfactant can act differently and have a different purpose on hydrate formations. Raman analysis and surfactant adsorption isotherms revealed each surfactants propensity towards hydrate interfaces. Dowfax C6L is able to adsorb onto hydrate interfaces with a significantly large amount and has no blue shift of the CP ring breathing band to indicate a hydrate-like environment. These behaviors make Dowfax C6L a favorable anti-agglomerate agent. Dowfax 2A1 is able to shift the CP ring breathing band to a hydrate-like position and its adsorption isotherm is similar to the most effective surfactant promoter molecule, SDS. This indicates that Dowfax 2A1 is a promoter molecule that may act similarly to SDS. Additional adsorption data will be added to finalize the types of isotherms of two Dowfax surfactants and high-pressure

methane hydrate formation experiments will be carried out to compare their promotion effect with that of SDS.

9.1.5. References

1. Sloan, E. D.; Koh, C. Clathrate Hydrates of Natural Gas, 3rd ed.; CRC: Boca Raton; 2008.
2. Liang, D., Guo, K., Wang, R., Fan, S. Hydrate equilibrium data of 1,1,1,2-tetrafluoroethane (HFC-134a), 1,1-dichloro-1-fluoroethane (HCFC-141b) and 1,1-difluoroethane (HFC-152a). Fluid Phase Equilibria. 2001. 187–188. 61–70.
3. Kang, S.-P., Lee, H. Recovery of CO2 from Flue Gas Using Gas Hydrate: Thermodynamic Verification through Phase Equilibrium Measurements. Environ. Sci. Technol. 2000. 34. 4397-4400
4. J. Javanmardi, M. Moshfeghian. Energy consumption and economic evaluation of water desalination by hydrate phenomenon. Applied Thermal Engineering. 2003. 23. 845–85
5. Zhong, Y.; Roger, R. E. Surfactant effects on gas hydrate formation. Chem. Eng. Sci. 2000. 55. 4175–4187.
6. Lo, C., Zhang, J.S., Somasundaran, P., Lee, J.W. Raman Spectroscopic Studies of Surfactant Effect on the Water Structure around Hydrate Guest Molecules. *J. Phys. Chem. Lett.* 2010. 1. 2676–2679.
7. Zhang, J. S.; Lo, C.; Somasundaran, P.; Couzis, A.; Lee, J. W. Adsorption of Sodium Dodecyl Sulfate at THF Hydrate/Liquid Interface J. Phys. Chem. C 2008. 112. 12381–12385.
8. Lo, C., Zhang, J.S., Couzis, A., Somasundaran, P., Lee, J.W. Adsorption of Cationic and Anionic Surfactants on Cyclopentane Hydrates. J. Phys. Chem. C. 2010. 114. 13385-13389.
9. Epton, S. R. A new method for the rapid titrimetric analysis of sodium alkyl sulphates and related compounds. Trans. Faraday Soc. 1948, 44, 226-230

10. Zhu, B. Y.; Gu, T. R. General isotherm equation for adsorption of surfactants at solid/liquid interfaces. Part 1. Theoretical. J. Chem. Soc., Faraday Trans. 1989, 85, 3813-3817.

9.2. Single Crystal Hydrate/ AFM

The goal of the study is implement a direct surface study on hydrates. By doing so we are poised to discover many facets of ice-like layers and even stiction. Hydrates are similar to ice however it has a different melt temperature, so it becomes an invaluable resource to evaluate hydrogen bonding at the nanometer scale. The problem with studying hydrates on an AFM is the large roughness. The way to circumvent this problem to create single crystal hydrates.

9.2.1. Single Crystal Hydrate

To form these single crystalline structures, an induced high magnetic or electric field is applied. Hydrates have a small to nonexistent dipole moment however; water molecules have a larger dipole[1]. By aligning the water molecules' dipole to an external field, water molecules reorient in one direction onto crystalline hydrate. The method that can be easily implemented is magnetic field manipulation. This is important in many spectroscopic studies and on microscopic techniques.

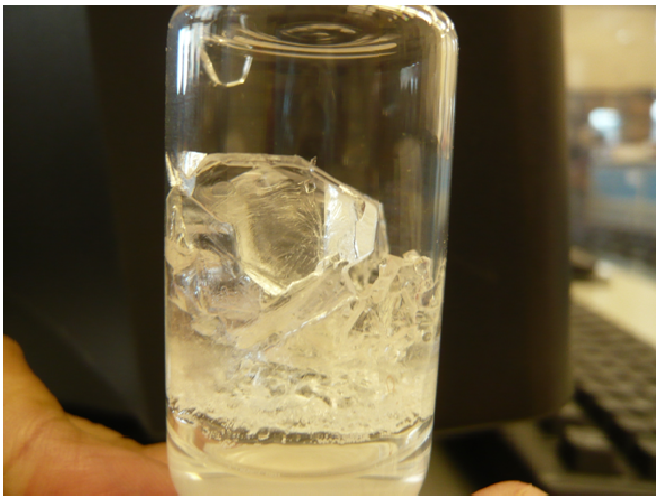

Figure 9.7. Large hydrate crystal formed under magnetic field.

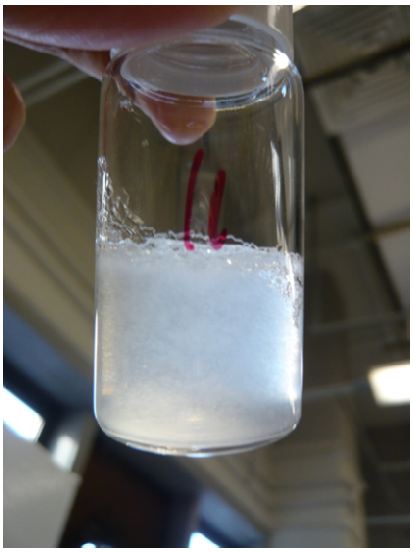

Figure 9.8. Coarse grain hydrate crystals with no field.

9.2.2. Wet AFM study

Only under wet conditions can we discover the hydrogen bonding forces around hydrate or hydrate-like material. This can also determine the most favorable orientation of the surfactant molecule on a hydrate surface. With a wet AFM implemented one can also study the surface attractions to different inhibitor and promoter compounds.

9.2.3. Reference

1. Davidson, D.W. The Motion of Guest Molecules in Clathrate Hydrates. Canadian Journal of Chemistry. 1971. 49. 1224-1242.

9.3. Mixed Micelle/ Salt and Alcohol

The research goal of this endeavor is to directly influence hydrate self-assembly using a synergistic mixed surfactant system. This study will attempt to promote hydrate formation even further by introducing synergistic molecules to the hydrate/water interface. Having a clearer understanding for inducing fast formation, we can further gas hydrate technology beyond storage and sequestration. Having direct influence over hydrophobicity and surfactant head groups, one can control the formation of hydrophobic gas hydrates. This project may lead to the use of greener technologies in the oil& gas fields, as a result of understanding the fundamental science related to fast formation. To investigate this idea of controlling formation rates of gas hydrates, several experiments can be carried out:

9.3.1. Adsorption of 1:1 = Surfactant:Alcohol on hydrate interfaces

Cyclopentane hydrates will act as the model hydrates on which the Surfactant:Alcohol mixture will adsorb. As adsorption is the first step in hydrate promotion it will allows us to identify the mechanism for formation.

9.3.2. ζ- Potential

Monolayer formation is an identification of which concentration will be an effective concentration for hydrate promotion. Zeta Potential will determine at which concentration a hydrate surface is saturated. A hemi-micelle layer can be detected once the surface charge of hydrate particles is saturated.

9.3.3. Adsorption Isotherm

An adsorption isotherm experiment will use the elemental analyzer to determine the amount of surfactant on the hydrate surface. The adsorption amount will determine whether these surfactants are significantly being attracted to the hydrate surface. A subsequent checking of the method will be done using titration methods

9.3.4. Adsorption of Salt and Surfactant on hydrate interfaces

Cyclopentane hydrates will be used as a model hydrate. Salt introduces another element of enhanced adsorption. This research leads to a more realistic model for sea floor hydrates.

9.3.5. Adsorption Isotherm

We will continue to resolve the adsorption Isotherm using titration and surfactant selective ion electrode. The quantitative amount of surfactant could lead to protocols on the use of surfactants at the seafloor, and whether adding increased amounts of surfactant is harmful or beneficial to the hydrate environment.

9.3.6. Surface-Enhanced Raman

Vibrational spectroscopy will deduce whether a model system under the constraints of the prior study is suitable to form hydrates. The vibrational bands of cyclopentane can evaluate whether the system is favorable for fast formation.

9.3.7. *High-Pressure Reactor*

As a proof of concept, methane hydrates will be made in an acquiescent system. We will follow the pressure and temperature of the formation of methane hydrates using a high pressure reactor. This will be the essential proof that will determine whether the hypothesis of increased hydrophobicity at the hydrate/water interface will increase fast formation.

Chapter 10. Bibliography

1. Anderson, B. J.; Tester, J. W.; Borghi, G. P.; Trout, B. L. Properties of Inhibitors of Methane Hydrate Formation via Molecular Dynamics Simulations. J. Am. Chem. Soc. 2005, 127, 17852–17862.

2. Anderson, R.; Chapoy, A.; Tohidi, B. Phase relations and binary clathrate hydrate formation in the system H2-THF-H2O. Langmuir 2007, 23, 3440–3444.

3. Anklam, M. R.; York, J. D.; Helmerich, L.; Firoozabadi, A. Effects of antiagglomerants on the interactions between hydrate particles. AIChE J. 2008, 54, 565-574.

4. Bales, B. L.; Zana, R. Cloud Point of Aqueous Solutions of Tetrabutylammonium Dodecyl Sulfate Is a Function of the Concentration of Counterions in the Aqueous Phase. Langmuir 2004, 20, 1579–1581.

5. Becraft, K.; Richmond, G. L. In Situ Vibrational Spectroscopic Studies of the CaF2/H2O Interface. Langmuir 2001, 17, 7721-7724.

6. Birks, J. B. Photophysics of Aromatic Molecules; Wiley-Interscience:London, 1970; p 318.

7. Carroll, J. J.; Mather, A. E. The system carbon dioxide-water and the Krichevsky-Kasarnovsky equation. J. Solution Chem. 1992, 21, 607–621.

8. Carver, T. J.; Drew, M. G. B.; Rodger, P. M. Characterisation of the {111} growth planes of a type II gas hydrate and study of the mechanism of kinetic inhibition by poly(vinylpyrrolidone). J. Chem. Soc., Faraday Trans. 1996, 92, 5209–5033.

9. Chandar, P.; Somasundaran, P.; Turro, N. J. Fluorescence probe studies on the structure of the adsorbed layer of dodecyl sulfate at the alumina—water interface. J. Colloid Interface Sci. 1987, 117, 31-46.

10. Chandar, P.; Somasundaran, P.; Turro, N. J. Fluorescence probe studies on the structure of the adsorbed layers of dodecyl sulfate at the alumina-water interface. J. Colloid Interface Sci. 1987, 117, 31–46.

11. Chapoy, A.; Anderson, R.; Tohidi, B. Low Pressure Molecular Hydrogen Storage in Semi-Clathrate Hydrates of Quaternary Ammonium Compounds. J. Am. Chem. Soc. 2007, 129, 746–747.

12. Collett, T.S., Detection and Evaluation of Natural Gas Hydrates from Well Logs, Prudhoe Bay Alaska, M.S. Thesis, University of Alaska. 1983.

13. Collett, T.S., National Assessment of U.S. Oil and Gas Resources on CD-ROM (Gautier, D.L., Goldton, G.L., Takahishi, K.I., eds.), USGS Digital Data Series 30, Washington D.C. (1995).

14. Compoint, M.; Toubin, C.; Picaud, S.; Hoang, P. N. M.; Girardet, C. Geometry and dynamics of formic and acetic acids adsorbed on ice. Chem. Phys. Lett. 2002, 365, 1–7.

15. Conrad, M.; Strauss, H. L. The Vibrational Spectrum of Water in Liquid Alkanes. Biophysical Journal, 48, 1985, 117-124.

16. Corso, J. V. Mixed Indicator Composition. U.S. Patent 2663692, 1953.

17. Davy. H. On a Combination of Oxymuriatic Gas and Oxygene Gas. Philosophical Transactions of the Royal Society. 1811. 101. 155-162.

18. Delahave, A.; Fournaison, L.; Marinhas, S.; Chatti, I.; Petitet, J. P.; Dalmzaaone, D.; Furst, W. Effect of THF on equilibrium pressure and dissociation enthalpy of CO2 hydrates applied to secondary refrigeration. Ind. Eng. Chem. Res. 2005, 45, 391–397.

19. Devarakonda, S.; Groysman, A.; Myerson, A. S. THF-water hydrate crystallization: an experimental investigation. J. Cryst. Growth 1999, 204, 525–538.

20. Di Profio, P.; Arca, S.; Germani, R.; Savelli, G. Surface promoting effects on clathrate hydrate formation: Are micelles really involved. Chem. Eng. Sci. 2005, 60, 4141–4145.

21. Dobbs, G. T.; Luzinova, Y.; Mizaikoff, B. Infrared Spectroscopy for Monitoring Gas Hydrates in Aqueous Solution. Proceedings of the 6th International Conference on Gas Hydrates (ICGH 2008)

22. Drzymala, J.; Sadowski, Z.; Holysz, L; Chibowski, E. Ice/water interface: Zeta potential, point of zero charge, and hydrophobicity. J. Colloid Interface Sci. 1999, 220, 229–234.

23. Englezos, P.; Kalogerakis, N.; Dholabhai, P. D.; Bishnoi, P. R. Kinetics of formation of methane and ethane gas hydrates. Chem. Eng. Sci. 1987, 42, 2647–2658.

24. Epton, S. R. A new method for the rapid titrimetric analysis of sodium alkyl sulphates and related compounds. Trans. Faraday Soc. 1948, 44, 226-230.

25. Fleyfel, F.; Devlin, J. P. Carbon Dioxide Clathrate Hydrate Epitaxial Growth: Spectroscopic Evidence for Formation of the Simple Type-II CO2 Hydrate. Journal of Physical Chemistry 95, 1991, 9, 3811-3815.

26. Gayet, P.; Dicharry, C.; Marion, G.; Graciaa, A.; Lachaise, J.; Nesterov, A. Experimental Determination of Methane Hydrate Dissociation Curve up to 55 MPa by Using a Small Amount of Surfactant as Hydrate Promoter Chem. Eng. Sci. 2005, 60, 5751– 5758.

27. Gregory, J. Particles in water: properties and processes; CRC: Boca Raton, FL, 2006; pp 90-92.

28. Gudmundsson, J. S.; Borrehaug, A. A Frozen Hydrate for Transport of Natural Gas. In The Second International Conference on Natural Gas Hydrate, Toulouse, France, 1996; pp 415− 422.

29. Hammerschmidt, E. G. Formation of Gas Hydrates in Natural Gas Transmission Lines Ind. Eng. Chem. 1934, 26, 851– 855.

30. Hutter, J. L.; King, H. E.; Lin, M. Y. Polymeric Hydrate-Inhibitor Adsorption Measured by Neutron Scattering. Macromolecules 2000, 33, 2670–2679.

31. Javanmardi, J., Moshfeghian, M. Energy consumption and economic evaluation of water desalination by hydrate phenomenon. Applied Thermal Engineering. 2003. 23. 845–85.

32. Jeffrey, G. A. Hydrate Inclusion Compounds. In Inclusion Compounds 1; Atwood, J. L., Davies, J. E. D., MacNichol, D. D., Eds.; Academic Press: London, 1983; p 135.

33. Jeffrey, G. A.; McMullan, R. W. The Clathrate Hydrates. Progress in Inorganic Chemistry; John Wiley: New York, 1967; 8, 43-108.

34. Kalyanasundaram, K.; Thomas, J. K. Environmental effects on vibronic band intensities in pyrene monomer fluorescence and their application in studies of micellar systems. J. Am. Chem. Soc. 1977, 97, 2039– 2044.

35. Kang, S.-P., Lee, H. Recovery of CO2 from Flue Gas Using Gas Hydrate: Thermodynamic Verification through Phase Equilibrium Measurements. Environ. Sci. Technol. 2000. 34. 4397-4400.

36. Kashchieva, D.; Firoozabadib, A. Induction time in crystallization of gas hydrates. J. Cryst. Growth 2003, 250, 499–515.

37. Kelland, M. A. History of the Development of Low Dosage Hydrate Inhibitors. Energy Fuels 2006, 20, 825–847.

38. King, H. E.; Hutter, J. L.; Lin, M. Y.; Sun, T. Polymer conformations of gas-hydrate kinetic inhibitors: A small-angle neutron scattering study. J. Chem. Phys. 2000, 112, 2523–2532.

39. Koh, C. A. Towards a fundamental understanding of natural gas hydrates. Chem. Soc. Rev. 2002, 31, 157–167.

40. Kutergin, O. B.; Mel'nikov, V. P.; Nesterov, A. N. Influence of Surfactants on the Mechanism and Kinetics of the Formation of Gas Hydrates Dokl. Akad. Nauk SSSR 1992, 323, 549– 553.

41. Kvamme, B.; Kuznetsova, T.; Aasoldsen, K. Molecular dynamics simulations for selection of kinetic hydrate inhibitors. J. Mol. Graphics Modell. 2005, 23, 524–536.

42. Liang, D., Guo, K., Wang, R., Fan, S. Hydrate equilibrium data of 1,1,1,2-tetrafluoroethane (HFC-134a), 1,1-dichloro-1-fluoroethane (HCFC-141b) and 1,1-difluoroethane (HFC-152a). Fluid Phase Equilibria. 2001. 187–188. 61–70.

43. Lipkowski, J. The Structure of Tetrabutylammonium Bromide Hydrate (C4H9)4NBr·21/3H2O. J. Supramol. Chem. 2002, 2, 435–439.

44. Lo, C., Zhang, J.S., Couzis, A., Somasundaran, P., Lee, J.W. Adsorption of Cationic and Anionic Surfactants on Cyclopentane Hydrates. J. Phys. Chem. C. 2010. 114. 13385-13389.

45. Lo, C., Zhang, J.S., Somasundaran, P., Lee, J.W. Raman Spectroscopic Studies of Surfactant Effect on the Water Structure around Hydrate Guest Molecules. J. Phys. Chem. Lett. 2010. 1. 2676–2679.

46. Lo, C.; Zhang, J. S.; Somasundaran, P.; Couzis, A.; Lee, J. W. Adsorption of Cationic and Anionic Surfactants on Cyclopentane Hydrates. J. Phys. Chem. C 2010, 114, 13385–13389.

47. Lo, C.; Zhang, J. S.; Somasundaran, P.; Couzis, A.; Lee, J. W. Adsorption of Surfactants on Two Different Hydrates Langmuir 2008, 24, 12723– 12726.

48. Lo, C.; Zhang, J. S.; Somasundaran, P.; Lee, J. W. Raman Spectroscopic Studies of Surfactant Effect on the Water Structure around Hydrate Guest Molecules. J. Phys. Chem. Lett. , 2010, 1, 2676–2679.

49. Long, D., Lovell, M.A., Rees, J.G., Rochelle, C.A. Sediment-Hosted Gas Hydrates: New Insights on Natural and Synthetic Systems, Geological Society, London, Special Publications. 2009. 319. 1-9.

50. Mao, W. L.; Mao, H. K.; Goncharov, A. F.; Struzhkin, V. V.; Guo, Q. Z.; Hu, J. Z.; Shu, J. F.; Hemley, R. J.; Somayazulu, M.; Zhao, Y. S. Hydrogen Clusters in Clathrate Hydrate Science 2002, 297, 2247– 2249.

51. Miller, F. A.; Inskeep, R. G. The Infra-Red and Raman Spectra of Cyclopentane, Cyclopentane-d1, and Cyclopentane-d10 J. Chem. Phys. 1950, 18, 1519– 1531.

52. Mullin, J. W., Crystallization, 4th ed., Butterworth-Heinemann: Oxford, U.K., 2001, Chapter 5.

53. North, W. J.; Blackwell, V. R.; Morgan, J. J. Studies of CO2 Hydrate Formation and Dissolution Environ. Sci. Technol. 1998, 32, 676– 681.

54. Okutani, K.; Kuwabara, Y.; Mori, Y. H. Surfactant Effects on Hydrate Formation in an Unstirred Gas/Liquid system: An Experimental Study Using Methane and Sodium Alkyl Sulfates Chem. Eng. Sci. 2008, 63, 183– 194.

55. Osawa, M. Surface-Enhanced Infrared Absorption. NEAR-FIELD OPTICS AND SURFACE PLASMON POLARITONS Topics in Applied Physics, 2001, 81, 163-187.

56. Patrykiejew, A.; Sokolowski, S.; Zientarski, T.; Binder, K. Monte Carlo Study of Dense Monolayer and Bilayer Films on the (100) Plane of Face-Centered Cubic Crystals. Langmuir 1999, 15, 3642-3652.

57. Pimentel, G. C.; McClellan, A. L. The Hydrogen Bond; WH Freeman: New York, 1960.

58. Pradines, V.; Lavabre, D.; Micheau, J.C.; Pimienta, V. Determining the Association Constant and Adsorption Properties of Ion Pairs in Water by Fitting Surface Tension Data. Langmuir 2005, 21, 11167–11172.

59. Prosser, A. J.; Franses, E. I. Adsorption and surface tension of ionic surfactants at the air-water interface: review and evaluation of equilibrium models. Colloid Surf. A. 2001, 178, 1–40.

60. Richmond, G. L. Molecular Bonding and Interactions at Aqueous Surfaces as Probed by Vibrational Sum Frequency Spectroscopy. Chem. Rev. 2002, 102, 2693-2724.

61. Rosano, H. L.; Nixon, A. L.; Cavallo, J. L. Interfacial Stoichiometry of a Microemulsion System J. Phys. Chem. 1989, 93, 4536– 4539.

62. Rosenbaum, E. J.; Jacobson, H. F. Raman Spectra of Cyclopentane and Some of Its Monoalkyl Derivatives J. Am. Chem. Soc. 1941, 63, 2841– 2842.

63. Schettino, V.; Marzocchi, M. P.; Califano, S. Infrared Spectra of Crystalline Cyclopentane and Cyclopentane-d10 J. Chem. Phys. 1969, 51, 5264– 5276.

64. Shin, J.-W.; Hammer, N.I.; Diken, E.G.; Johnson, M.A.; Walters, R.S.; Jaeger, T.D.; Duncan, M.A.; Christie, R.A.; Jordan, K.D. Infrared Signature of Structures Associated with the H+ (H2O)n (n=60 to 27) Clusters. Science , 2004, 304, 1137-1140.

65. Sloan, E. D. Clathrate Hydrates of Natural Gas, 2nd ed.; Dekker: New York, 1998.

66. Sloan, E. D. Fundamental Principles and Applications of Natural Gas Hydrates Nature 2003, 426, 353– 359.

67. Sloan, E. D.; Koh, C. Clathrate Hydrates of Natural Gas, 3rd ed.; CRC: Boca Raton, FL, 2008.

68. Somasundaran, P; Moudgil, B. M. The effect of dissolved hydrocarbon gases in surfactant solutions on froth floatation of minerals. J. Colloid Interface Sci. 1974, 47, 290–299.

69. Steveninck, J. V.; Riemersma, J. C. Determination of Long-Chain Alkyl Sulfates as Chloroform-Soluble Azure A Salts. Anal. Chem. 1966, 38, 1250-1251.

70. Storr, M. T.; Taylor, P. C.; Monfort, J. P.; Rodger, P. M. Kinetic Inhibitor of Hydrate Crystallization. J. Am. Chem. Soc. 2004, 126, 1569–1576.

71. Suga, H.; Matsuo, T.; Yamamuro, O. Thermodynamic study of ice and clathrate hydrates. Pure Appl. Chem. 1992, 64, 17–26.

72. Thompson, H.; Soper, A. K.; Buchanan, P.; Aldiwan, N.; Creek, J. L.; Koh, C. A. Methane hydrate formation and decomposition: Structural studies via neutron diffraction and empirical potential structure refinement. J. Chem. Phys. 2006, 124, 164508.

73. Tian, C.S.; Shen, Y.R. Isotopic Dilution Study of the Water/Vapor Interface by Phase-Sensitive Sum-Frequency Vibrational Spectroscopy. J.AM. CHEM. SOC. 2009, 131, 2790–2791.

74. Tréhu, A.M., Bohrmann, G., Torres, M.E., Colwell, F.S. (eds.), in Proc. Ocean Drill. Program, Scientific Results 2006, TAMU, College Station, TX, 204.

75. Tréhu, A.M., Ruppel, C., Holland, M., Dickens, G.R., Torres, M.E., Collett, T.S., Goldberg, D.S., Riedel, M., Schultheiss, P., Oceanography. 2006. 19. 124-143.

76. Wang, L. K.; Panzardi, P. Determination of anionic surfactants with Azure A and quaternary ammonium salt. J. Anal. Chem. 1975, 47, 1472-1475.

77. Wang, W. X.; Bray, C. L.; Adams, D. J.; Cooper, A. I. Methane Storage in Dry Water Gas Hydrates. J. Am. Chem. Soc. 2008, 230, 11608-11609.

78. Wang, W. X.; Carter, B. O.; Bray, C. L.; Steiner, A.; Bacsa, J.; Jones, J. T.; Croper, C.; Khimyak, Y. Z.; Adams, D. J.; Cooper, A. I. Reversible Methane Storage in a Polymer-Supported Semi-Clathrate Hydrate at Ambient Temperature and Pressure. Chem. Mater. 2009, 21, 3810-3815.

79. Watanabe, K.; Imai, S.; Mori, Y. H. Surfactant effects on hydrate formation in an unstirred gas/liquid system: An experimental study using HFC-32 and sodium dodecyl sulfate. Chem. Eng. Sci. 2005, 60, 4846–4857.

80. Watanabe, K.; Niwa, S.; Mori, Y. H. Surface tensions of aqueous solutions of sodium alkyl sulfates in contact with methane under hydrate forming conditions. J. Chem. Eng. Data 2005, 50, 1672–1676.

81. Werezak, G. N. Aqueous solution concentration by a clathrate type of gas hydrate formation. Chem. Eng. Prog. Symp. Ser. 1969, 65, 6–18.

82. Zana, R.; Benrraou, M.; Bales, B. L. Effect of the Nature of the Counterion on the Properties of Anionic Surfactants. 3. Self-Association Behavior of Tetrabutylammonium Dodecyl Sulfate and Tetradecyl Sulfate: Clouding and Micellar Growth. J. Phys. Chem. 2004, 108, 18195– 18203.

83. Zhang, J. S.; Lee, J. W. Effect of Sodium Dodecyl Sulfate on the Supercooling Point of Ice and Clathrate Hydrates. Energy Fuel 2009, 23, 3045-3047.

84. Zhang, J. S.; Lee, J. W. Equilibrium of Hydrogen + Cyclopentane and Carbon Dioxide + Cyclopentane Binary Hydrates. J. Chem. Eng. Data 2009, 54, 659-661.

85. Zhang, J. S.; Lee, S. Y.; Lee, J. W. Does SDS Micellize under Methane Hydrate-Forming Conditions below the Normal Ambient Krafft Point? J. Colloid Interface Sci. 2007, 315, 313– 318.

86. Zhang, J. S.; Lee, S. Y.; Lee, J. W. Does SDS micellize under methane hydrate-forming conditions below the normal Krafft point? J. Colloid Interface Sci. 2007, 315, 313–318.

87. Zhang, J. S.; Lee, S. Y.; Lee, J. W. Kinetics of Methane Hydrate Formation from SDS Solution. Ind. Eng. Chem. Res. 2007, 46, 6353– 6359.

88. Zhang, J. S.; Lee, S. Y.; Lee, J. W. Solubility of sodium dodecyl sulfate near propane and carbon dioxide hydrate-forming conditions. J. Chem. Eng. Data 2007, 52, 2480–2483.

89. Zhang, J. S.; Lo, C.; Somasundaran, P.; Couzis, A.; Lee, J. W. Adsorption of Sodium Dodecyl Sulfate at THF Hydrate/Liquid Interface J. Phys. Chem. C 2008, 112, 12381–12385.

90. Zhang, J. S.; Lo, C.; Somasundaran, P.; Lu, S.; Couzis, A.; Lee, J. W. Adsorption of Cationic and Anionic Surfactants on Cyclopentane Hydrates. J. Phys. Chem. C 2008, 112, 12381–12385.

91. Zhang, J. S.; Lo, C.; Somasundaran, P.; Lu, S.; Couzis, A.; Lee, J. W. Adsorption of Sodium Dodecyl Sulfate at THF Hydrate/Liquid Interface. J. Phys. Chem. C 2008, 112, 12381-12385.

92. Zhang, Y.; Debenedetti, P. G.; Prud'homme, R. K.; Pethica, B. A. Differential Scanning Calorimetry Studies of Clathrate Hydrate Formation. J. Phys. Chem. B 2004, 108, 16717–16722.

93. Zhong, Y.; Rogers, R. E. Surfactants Effects on Gas Hydrate Formation Chem. Eng. Sci. 2000, 55, 4175– 4787.

94. Zhu, B. Y.; Gu, T. R. General isotherm equation for adsorption of surfactants at solid/liquid interfaces. Part 1. Theoretical. J. Chem. Soc., Faraday Trans. 1989, 85, 3813-3817.